

27
8-27-80
+ 15 NTIS

ornl

ORNL/TM-5684

OAK
RIDGE
NATIONAL
LABORATORY



MASTER

**The Performance of
Hydroclones for Removing
Particles from Viscous Liquids**

Jan B. Talbot

OPERATED BY
UNION CARBIDE CORPORATION
FOR THE UNITED STATES
DEPARTMENT OF ENERGY

DISTRIBUTION OF THIS DOCUMENT IS UNLIMITED

DISCLAIMER

This report was prepared as an account of work sponsored by an agency of the United States Government. Neither the United States Government nor any agency Thereof, nor any of their employees, makes any warranty, express or implied, or assumes any legal liability or responsibility for the accuracy, completeness, or usefulness of any information, apparatus, product, or process disclosed, or represents that its use would not infringe privately owned rights. Reference herein to any specific commercial product, process, or service by trade name, trademark, manufacturer, or otherwise does not necessarily constitute or imply its endorsement, recommendation, or favoring by the United States Government or any agency thereof. The views and opinions of authors expressed herein do not necessarily state or reflect those of the United States Government or any agency thereof.

DISCLAIMER

Portions of this document may be illegible in electronic image products. Images are produced from the best available original document.

Printed in the United States of America. Available from
National Technical Information Service
U.S. Department of Commerce
5285 Port Royal Road, Springfield, Virginia 22161
NTIS price codes—Printed Copy: A06; Microfiche A01

This report was prepared as an account of work sponsored by an agency of the United States Government. Neither the United States Government nor any agency thereof, nor any of their employees, makes any warranty, express or implied, or assumes any legal liability or responsibility for the accuracy, completeness, or usefulness of any information, apparatus, product, or process disclosed, or represents that its use would not infringe privately owned rights. Reference herein to any specific commercial product, process, or service by trade name, trademark, manufacturer, or otherwise, does not necessarily constitute or imply its endorsement, recommendation, or favoring by the United States Government or any agency thereof. The views and opinions of authors expressed herein do not necessarily state or reflect those of the United States Government or any agency thereof.

Contract No. W-7405-eng-26

CHEMICAL TECHNOLOGY DIVISION

THE PERFORMANCE OF HYDROCLONES FOR REMOVING
PARTICLES FROM VISCOUS LIQUIDS

Jan B. Talbot

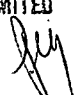
Date Published - August 1980

OAK RIDGE NATIONAL LABORATORY
Oak Ridge, Tennessee 37830
operated by
UNION CARBIDE CORPORATION
for the
DEPARTMENT OF ENERGY

DISCLAIMER

This book was prepared as an account of work sponsored by an agency of the United States Government. Neither the United States Government nor any agency thereof, nor any of their employees, makes any warranty, express or implied, or assumes any legal liability or responsibility for the accuracy, completeness, or usefulness of any information, apparatus, product, or process disclosed, or represents that its use would not infringe privately owned rights. Reference herein to any specific commercial product, process, or service by trade name, trademark, manufacturer, or otherwise, does not necessarily constitute or imply its endorsement, recommendation, or favoring by the United States Government or any agency thereof. The views and opinions of authors expressed herein do not necessarily state or reflect those of the United States Government or any agency thereof.

DISTRIBUTION OF THIS DOCUMENT IS UNLIMITED



THIS PAGE
WAS INTENTIONALLY
LEFT BLANK

CONTENTS

	<u>Page</u>
ABSTRACT	1
1. INTRODUCTION	1
2. HYDROCLONE PERFORMANCE CRITERIA.	6
2.1 Hydroclone Pressure Drop.	6
2.2 Hydroclone Efficiency	8
2.3 Volume Split or Flow Ratio.	12
2.4 Operating Variables	13
3. SMALL-DIAMETER HYDROCLONES	14
4. EXPERIMENTAL APPARATUS AND PROCEDURE	15
5. EXPERIMENTAL RESULTS AND PERFORMANCE CALCULATIONS.	20
5.1 Test Data	20
5.2 Hydroclone Performance Calculations	22
5.3 Particle-Size-Distribution Data and Point Efficiencies.	31
5.4 Hydroclone Attrition.	38
6. CORRELATION OF DATA AND DISCUSSION OF RESULTS.	42
6.1 Pressure Drop as a Function of Flow Rate and Viscosity.	42
6.2 Hydroclone Performance Parameters	54
6.3 Hydroclone Efficiency	62
7. CONCLUSIONS.	86
8. ACKNOWLEDGMENTS.	90
9. APPENDIX	91
10. REFERENCES	99

THIS PAGE
WAS INTENTIONALLY
LEFT BLANK

LIST OF SYMBOLS

a, b	constants used in data correlations
C	solids concentration, g/cm^3
D	hydroclone diameter, cm
D_c	diameter of the cylindrical section of the hydroclone, cm
d	particle diameter, μm
dm	mean particle diameter, μm
d_{50}	particle diameter which exhibits a 50% point efficiency
E	hydroclone efficiency
E_c	centrifugal efficiency
F_k	weight percent less than a particle diameter, d_k , in the feed
ΔF	$F_{k+1} - F_k$
G	gross efficiency
g_c	gravitational constant, $1 \text{ m}\cdot\text{kg}/\text{N}\cdot\text{sec}^2$
k	proportionality constant
N_{Eu}	Euler number
N_{Re}	Reynolds number
n	coefficient of tangential velocity distribution
O_k	weight percent less than a particle diameter, d_k , in the overflow
ΔO	$O_{k+1} - O_k$
P	pressure, lb/in.^2
ΔP	inlet-to-overflow pressure drop, lb/in.^2
Q	flow rate, cm^3/min
Rf	flow ratio
r	radial position in hydroclone, cm

r^2	coefficient of determination
S	volume split
s	standard deviation
U_k	weight percent less than a particle diameter, d_k , in the underflow
ΔU	$U_{k+1} - U_k$
V	tangential velocity, cm/sec
V_i	inlet feed velocity, cm/sec
x,y,z	exponential coefficients

Greek Letters

α	inlet-velocity loss coefficient [in Eq. (4)]
β	coefficient in Eq. (51)
ϵ	corrected point efficiency
ϵ_k	corrected point efficiency for a particle diameter, d_k
θ	hydroclone included angle, degrees
μ	liquid viscosity, cP
ρ	liquid density, g/cm ³
σ	solid density, g/cm ³

Subscripts

f	feed stream
o	overflow stream
u	underflow stream

Superscripts

'	cumulative method
---	-------------------

THE PERFORMANCE OF HYDROCLONES FOR REMOVING
PARTICLES FROM VISCOUS LIQUIDS

Jan B. Talbot

ABSTRACT

The performance of a 1-cm diam, Dorr-Oliver hydroclone with slurries containing 0.5 wt % solids in water-glycerin solutions was studied to evaluate the effects of fluid viscosity. Micron-sized particles of low-density solids (aluminum oxide, test dust, fly ash, or kaolin) were removed from solutions with viscosities ranging from 1 to 85 cP. Pressure drop across the hydroclone increased with increasing feed rate and viscosity. Gross and centrifugal efficiencies were found to increase with flow rate and decrease with viscosity. Liquid viscosities >10 cP had deleterious effects on the pressure drop and efficiency; thus useful separations were not attained. The particle diameter, corresponding to a point efficiency of 50%, decreased as the product of the inlet Reynolds number and the solid-to-liquid density ratio increased. The reduced efficiency curve was found to characterize the hydroclone performance.

1. INTRODUCTION

Since the first hydroclone patent was granted in the United States in 1891 to Bretney,¹ hydroclones have found many uses in the physical removal of solids from liquids or in the concentration of solids. However, the hydroclone (which is also called hydrocyclone, hydraulic cyclone, and liquid cyclone) was seldom exploited until 1939 when Driessen² developed its use for coal preparation (i.e., washing and desliming) at the Dutch State Mines in Limburg, Holland. The largest application of hydroclones has been in the pulp and paper industry and in coal preparation. However, other industries have used hydroclones

as thickeners, classifiers, washers, liquid-liquid separators, gas-liquid separators, and mass-transfer promoters.

In general, the operation of a hydroclone uses fluid pressure energy to create rotational fluid motion which causes the phase separation. The idealized flow pattern within a hydroclone is shown in Fig. 1. A suspension of solid particles in a liquid is injected tangentially into the cylindrical section of a hydroclone and adopts a downward spiral motion into the conical section. The small apex prevents total discharge of the swirling slurry to the underflow. Part of the suspension changes direction into the inner helix and exits as the overflow through the vortex finder at the center of the hydroclone. The selective separation of solid particles from the liquid is the result of two opposing forces acting on the particles--an outward centrifugal force and an inward viscous drag. The magnitude of these forces depends upon the physical dimensions of the hydroclone and the physical properties of both the fluid and solid material.

The basic advantages of a hydroclone over other solid-liquid separation techniques are simplicity, economy, and the possibility of operation at temperatures up to 450°C. Hydroclones are simple devices with no moving parts or mechanical seals. They require minimum maintenance, compared to a centrifugal or a continuous filter. The required energy of separation is the fluid pressure drop, which can be supplied by a standard pump.

Hydroclones are potentially useful for removing solids from coal-derived liquids, either alone or in series with filtration equipment. The separation and concentration of micron-sized ash-char-catalyst solids

ORNL DWG 75-59

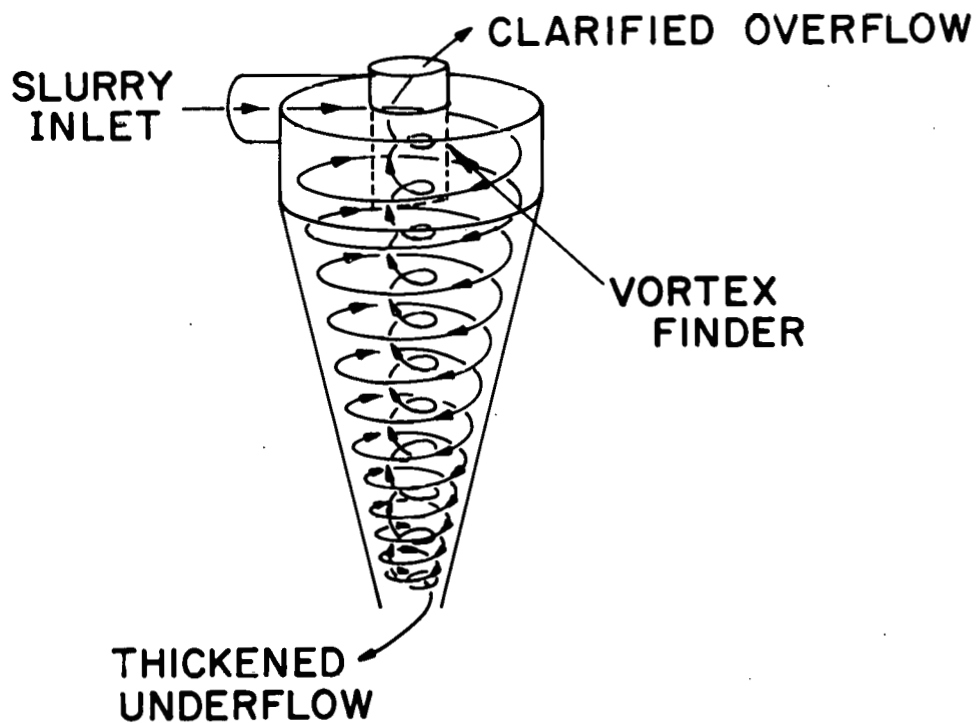


Fig. 1. Idealized flow pattern within a hydroclone.

from viscous liquid streams that result from hydroliquefaction and pyrolysis of coal is a crucial technical problem in the development and application of these processes. From a survey of the supporting research and development of separations technology for coal liquefaction processes,³ three pilot plant ventures were found to have demonstrated the efficacy of hydroclones. Hydrocarbon Research, Inc. (Trenton, N.J.) made small-scale tests to concentrate solids contained in the reactor slurry product of vacuum flash bottoms from their H-Coal process. These tests were made with one unit of a Dorr-Oliver six cyclone "DOXIE." The solids content of the underflow stream ranged from 28 to 75 wt % of the solids in the feed. This work indicated that, with an oil having a density of about 0.9 g/cm³ and a viscosity of 3-5 cP, the clarified liquid would contain about one-third of the solids content. An estimated operating temperature to achieve these properties with H-Coal products would be ~260°C. Also, a hydroclone test loop was studied by Hydrocarbon Research, Inc. (Lawrenceville, N.J.)⁴ to evaluate a 1-cm Dorr-Oliver hydroclone as a means of separating ash and unreacted coal from nondistillable residual oil. After adjusting the liquid viscosity with hydrogenated anthracene and No. 2 fuel oils, the vacuum bottoms product was fed into the test loop. Their results showed that separation efficiencies, defined as $100 - [1 - (\% \text{ ash in overflow} / \% \text{ ash in feed})]$, varied from ~78% for dilute feed (1.1% ash) at 218°C down to 7.5% for feed containing 7.6% ash at 203°C. Increasing the pressure drop from 30 to 60 psi increased the separation efficiency from 36 to 65%. An approximate correlation of viscosity (not a true viscosity since the fluids were non-Newtonian)

and efficiency showed that as viscosity increased from 0.1 to 6 cP, the separation efficiency decreased from about 80 to 15%.

The Consolidation Coal Company pilot plant (Cresap, W. Va.) tested a solids separation system consisting of three 3-in. (main diameter) hydroclones, two in parallel as separators and one as a washer unit.³ The resulting material balances indicated average removal of solids, ash, and extract as 94.9, 93.2, and 93.4 wt %, respectively; the total solids content in the feed ranged from 2.03 to 3.35 wt %. Solid particles larger than 40 μ in diameter did not appear in the overflow, although the feed contained 50 to 60% solids above 40 μ and 1% above 300 μ in diameter.

The hydroclone applications discussed have been adjudged as complete separation methods, not as a solids concentrating technique to be used prior to filtration. A limited amount of data were taken and a relationship between efficiency and the operating parameters was not determined. The performance of hydroclones with relatively viscous liquids and micron-sized particles, such as those produced in coal hydro-liquefaction processes, has not been studied adequately.

The main objective of this study was to experimentally measure the performance of a 1-cm diam Dorr-Oliver "Doxie" hydroclone as a function of applied pressure drop, liquid viscosity, solids density, and particle diameter. A typical synthetic coal oil stream has a viscosity range of 140 cP at 90°C to 7.5 cP at 175°C and contains about 3 to 10 wt % solids.³ These low-density solids (~ 1.5 to 2.5 g/cm³) are usually < 20 μ m in diameter ($\sim 70\%$ < 5 μ m in diameter).³ Therefore, micron-sized powders of low density were suspended in water-glycerin solutions in the viscosity range

of 1 to 85 cP to simulate a coal-derived liquid stream. The relationship between pressure drop (inlet-to-overflow) and flow rate at varying viscosities was determined, and a correlation was developed to describe particle size classification as a function of the physical properties of the solid particles and liquid medium.

2. HYDROCLONE PERFORMANCE CRITERIA

The general performance of a hydroclone depends upon the physical dimensions of the unit, the feed capacity, and the physical properties of the feed. Performance criteria are usually defined by hydroclone efficiency, pressure drop, and the ratio of underflow-to-overflow rates. The literature has numerous papers concerning hydroclones, which fall into two basic categories: (1) works dealing with theory and design, and (2) works related to industrial applications. The most complete bibliography is contained in a book titled The Hydroclone.⁵

2.1 Hydroclone Pressure Drop

The hydroclone develops its separational power through the use of fluid pressure energy. Therefore, the pressure drop across the unit, from the feed entry to the overflow exit, is an important operating variable. A semi-theoretical relationship⁶ has been developed to relate the pressure difference across an annular layer of rotating fluid to the inlet velocity for nonviscous fluid by considering the simplified equation of motion:

$$\frac{dP}{dr} = \frac{\rho V^2}{r}, \quad (1)$$

and an empirical relationship describing the tangential velocity distribution:

$$Vr^n = k_1, \quad (2)$$

where $0 \leq n \leq 1$ in the outer region, and $n = 1$ in the inner region of the hydroclone; k_1 is a constant. After substituting Eq. (2), the total pressure loss due to the change in centrifugal head from the inlet to overflow is determined by integrating Eq. (1) from $r = D_o/2$ to $r = D_c/2$ to give:

$$\Delta P = \frac{2^{2n-1}}{n} \rho k_1^2 D_c^{-2n} \left[\left(\frac{D_c}{D_o} \right)^{2n} - 1 \right]. \quad (3)$$

Expressing the constant k_1 in terms of inlet feed velocity:

$$k_1 = Vr^n = \alpha V_i (D_c/2)^n, \quad (4)$$

and substituting this value for k_1 into Eq. (3) yields:

$$\Delta P = \frac{1}{2n} \rho \alpha^2 V_i^2 \left[\left(\frac{D_c}{D_o} \right)^{2n} - 1 \right]. \quad (5)$$

Equation (5) is dependent on the knowledge of n and α , which are in turn dependent on the hydroclone design and fluid properties. For a particular hydroclone design and fluid conditions, the above correlation developed by Bradley in Eq. (5) and empirical expressions by other workers reduce to the following general relationship for pressure drop as a function of inlet flow rate and the cylindrical section diameter of the hydroclone:

$$\Delta P = k_2 \frac{Q_f^2}{D_c^4}. \quad (6)$$

2.2 Hydroclone Efficiency

There is a difficulty in expressing efficiency in phase separations because a single efficiency number can describe the separation only when the separation is ideal (i.e., when the phases are completely separated from each other). Hydroclone efficiency is defined in several different ways in the literature.⁵ Gross efficiency, G , is the ratio of the solids discharge rate at the underflow to the solids feed rate. Since liquid is continuously removed with the underflow solids, two liquid and two solid flow rates are involved in any useful definition of efficiency. Therefore, the hydroclone efficiency more commonly used is the centrifugal efficiency, E_c , which is defined as follows:

$$E_c = \frac{G - R_f}{1 - R_f}, \quad (7)$$

where

R_f = ratio of the underflow rate to feed rate.

For example, if all solids entering the hydroclone leave at the underflow, $G = 1$. If all the liquid leaves at the overflow, $R_f = 0$, and the centrifugal efficiency equals unity. Centrifugal efficiency is also called the separation number.⁷

Since all of the solids in the feed material may not be the same size, efficiency must be referenced to a size distribution. The point efficiency, E' , expresses the centrifugal efficiency for a given particle size or fraction of a given particle size interval which is removed from the feed stream through the underflow. Point efficiency is calculated in the literature from the particle size distributions and operating data

by two methods. Bradley⁸ uses a differential relationship, assuming the differences for the feed, overflow, and underflow analyses are calculated over the same size interval, and the interval is small. The differential relationship is

$$E = G \frac{\Delta U}{\Delta F} = \frac{1}{1 + \frac{\Delta O}{\Delta U} \left(\frac{1-G}{G} \right)}, \quad (8)$$

where

$$\Delta U = U_{k+1} - U_k,$$

$$\Delta O = O_{k+1} - O_k,$$

$$\Delta F = F_{k+1} - F_k = G\Delta U + (1-G)\Delta O.$$

This point efficiency, E , is the following with respect to a mean particle diameter for a particular size interval:

$$d_m = \frac{d_k + d_{k+1}}{2}. \quad (9)$$

Another technique used to calculate point efficiency⁹ is to use a cumulative relationship, such that with respect to a particle size, d_k , point efficiency is defined as

$$E'_k = \left(\frac{U_k}{F_k} \right) \left(\frac{C_u}{C_f} \right) \left(\frac{Q_u}{Q_f} \right). \quad (10)$$

Point efficiency is often corrected to take account of the liquid that is split between the overflow and underflow streams. The corrected point efficiency is described by the following equations:

$$\epsilon = \frac{E - Rf}{1 - Rf}, \quad (11)$$

and

$$\epsilon'_k = \frac{E'_k - Rf}{1 - Rf} \quad (12)$$

Typical results are given in Fig. 2, which relate point efficiency to particle diameter for a particular hydroclone and flow rate. The quality of separation can be predicted from the shape of this curve. A steep slope in Fig. 2 would correspond to a sharp separation.

The particle diameter that gives a point efficiency of 50%, d_{50} , has become a useful reference point for defining hydroclone efficiency. Utilizing the d_{50} concept and the validity of Stoke's Law,⁶ there have been two general attempts to correlate theoretically the efficiency of hydroclones. One approach considers equilibrium orbiting of various-sized particles at different radii; the other considers nonequilibrium conditions with separation dictated by residence time. The equilibrium orbit theory considers an orbit at which a particle is balanced between the centrifugal force and inward drag force. Bradley¹⁰ developed a theoretical correlation of efficiency by assuming that the particles find their equilibrium positions in the hydroclone core. The dimensionless form of the equation is expressed as

$$\frac{d_{50}^n n_c}{D_f^2} = \frac{3 (0.38)^n}{\alpha} \left[\frac{\mu D_c (1-Rf) \tan \frac{\theta}{2}}{Q_f (\sigma - \rho)} \right]^{0.5} \quad (13)$$

where α and n were factors dependent on cyclone design and fluid properties [see Eqs. (2) and (4)]. The factor, α , is also dependent on feed rate, Q_f .

ORNL DWG 77-871

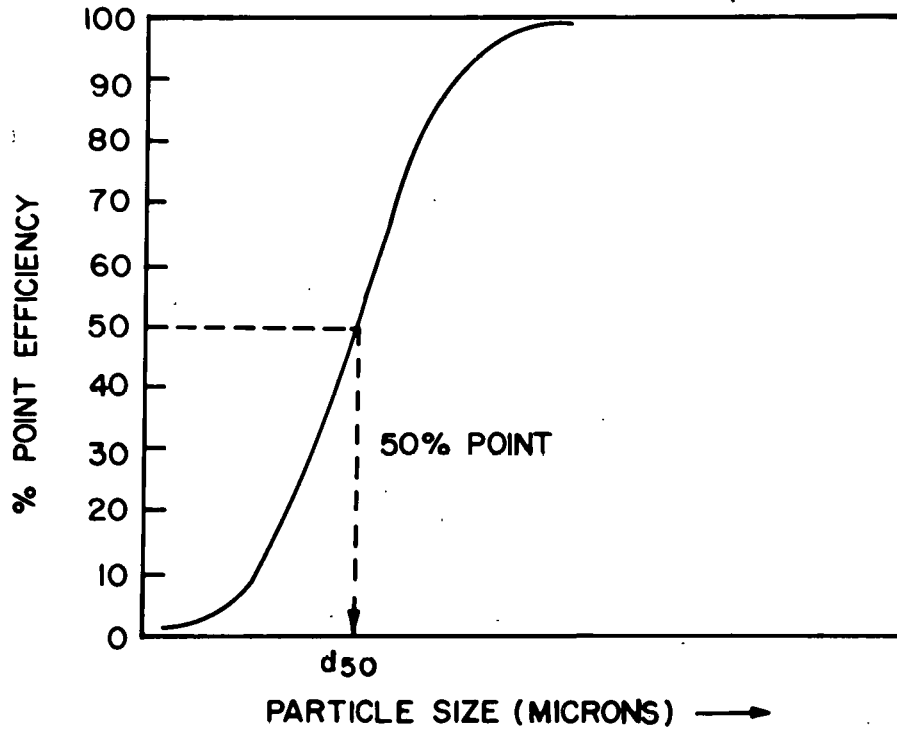


Fig. 2. Typical point efficiency curve.

The residence time theory¹¹ considers the time taken by a particle to travel from the inlet to the cyclone wall. This approach is similar to the theory used for gravity settling tanks. Interestingly, the theoretical correlations for hydroclone efficiency reduce to the form:

$$d_{50} = k_3 \left[\frac{D_c^3 \mu}{Q_f (\sigma - \rho)} \right]^{0.5} \quad (14)$$

Also, a graphical representation of efficiency by means of a "reduced efficiency curve" is obtained by plotting centrifugal efficiency versus the ratio of the particle size to d_{50} .¹² This normalized curve remains approximately constant for a particular hydroclone design and feed material over a range of operating conditions.

2.3 Volume Split or Flow Ratio

In phase separations, it is important to split the feed into the appropriate volumetric proportions. The terms to describe this aspect of hydroclone performance are the following:

$$\text{volume split, } S = \frac{Q_u}{Q_o} \quad (15)$$

and

$$\text{flow ratio, } Rf = \frac{Q_u}{Q_f} \quad (16)$$

Back pressure conditions at the overflow and underflow exits alter volume split data. Therefore, data for theoretical or empirical correlations are only applicable for free discharge or balanced back pressure

conditions (i.e., the same pressure at the overflow and underflow ports of the hydroclone). The empirical relationships developed in the literature⁶ conclude that the volume split for $S < 0.5$ can be expressed as

$$S = k_4 (D_u/D_o)^x Q_f^y, \quad (17)$$

where k_4 has a value of ~ 5 for Q_f in Imperial gallons per minute (I gal/min). The value of x ranges from 1.75 to 4.4, and y varies from -0.75 to -0.44. The first x and y limits are applicable to small-diameter hydroclones. For $S > 0.5$, however, the split is independent of flow rate. The theoretical relationships⁶ for the flow ratio are of the following form:

$$Rf = 1 - \frac{k_5}{1 + k_6 (D_u/D_o)^z}, \quad (18)$$

where constants k_5 and k_6 are both approximately unity, and z has a value of 3 to 4.

2.4 Operating Variables

The operating variables of interest in this study are solid density, liquid medium viscosity, and particle size. Specifically, the hydroclone performance was evaluated as a function of a small solid-liquid density difference, a relatively high liquid viscosity, and micron-sized particles. As explained in Sect. 2.2, with other conditions held constant, the smaller particle size yields a lower separation efficiency. From the d_{50} efficiency relationship shown in Eq. (14), which assumes Stokes'

Law, the d_{50} value is inversely proportional to the square root of the solid-liquid density difference. The Stokes' Law limit is reached at a particle Reynolds number of two; thus, in an intermediate particle N_{Re} range ($30 < N_{Re} < 300$), a better correlation for small-diameter hydroclones⁶ is

$$d_{50} \propto (\sigma - \rho)^{-0.62} \quad (19)$$

The d_{50} value is also related through the laws of motions to fluid viscosity by the following:

$$\text{Stokes' Law: } d_{50} \propto \mu^{0.5}, \quad (20)$$

$$\text{Intermediate Range: } d_{50} \propto \mu^{0.38} \quad (21)$$

Therefore, an increase in viscosity lowers the separation point efficiency and the gross efficiency.¹³ Also an increase in viscosity produces a higher flow rate at a given pressure drop.¹⁴ Bradley⁶ reports that although a viscosity term does not enter into the pressure drop relationship, an increase in viscosity causes a decrease in pressure drop for the same feed capacity. Increasing viscosity also increases the volume split or flow ratio.⁶ Bradley⁶ concluded that viscosity effects can be very significant, and hydroclones can become ineffective separation devices at viscosities >30 cP.

3. SMALL-DIAMETER HYDROCLONES

The hydroclone size required for a given application is defined by the particle size to be separated. Smaller-diameter hydroclones are

generally more efficient for removing smaller (e.g., micron-sized) particles. The smallest hydroclone available commercially has a 1-cm major diameter; hydroclones with smaller diameters have not improved separation efficiencies significantly.¹⁵ For commercial applications, such as in coal liquefaction processing, a type TMC Dorrclone is available with 1-cm-diam hydroclones in manifolds containing 60, 162, and 300 units. The hydroclones are arranged in parallel, thus for a 100 psig pressure differential, the TMC-300 unit has a maximum capacity of ~15,000 bbl/day.

Previous studies or applications with 0.4- to 4.0-cm diam hydroclones included (a) the recovery of catalysts from fluidized catalytic cracker distillation bottoms in petroleum refineries,¹⁶ (b) the removal of precipitated fission and corrosion products from uranyl sulfate solutions in an aqueous homogeneous nuclear reactor,¹⁵ (c) the separation of starch from gluten, and (d) the removal of fine particles from green liquor in the recausticizing steps of sulfate kraft mills.¹⁷ A summary of efficiency and pressure drop correlations for small-diameter hydroclones is shown in Table 1.

4. EXPERIMENTAL APPARATUS AND PROCEDURE

A schematic diagram of the system used to study hydroclones is shown in Fig. 3. Slurry from a 20-ℓ stirred tank was recirculated by a Moyno slurry pump through a hydroclone and returned to the feed tank. The hydroclone tested was a 1-cm Dorr-Oliver Doxic Type A (Fig. 4). Pressure gauges were located as close to the hydroclone inlet and outlets as possible.

Table 1. Small-diameter hydroclone efficiency and pressure-drop correlations

Source	Size of hydroclone (D_c , mm)	Equation	Units
<u>Theoretical</u>			
Bradley ^a	Any	$\frac{d_{50} D_c}{D_i^2} = \frac{3(0.38)^n}{\alpha} \left[\frac{\mu D_c (1-RF)}{Q_f (\sigma-\rho)} \tan \frac{\theta}{2} \right]^{0.5}$ $\frac{\Delta P / \rho}{V_i^{2/2}} = \frac{\alpha^2}{n} \left[\left(\frac{D_c}{D_o} \right)^{2n} - 1 \right]$	Dimensionless
<u>Empirical</u>			
Haas ^b	4.1 to 10.2	$d_{50} = 1.07 \times 10^3 \left[\frac{D_c^{3.05} \mu}{Q_f^{1.14} (\sigma-\rho)} \right]^{0.5}$ $\Delta P = \frac{0.07 Q_f^{2.27}}{D_c^{0.8} D_i^{1.5} D_o^{2.0}}$	d_{50} , μm , μ , lb/ft sec, Q_f , gal/min, σ , ρ , lb/ft ³ , D_c , D_i , D_o , in., ΔP , ft of fluid
Matschke and Dahlstrom ^c	10 to 40	$d_{50} = \frac{87.2 (D_o D_i)^{0.65}}{Q_f^{0.6}} \left[\frac{1}{\sigma-\rho} \right]^{0.5}$ <p>(water flow in 10° cyclone)</p> $\Delta P = \frac{0.021 Q_f^2}{(D_i D_c)^{1.8}}$	d_{50} , μm , σ , ρ , g/cc, D_o , D_c , D_i , in., Q_f , gal/min, ΔP , ft of fluid
Wagner and Murphy ^d	8.9 to 22.9	$d_{50} = \frac{99.6 (D_o D_i)^{0.68}}{Q_f^{0.53}} \left[\frac{\mu}{\sigma-\rho} \right]^{0.5}$ <p>(5° cyclone)</p> $\Delta P = \frac{0.004 Q_f^{2.07}}{(D_i D_c)^2} \left[\frac{\mu}{\rho} \right]^{n.4}$	d_{50} , μm , Q_f , gal/min, σ , ρ , g/cc, D_i , D_c , D_o , in., ΔP , ft of fluid, μ , cP, θ , degrees

^aEquations taken from refs. 6 and 10.^bEquations taken from ref. 15.^cEquations taken from refs. 10 and 17.^dEquations taken from ref. 18.

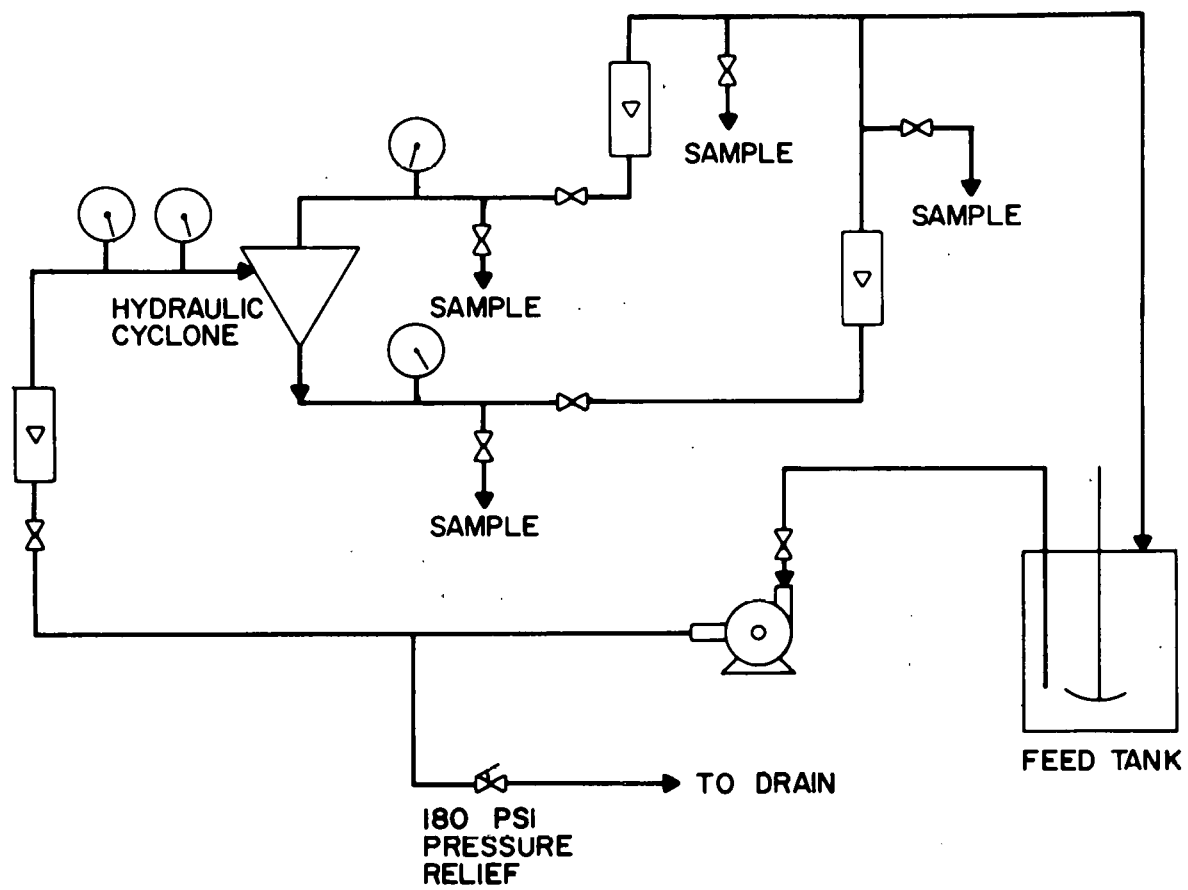


Fig. 3. System to study hydroclone performance.

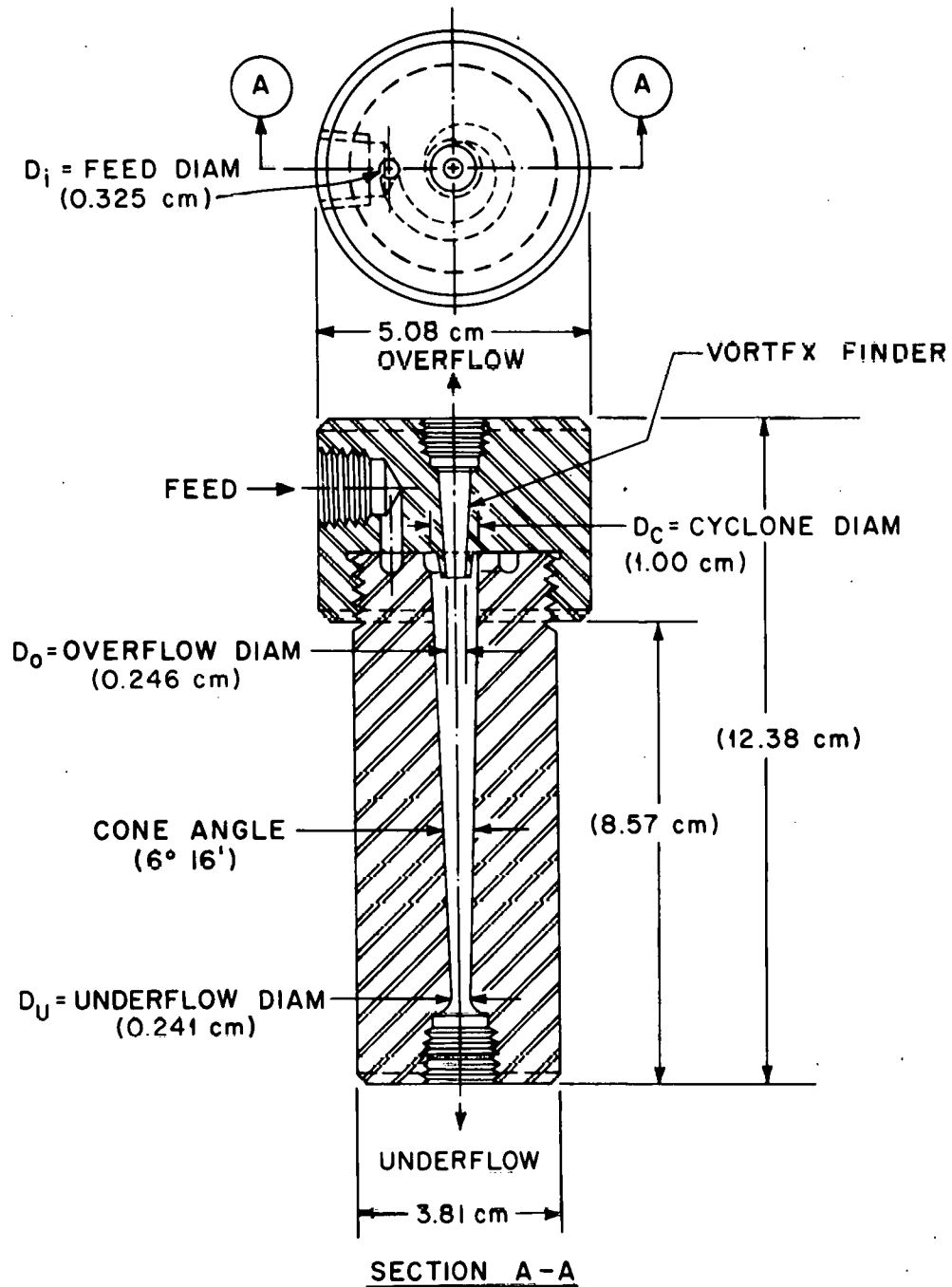


Fig. 4. Dorr-Oliver Doxie Type A (1-cm-diam) hydrocyclone.

A variety of solids were used to prepare a feed slurry of 5 wt % particles in water-glycerin solutions with viscosities ranging from 1 to 85 cP. The particles tested were aluminum oxide, Air Cleaner Test Dust,* fly ash, and kaolin. The aluminum oxide and fly ash were sieved through a 400-mesh screen (37 μm) using a Ro-Tap. The particle size distribution of the Test Dust, which is primarily SiO_2 and Al_2O_3 , is reported in Table 2.¹⁹

Table 2. Particle size distribution of Air Cleaner Test Dust

Size (μ)	Wt %
0-5	39 \pm 2
5-10	18 \pm 3
10-20	16 \pm 3
20-40	18 \pm 3
40-80	9 \pm 3

The kaolin particles are $<10 \mu\text{m}$ in diameter with ~ 70 wt % of the particles $<5 \mu\text{m}$. Particle densities and liquid viscosities were determined with a 50-cm^3 pycrometer and a Brookfield viscometer respectively.

To begin an experiment, solutions were prepared with the desired viscosity and solids concentration and then stirred until the solids were suspended. Next the pump was started with the flow rate and pressure

*Obtained from Keene Corporation, Fluid Handling Division, Cookeville, Tennessee.

drop controlled by the pump throttle. At a desired pressure drop, inlet, overflow, and underflow pressures were recorded. Underflow and overflow rates were measured with a graduated cylinder and stopwatch. Samples were taken of the overflow and underflow to determine the solids concentrations and particle size distributions. To measure solids concentration, the liquid from 10-cm³ aliquots were evaporated for ~4 hr on a hot plate at 400°C. Then the samples were dried further in an oven at 500°C. Also a Vitrin freeze drier was used to evaporate the liquid for some of the initial samples.²⁰ A photolemetric technique was used to measure the size distributions of small particles for slurries of kaolin in water-glycerin solutions with average viscosities of 1, 4.3, 10.7, 11.8, and 12.8 cP.

5. EXPERIMENTAL RESULTS AND PERFORMANCE CALCULATIONS

5.1 Test Data

Experiments to determine a relationship between pressure drop and both flow rate and viscosity were conducted with water-glycerin slurries containing solid particles of either test dust, fly ash, aluminum oxide, or kaolin. Preliminary measurements were made, however, using water only. These water capacity data are presented in Table 3. The inlet-to-overflow pressure drop varied from 17.0 to 102.3 psi in these runs. The test data for the runs with various slurries consist of pressure drop, feed liquid viscosity, overflow and underflow rate, and solids concentration in both the overflow and underflow streams. The data for slurries of aluminum oxide, test dust, and fly ash solids²⁰ are presented in the Appendix, along with the data for kaolin slurry experiments.

Table 3. Water capacity data

Run number	Pressure drop (psi)	Overflow rate (cm ³ /min)	Underflow rate (cm ³ /min)
1	17.0	871	768
2	23.8	984	893
3	33.1	1208	1018
4	43.0	1393	1109
5	56.6	1616	1204
6	74.8	1840	1461
7	96.8	1915	1745
8	115.3	2101	1828

Series of tests were run at varying liquid feed viscosities; each series was conducted at several different pressure drops. A summary of the test conditions are given in Table 4.

The density of the solids and the viscosity of the feed liquid were measured for each series of tests. The temperature of the feed solution and the measured values for the viscosities are given in the Appendix, with adjustments for any temperature change from the initial viscosity measurement. Liquid density was determined using the liquid viscosity at 25°C and literature data²¹ relating density, viscosity, and composition. Table 5 lists the solid and liquid density data at average values of viscosity. Also the solid-liquid density difference, $\sigma - \rho$, and a density ratio, $(\sigma - \rho)/\rho$, are given in Table 5.

The effect of solids content on the viscosity of the kaolin-glycerol solutions was also determined, since correlations in the literature indicate either liquid viscosity or viscosity of the total solution may be used in correlations of hydroclone performance. The results are tabulated in Table 6. The solids content has a pronounced effect on the viscosity of the kaolin mixtures, more than doubling the viscosity.

5.2 Hydroclone Performance Calculations

Performance data were calculated and are presented in Tables 7 and 8, using the operating data collected for the different test runs. The feed flow rate is the sum of the underflow and overflow rates. The solids concentration of the feed was calculated from the solids concentration and flow rate of the overflow and underflow streams. The volume split, S , flow ratio, R_f , and the dimensionless inlet Reynolds number

Table 4. Summary of test conditions

Type of solid	Viscosities investigated (cP)	Pressure drop range (psi)
Aluminum oxide	1.0	6.6-92.8
Test dust	1.0	6.8-54.2
	10.7	7.1-43.0
	33.0	15.5-45.5
	59.0	11.5-17.0
	85.0	8.5-18.8
Fly ash	1.0	7.4-34.5
	10.6	13.8-62.0
	35.0	11.2-35.0
Kaolin	1.0	13.6-97.7
	3.8	12.7-64.7
	4.3	12.8-66.6
	7.0	12.0-65.0
	10.7	34.0-65.3
	11.8	11.2-59.7
	12.8	12.0-35.2

Table 5. Solid and liquid density data

Type of solid	Solid density, σ (g/cm ³)	Liquid viscosity, μ (cP)	Liquid density, ^a $\rho(20)$ (g/cm ³)	$\sigma - \rho$ (g/cm ³)	$(\sigma - \rho) / \rho$
Test dust	2.64	1.0	1.00	1.54	1.54
		10.7	1.16	1.48	1.27
		33.0	1.20	1.44	1.20
		59.0	1.21	1.43	1.17
		85.0	1.22	1.42	1.16
Fly ash	2.28	1.0	1.00	1.28	1.28
		10.6	1.16	1.12	0.96
		35.0	1.20	1.08	0.90
Aluminum oxide	3.72	1.0	1.00	2.72	2.72
Kaolin	2.40	1.0	1.00	1.40	1.40
		3.8	1.11	1.29	1.16
		4.3	1.12	1.28	1.15
		7.0	1.14	1.26	1.10
		10.7	1.16	1.24	1.07
		11.8	1.17	1.23	1.06
		12.8	1.17	1.23	1.05

^aSp. gr. at 25/25°C from viscosity at 25°C.

Table 6. Effect of solids content on the viscosity of kaolin-water^a and kaolin-glycerol^b mixtures

Wt % solids	Viscosity (cP)
<u>Kaolin-water</u>	
0	0.99
1.98	1.30
4.97	1.57
9.20	2.41
<u>Kaolin-glycerol</u>	
0	6.50
2.00	6.83
5.00	7.82
10.0	14.26

^aDeterminations made at 23.2°C.

^bDeterminations made at 23.6°C.

Table 7. Performance results for water capacity tests

Run number	Pressure drop (psi)	Feed flow rate (cm ³ /min)	Split ^a	Rf ^b	Inlet Reynolds number	Euler number
1	17.0	1639	0.8817	0.4686	10,700	10.8
2	23.8	1877	0.9075	0.4758	12,246	11.6
3	33.1	2226	0.8427	0.4573	14,500	11.5
4	43.0	2502	0.7961	0.4432	16,400	11.8
5	56.5	2820	0.7450	0.4270	18,400	12.1
6	74.3	3301	0.7940	0.4426	21,500	11.7
7	95.8	3660	0.9112	0.4768	23,900	12.3
8	115.5	3929	0.8701	0.4653	25,700	12.8

$${}^a\text{Split} = \frac{\text{underflow rate}}{\text{overflow rate}}$$

$${}^b\text{Rf} = \frac{\text{underflow rate}}{\text{feed flow rate}}$$

Table 8. Performance results for slurry tests

Run number	Average viscosity (cP)	Pressure drop (psi)	Feed flow rate (cm ³ /min)	Solids in feed (g/cm ³)	Split ^a	R _F ^b	Gross efficiency	Overall centrifugal efficiency	Inlet Reynolds number	Euler number
<u>Aluminum Oxide Particles</u>										
1	1.0	6.6	1240		0.771	0.4355			8,090	7.3
2		21.2	2185		1.005	0.5011			14,300	7.6
3		37.0	2685		1.174	0.5400			17,500	8.8
4		62.7	3570		1.217	0.5490			23,300	8.4
5		74.8	3967		1.334	0.5715			25,900	8.1
6		92.8	4437		1.507	0.6011			29,000	8.0
<u>Test Dust Particles</u>										
18	1.0	6.8	1200	0.0449	1.182	0.5417	0.831	0.630	7,840	8.0
19		10.0	1490	0.0465	1.191	0.5436	0.859	0.690	9,730	7.7
20		17.7	2050	0.0450	1.384	0.5805	0.860	0.665	13,400	7.2
21		22.0	2200	0.0455	1.444	0.5909	0.881	0.710	14,400	7.8
22		27.0	2360	0.0434	1.408	0.5847	0.877	0.705	15,400	8.3
23		39.7	2890	0.0420	1.535	0.6055	0.891	0.723	18,900	8.1
24		46.5	3100	0.0483	1.541	0.6065	0.910	0.772	20,200	8.3
25		54.2	3300	0.0406	1.539	0.6061	0.895	0.734	21,500	8.5
26		29.7	2370	0.0418	1.495	0.5992	0.877	0.693	15,500	9.0
27		35.5	2640	0.0461	1.640	0.6212	0.899	0.733	17,200	8.7
35	10.7	7.1	1080	0.0583	0.742	0.4259	0.476	0.0868	659	10.4
36		11.2	1640	0.0612	0.952	0.4878	0.590	0.200	1,000	7.1
37		15.0	1940	0.0601	1.064	0.5155	0.637	0.250	1,180	6.8
38		20.4	2290	0.0617	1.267	0.5590	0.697	0.313	1,400	6.6
39		25.5	2600	0.0487	1.281	0.5615	0.646	0.192	1,590	6.4
40		31.2	2860		1.344	0.5734			1,750	6.5
41		36.8	3120		1.328	0.5705			1,900	6.5
42		43.0	3400		1.297	0.5647			2,070	6.4
45	33.0	22.2	1550	0.0601	2.100	0.6774	0.674	-0.0108	307	15.8
46		15.5	1280	0.0562	1.909	0.6563	0.671	0.0432	253	16.2
47		19.8	1440	0.0570	2.600	0.7222	0.732	0.0342	285	16.3
48		27.0	1770	0.0578	2.933	0.7458	0.763	0.0666	350	14.7
49		30.5	1890	0.0580	2.938	0.7460	0.766	0.0787	374	14.6
50		35.5	2210	0.0590	3.018	0.7511	0.775	0.0944	437	12.4
51		41.5	2330	0.0605	3.481	0.7768	0.816	0.175	461	13.1
52		45.5	2510	0.0602	3.482	0.7769	0.813	0.160	497	12.3
60	59.0	11.5	1230	0.0614	0.6622	0.3984	0.406	0.0123	136	13.0
61		15.1	1560	0.0628	0.7333	0.4231	0.437	0.0245	177	10.6
62		17.0	1590	0.0620	0.8068	0.4465	0.457	0.0186	176	11.5
63		14.0	1460	0.0609	0.7381	0.4247	0.433	0.0148	162	11.3
11	85.0	11.8	1210	0.0465	0.6133	0.3802	0.382	0.0025	92.9	13.8
12		14.9	1660	0.0452	0.6934	0.4096	0.386	-0.0403	128	9.2
13		18.8	1940	0.0451	0.7168	0.4175	0.424	0.0117	149	8.5
14		17.5	1750	0.0527	0.7677	0.4343	0.448	0.0236	134	9.8
15		8.5	960	0.0556	0.8462	0.4583	0.450	-0.0153	73.7	15.6
16		10.5	1210	0.0530	0.8333	0.4545	0.457	0.0053	92.9	12.2
17		14.5	1530	0.0531	0.8888	0.4706	0.490	0.0365	118	10.6

Table 8 (continued)

Run number	Average viscosity (cP)	Pressure drop (psi)	Feed flow rate (cm ³ /min)	Solids in feed (g/cm ³)	Split ^a	Rf ^b	Gross efficiency	Overall centrifugal efficiency	Inlet Reynolds number	Euler number
<u>Fly-Ash Particles</u>										
28	1.0	7.4	1190	0.0267	1.245	0.5546	0.904	0.785	7,770	8.9
29		11.2	1520	0.0447	1.171	0.5395	0.957	0.906	9,920	8.3
30		14.1	1790	0.0478	1.295	0.5642	0.939	0.862	11,700	7.5
31		18.6	1970	0.0486	1.558	0.6091	0.960	0.898	12,900	8.2
32		24.1	2150	0.0450	1.500	0.6000	0.974	0.936	14,000	8.9
33		28.5	2370	0.0413	1.279	0.5612	0.976	0.945	15,500	8.7
34		34.5	2690	0.0455	1.612	0.6171	0.974	0.933	17,600	8.1
64	10.6	13.8	1190	0.0575	0.9833	0.4958	0.521	0.0490	733	16.6
65		18.5	1490	0.0581	0.9605	0.4899	0.540	0.0983	918	14.2
66		26.0	1720	0.0576	1.000	0.5000	0.562	0.124	1,060	15.0
67		32.0	1930	0.0574	1.218	0.5492	0.624	0.166	1,190	14.7
68		39.0	2110	0.0573	1.269	0.5592	0.647	0.199	1,300	15.0
69		43.7	2260	0.0569	1.283	0.5619	0.667	0.240	1,390	14.6
70		48.3	2440	0.0563	1.302	0.5656	0.692	0.292	1,500	13.9
71		55.2	2600	0.0554	1.321	0.5692	0.702	0.307	1,600	14.0
72		62.0	2820	0.0564	1.350	0.5745	0.729	0.362	1,740	13.9
53	35.0	11.2	1220		0.6944	0.4098			228	12.9
54		14.0	1480		0.7619	0.4324			276	10.9
55		18.0	1800	0.0596	0.8000	0.4444	0.439	-0.0098	336	9.5
56		23.5	2100	0.0611	0.8421	0.4571	0.462	0.0088	392	9.1
57		27.0	2280	0.0599	0.8387	0.4561	0.477	0.0375	425	8.9
58		31.8	2430	0.0564	0.8550	0.4609	0.497	0.0664	453	9.2
59		35.0	2530		1.008	0.5020			472	9.3
<u>Kaolin Particles</u>										
1	1.0	13.6	1617	0.0425	1.156	0.5362	0.701	0.355	10,600	8.9
2		18.0	1742	0.0413	1.219	0.5493	0.735	0.412	11,400	10.1
3		23.0	2002	0.0417	1.181	0.5415	0.733	0.418	13,100	9.8
4		27.8	2160	0.0410	1.143	0.5333	0.746	0.456	14,100	10.2
5		33.8	2357	0.0422	1.149	0.5346	0.754	0.472	15,400	10.4
6		37.5	2543	0.0418	1.157	0.5364	0.764	0.491	16,600	9.9
7		47.5	2823	0.0423	1.076	0.5182	0.769	0.520	18,400	10.2
8		57.8	3237	0.0417	1.062	0.5150	0.789	0.564	21,100	9.4
9		67.5	3633	0.0447	1.205	0.5464	0.819	0.600	23,700	8.7
10		77.5	3810	0.0444	1.159	0.5367	0.810	0.590	24,900	9.1
11		87.3	3944	0.0433	1.104	0.5246	0.799	0.578	25,800	9.6
12		97.7	4149	0.0416	1.167	0.5384	0.802	0.570	27,100	9.7
13	3.8	12.7	1800	0.0321	1.196	0.5446	0.627	0.181	3,130	6.7
14		17.3	2005	0.0369	1.193	0.5440	0.589	0.100	3,490	7.3
15		22.1	2278	0.0498	1.228	0.5512	0.603	0.116	3,970	7.3
16		27.0	2562	0.0433	1.205	0.5464	0.601	0.120	4,460	7.0
17		31.7	2654	0.0452	1.202	0.5460	0.616	0.154	4,620	7.7
18		36.4	2843	0.0502	1.144	0.5335	0.595	0.132	4,950	7.7
19		41.6	3033	0.0510	1.187	0.5428	0.602	0.130	5,280	7.2

Table 8 (continued)

Run number	Average viscosity (cP)	Pressure drop (psi)	Feed flow rate (cm ³ /min)	Solids in feed (g/cm ³)	Split ^a	Rf ^b	Gross efficiency	Overall centrifugal efficiency	Inlet Reynolds number	Euler number
<u>Kaolin Particles</u>										
20		46.4	3235	0.0529	1.242	0.5540	0.616	0.139	5,630	7.6
21		51.2	3392	0.0535	1.172	0.5396	0.603	0.138	5,910	7.6
22		56.2	3526	0.0506	1.157	0.5363	0.588	0.112	6,140	7.7
23		61.0	3737	0.0447	1.159	0.5369	0.563	0.0553	6,510	7.5
24		64.7	3847	0.0480	1.132	0.5309	0.578	0.0996	6,700	7.5
37	4.3	12.8	1725	0.0169	1.226	0.5508	0.623	0.160	2,500	7.3
38		17.6	2059	0.0142	1.264	0.5583	c		2,990	7.1
39		22.3	2269	0.0190	1.268	0.5590	0.628	0.156	3,370	7.4
40		27.0	2565	0.0180	1.256	0.5566	c		3,850	7.0
41		31.8	2733	0.0204	1.243	0.5542	0.639	0.190	4,150	7.3
42		36.6	2850	0.0219	1.238	0.5531	0.642	0.200	4,430	7.7
43		41.2	3042	0.0237	1.251	0.5558	0.651	0.214	4,730	7.6
44		46.5	3211	0.0233	1.253	0.5562	0.653	0.218	4,990	7.7
45		51.5	3393	0.0236	1.262	0.5579	0.657	0.225	5,210	7.6
46		56.7	3536	0.0243	1.251	0.5558	0.666	0.247	5,500	7.7
47		61.0	3683	0.0249	1.294	0.5542	0.664	0.229	5,870	7.7
48		66.6	3761	0.0250	1.248	0.5551	0.671	0.260	5,920	8.0
25	7.0	12.0	1674	0.0437	0.8976	0.4730	0.481	0.0152	1,560	7.3
26		16.7	1930	0.0432	0.9300	0.4819	0.496	0.0268	1,800	7.7
27		21.3	2241	0.0473	0.9723	0.4930	0.502	0.0177	2,090	7.2
28		26.0	2368	0.0483	0.9541	0.4883	0.499	0.0223	2,210	7.9
29		30.7	2681	0.0495	1.068	0.5165	0.537	0.0418	2,500	7.3
30		35.4	2921	0.0514	1.107	0.5254	0.544	0.0398	2,720	7.1
31		40.6	3143	0.0552	1.083	0.5198	0.540	0.0414	2,930	7.0
32		45.5	3294	0.0543	1.158	0.5367	0.552	0.0336	3,070	7.2
33		50.3	3539	0.0536	1.147	0.5343	0.555	0.0449	3,300	6.9
34		55.7	3717	0.0539	1.214	0.5484	0.555	0.0153	3,470	6.9
35		60.2	3818	0.0564	1.197	0.5448	0.582	0.0812	3,560	7.0
36		65.0	3942	0.0545	1.226	0.5507	0.584	0.0748	3,680	7.2
54	10.7	34.0	2930	0.0555	0.9415	0.4849	0.485	0.0009	1,700	6.8
55		38.7	3139	0.0562	0.9955	0.4989	0.512	0.0266	1,850	6.7
56		43.7	3197	0.0574	1.030	0.5073	0.516	0.0168	1,910	7.3
57		48.7	3453	0.0585	1.055	0.5135	0.525	0.0237	2,100	7.0
58		53.8	3636	0.0596	1.069	0.5166	0.529	0.0260	2,260	7.0
59		58.4	3722	0.0585	1.145	0.5338	0.546	0.0256	2,380	7.2
60		64.0	3820	0.0605	1.145	0.5338	0.555	0.0450	2,480	7.5
72		65.3	4083	0.0463	1.221	0.5497	0.593	0.0950	2,400	6.7
49	11.8	11.2	1652	0.0421	0.8509	0.4597	0.463	0.0055	899	7.0
50		15.8	1893	0.0439	0.8676	0.4646	0.471	0.0116	1,030	7.5
51		20.1	2210	0.0474	0.9439	0.4856	0.492	0.0123	1,230	7.0
52		24.9	2426	0.0492	0.9390	0.4843	0.489	0.0098	1,400	7.2
53		29.4	2687	0.0522	0.9159	0.4781	0.487	0.0174	1,550	7.0
67		40.0	3113	0.0405	1.209	0.5472	0.581	0.0743	1,660	7.1
68		44.3	3242	0.0418	1.193	0.5440	0.582	0.0833	1,760	7.2
69		50.4	3453	0.0428	1.206	0.5468	0.587	0.0894	1,880	7.2
70		55.4	3678	0.0448	1.323	0.5695	0.607	0.0865	2,020	7.0
71		59.7	3926	0.0453	1.259	0.5574	0.591	0.0751	2,190	6.6

Table 8 (continued)

Run number	Average viscosity (cP)	Pressure drop (psi)	Feed flow rate (cm ³ /min)	Solids in feed (g/cm ³)	Split ^a	Rf ^b	Gross efficiency	Overall centrifugal efficiency	Inlet Reynolds number	Euler number
<u>Kaolin Particles</u>										
61	12.8	12.0	1680	0.0259	0.9304	0.4820	0.497	0.0298	828	7.3
62		16.5	2018	0.0289	0.9442	0.4857	0.506	0.0404	1,010	6.9
63		21.0	2251	0.0316	1.005	0.5012	0.524	0.0461	1,130	7.1
64		25.7	2440	0.0343	1.044	0.5108	0.538	0.0565	1,230	7.4
65		30.5	2622	0.0370	1.134	0.5314	0.566	0.0748	1,340	7.6
66		35.2	2974	0.0396	1.185	0.5424	0.581	0.0850	1,550	6.8

$$^a_{\text{Split}} = \frac{\text{underflow rate}}{\text{overflow rate}}$$

$$^b_{\text{Rf}} = \frac{\text{underflow rate}}{\text{feed rate}}$$

^cCalculated values inconsistent.

and Euler number were calculated to correlate performance criteria. Gross efficiency and overall centrifugal efficiency were determined for tests where solids concentrations were measured.

5.3 Particle-Size-Distribution Data and Point Efficiencies

Particle size distributions were determined for the kaolin-slurries with average viscosities of 1.0, 4.3, 10.7, 11.8, and 12.8 cP. The particle size distributions for the overflow and underflow streams were measured, and the particle size distribution in the feed was calculated from these data on the outlet streams. Figure 5 shows typical size distributions for the slurry feed, overflow, and underflow streams of a kaolin-aqueous solution with a liquid viscosity of 1 cP. The slurry feed contains 40 wt % particles $<3 \mu\text{m}$ in diameter. The overflow and underflow streams contained respective 98 and 13 wt % particles $<3 \mu\text{m}$ in diameter when the pressure drop was 87.3 psi.

The effect of viscosity on the particle-size-distribution curves is shown in Figs. 6 and 7. Figure 6 shows the overflow particle-size-distribution curves for three runs at an average pressure drop of 28.1 psi for liquid viscosities of 1, 4.4, and 11.4 cP. As viscosity increases, the curve shifts to the right, indicating that larger size particles are not being separated as effectively. The particle diameters corresponding to <50 wt % removed in the 1, 4.4, and 11.4 cP viscosity runs are 1.88, 2.04, and $3.20 \mu\text{m}$ respectively. Figure 7 also shows the shift of the overflow particle-size-distribution curves with increasing viscosity at a higher average pressure drop, 66.0 psi. The corresponding particle diameters where <50 wt % are removed at fluid viscosities of

ORNL-DWG 78-5376 R

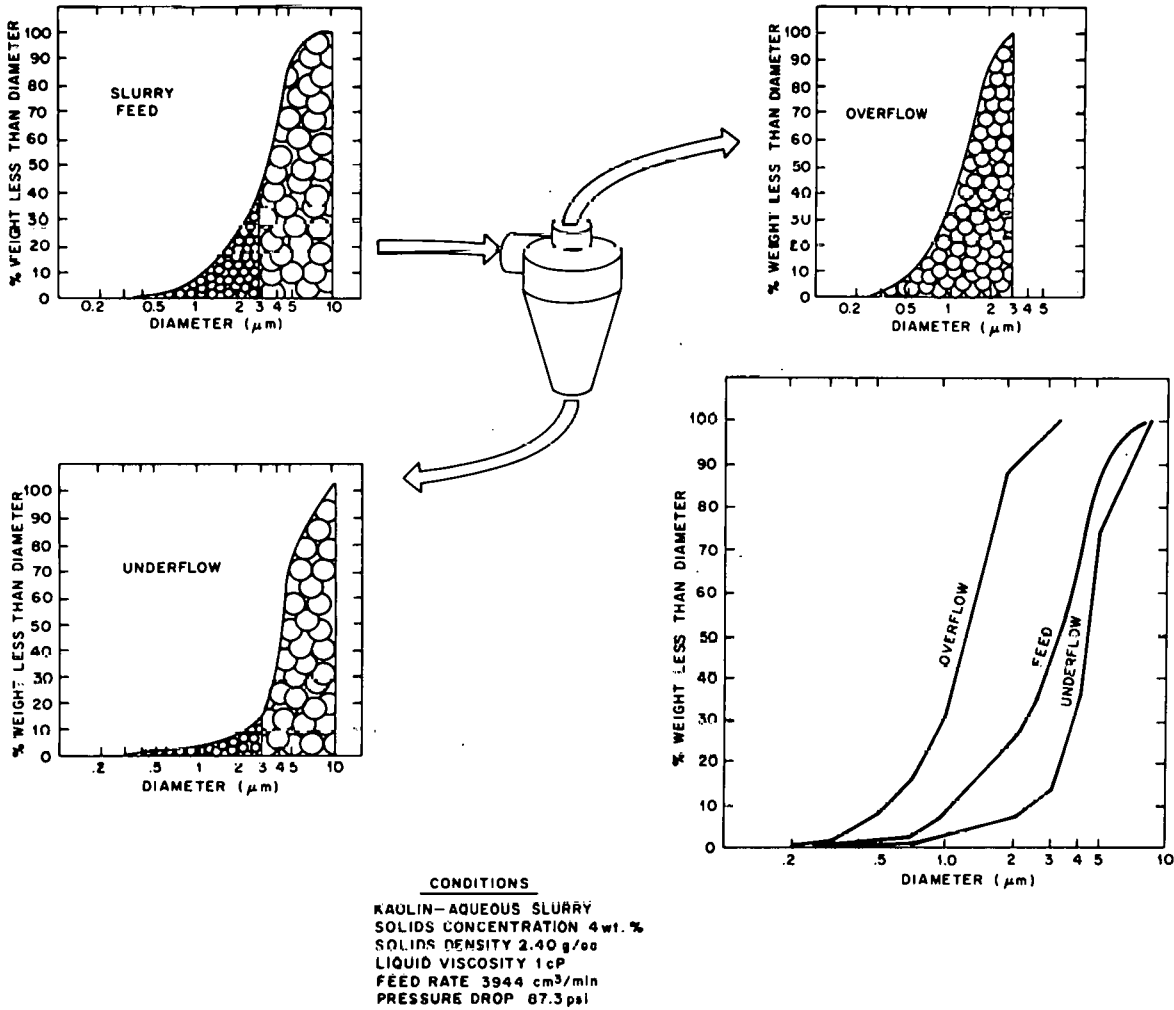


Fig. 5. Typical size distribution curves for kaolin-aqueous solution.

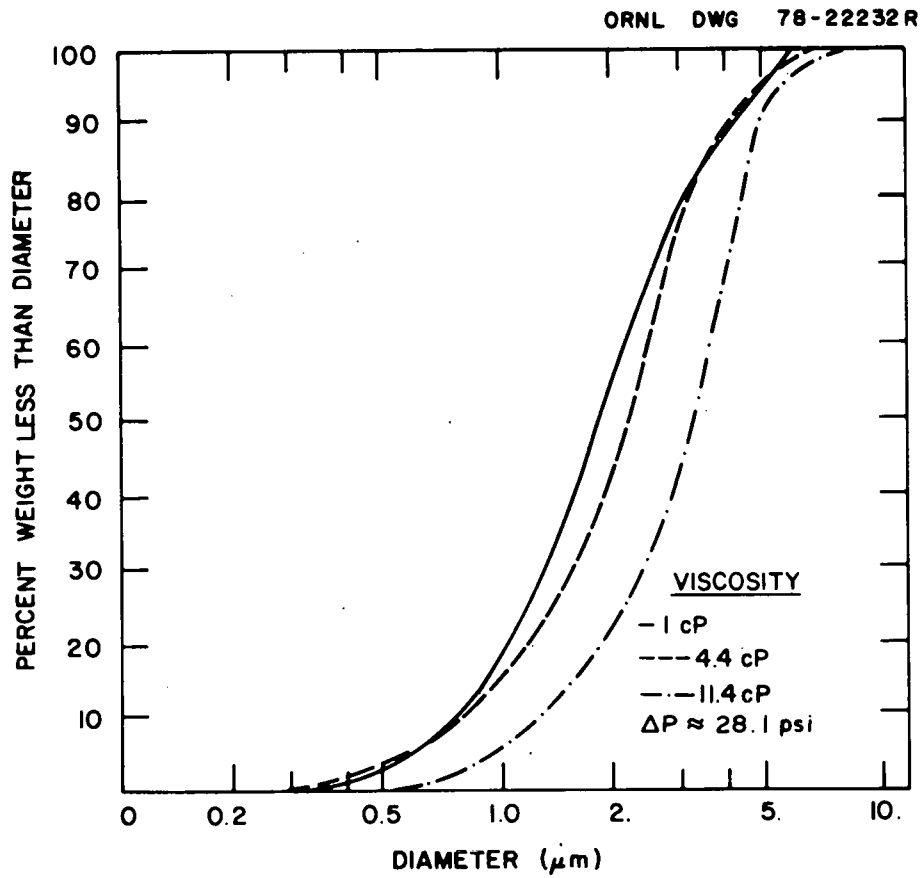


Fig. 6. The effect of viscosity on the overflow particle-size-distribution curve for $\Delta P \approx 28.1 \text{ psi}$.

ORNL DWG 78-22231

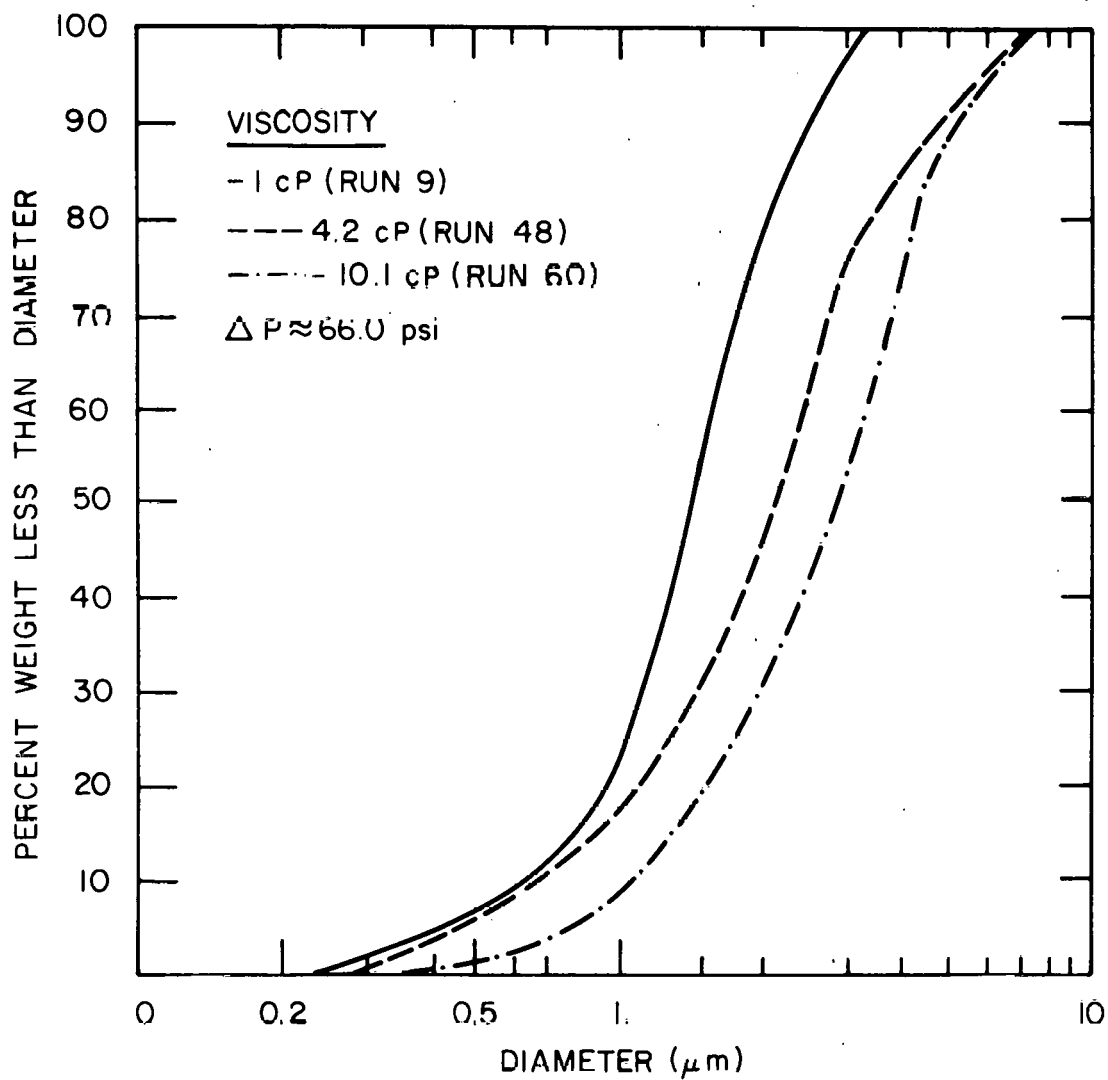


Fig. 7. The effect of viscosity on the overflow particle-size-distribution curve for $\Delta P \approx 66.0$ psi.

1, 4.2, and 10.1 cP are 1.39, 2.20, and 3.30 μm respectively. The increase in pressure drop (and flow rate) produced a steeper size-distribution curve for the 1 cP run. However, the increase in pressure drop did not improve the separation for the higher viscosities.

An increasing pressure drop has a pronounced effect on the particle-size-distribution curve at a viscosity of 1 cP. As the pressure drop increased from 18.0 to 87.3 psi in Fig. 8, the overflow particle-size-distribution curve for the 1 cP viscosity runs shifted to the left, increasing the pressure drop improved the separation of solids. A similar effect, but to a lesser degree, is seen in the curve for the 4.0 cP viscosity runs. At the higher viscosity of 11.8 cP, this trend reverses, and the shift of the particle-size-distribution curves is to the right (the extent of separation diminishes), with increasing pressure drop.

Another indication that hydroclone performance decreases with increasing viscosity is that the particle-size-distribution curves for the overflow and underflow fluids come closer together. Figure 9 shows a plot of the particle size distribution in the overflow vs the distribution in the underflow at equal particle diameters, and at an average pressure drop of 28.1 psi and viscosities of 1, 4.4, and 11.4 cP. The dashed line, with a slope of 1, would occur if the overflow and underflow size distributions were identical. The curves in Fig. 9 are drawn to identify the trend of the data. The 1 cP data are the most distant from the dashed line; increasing viscosity causes the overflow and underflow size-distribution curves to become more similar.

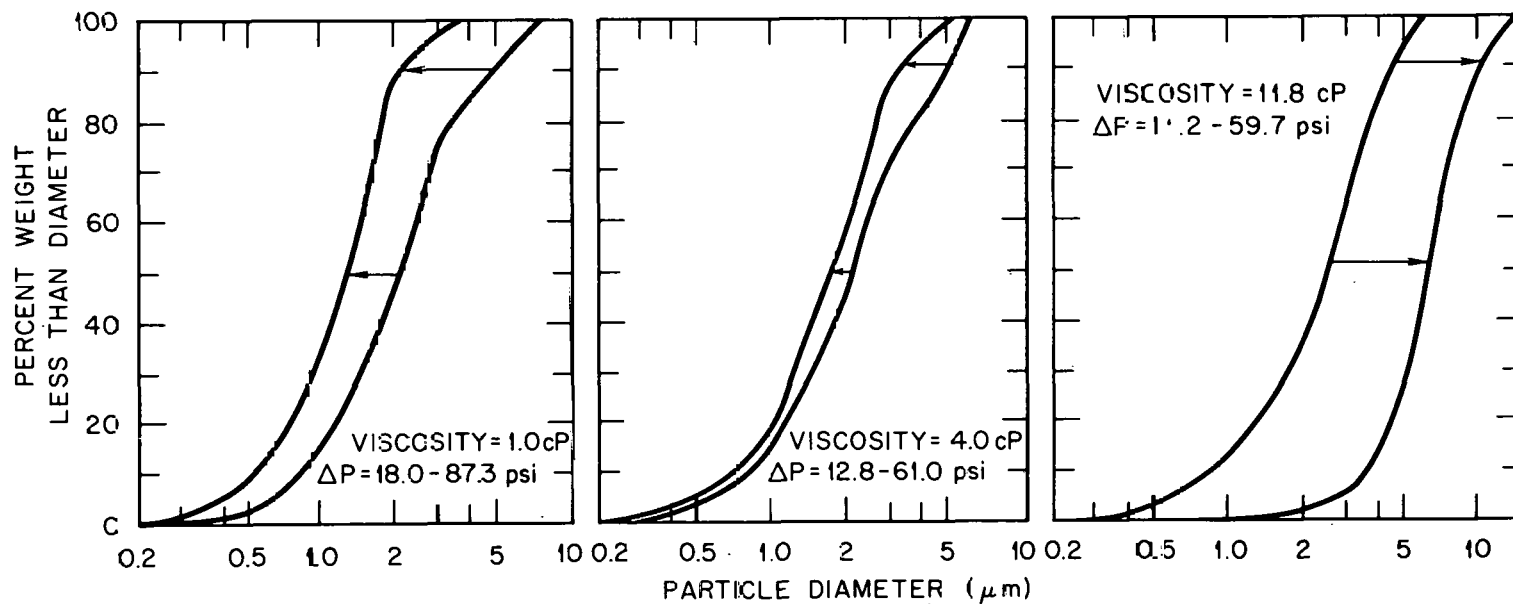


Fig. 8. The effect of pressure drop on overflow particle-size-distribution curves at viscosity of 1.0, 4.0, and 11.8 cP.

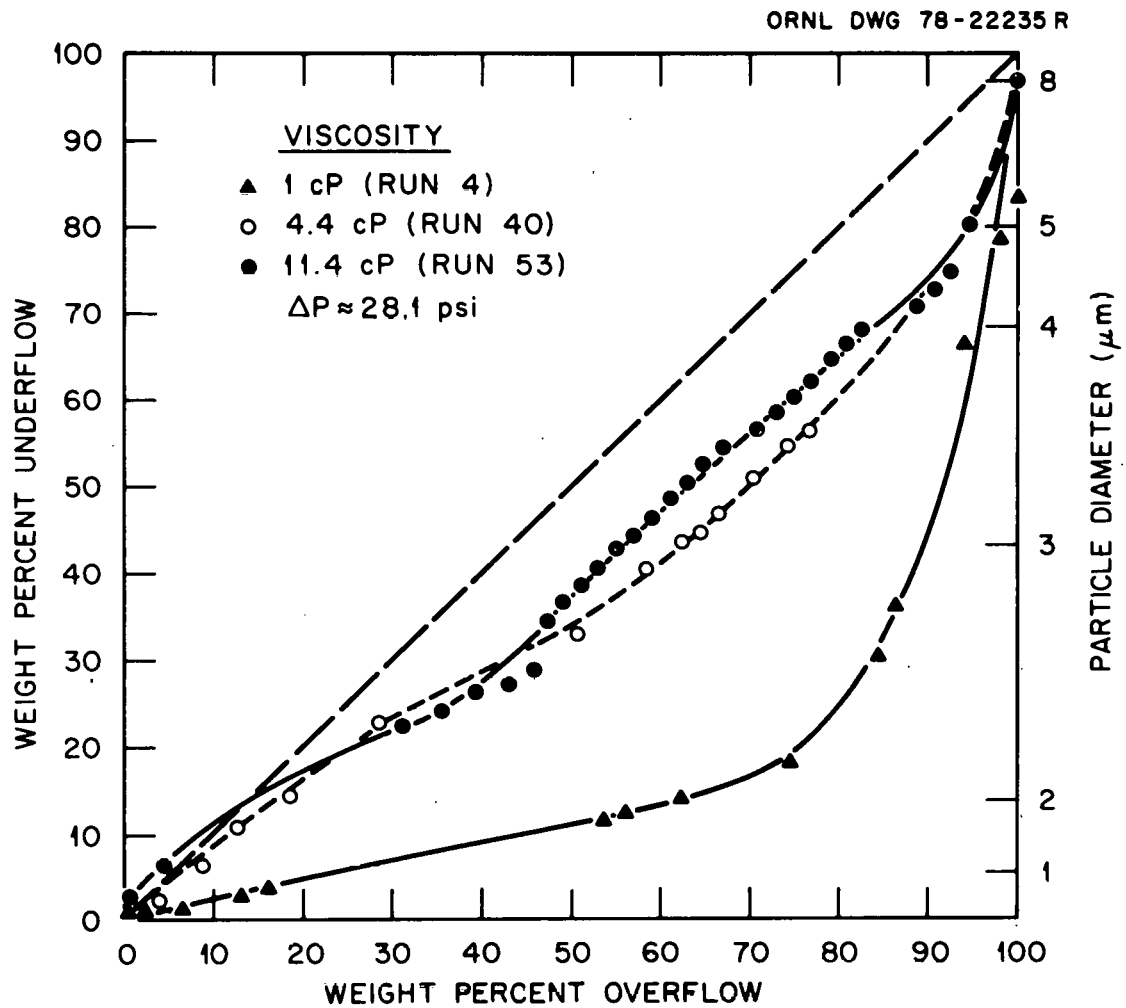


Fig. 9. The effect of viscosity on the variation in overflow and underflow particle-size-distribution curves for $\Delta P \approx 28.1$ psi.

Point efficiencies are calculated from the particle size analyses and operating data using Eqs. (8) and (10). The point efficiency data are plotted as a function of the appropriate particle diameters, as in Fig. 10. The point efficiencies determined from the differential relationship shown in Eq. (8) are greater than the efficiencies calculated by the cumulative method indicated in Eq. (10). The d_{50} value would be interpolated for each curve. Since the overflow and underflow size analyses were nearly identical for the high viscosity runs, the point efficiency data exhibited more variation with increasing viscosity. Therefore, d_{50} values could be interpolated from only a few of the runs. Table 9 lists the particle diameters corresponding to a point efficiency of 50%; d_{50} and d'_{50} denote the values interpolated from calculations using definitions for point efficiencies given in Eqs. (8) and (10) respectively.

A reduced efficiency correlation,⁵ which remains fairly constant for a range of operating variables, has been used to characterize a particular hydroclone operation. A reduced efficiency curve is obtained by plotting point efficiency vs a normalized particle size. The particle size is normalized by the d_{50} (or d'_{50}) value. Figure 11 shows reduced efficiency curves for both differential and cumulative point efficiency calculations.

5.4 Hydroclone Attrition

The same 1-cm diam Dorr-Oliver "Doxie" hydroclone was used for all experiments. Upon completion of the performance experiments, measurements of the hydroclone internal dimensions were repeated to determine the

ORNL-DWG 78-17912

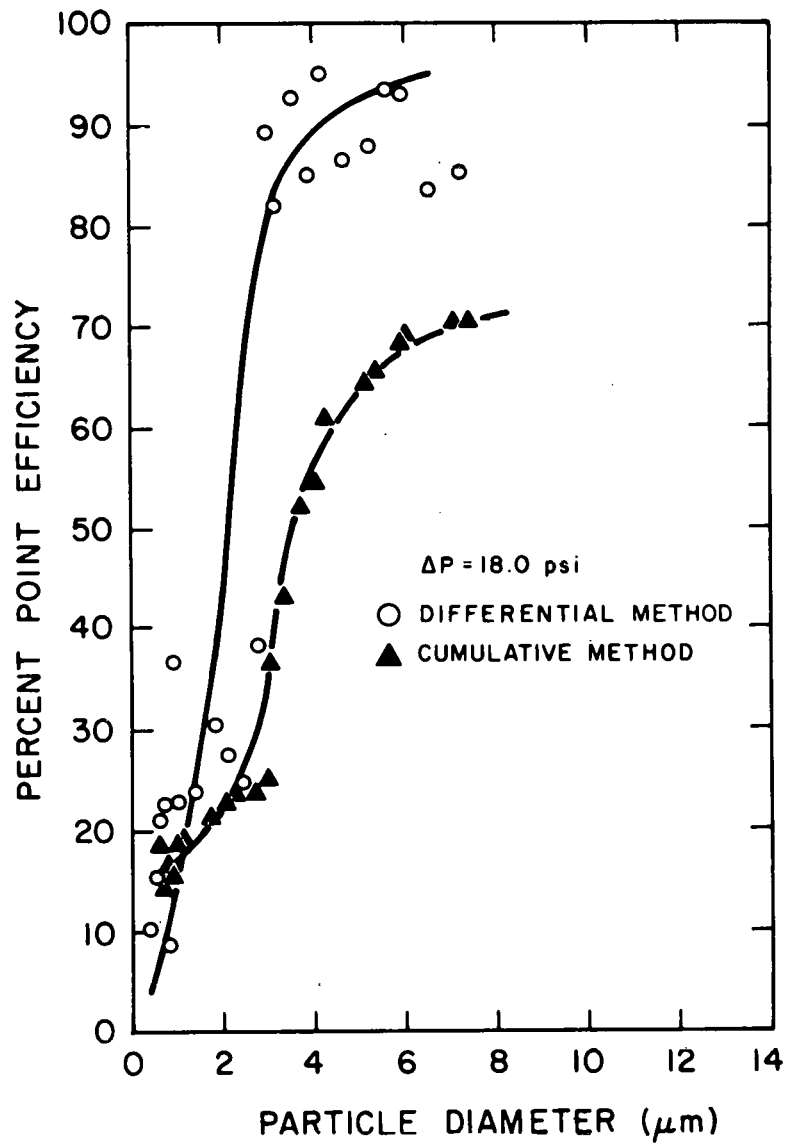


Fig. 10. Point efficiency curves for differential and cumulative methods for $\Delta P = 18.0$ psi.

Table 9. Particle diameters corresponding
to a point efficiency of 50%

Run number	Viscosity (cP)	Interpolated from values calculated by:	
		Equation (8) d_{50}	Equation (10) d'_{50}
2	1.0	2.2	3.5
3	1.0	2.3	3.4
4	1.0	1.9	3.3
5	1.0	2.4	4.5
6	1.0	2.1	4.8
9	1.0	1.3	-
11	1.0	1.3	3.5
12	1.0	2.3	3.0
37	4.5	1.9	-
42	4.2	1.8	3.4
43	4.2	1.8	-
56	10.9	3.8	-
58	10.5	3.0	-
59	10.2	2.6	-
60	10.1	3.1	-

ORNL-DWG 78-17913

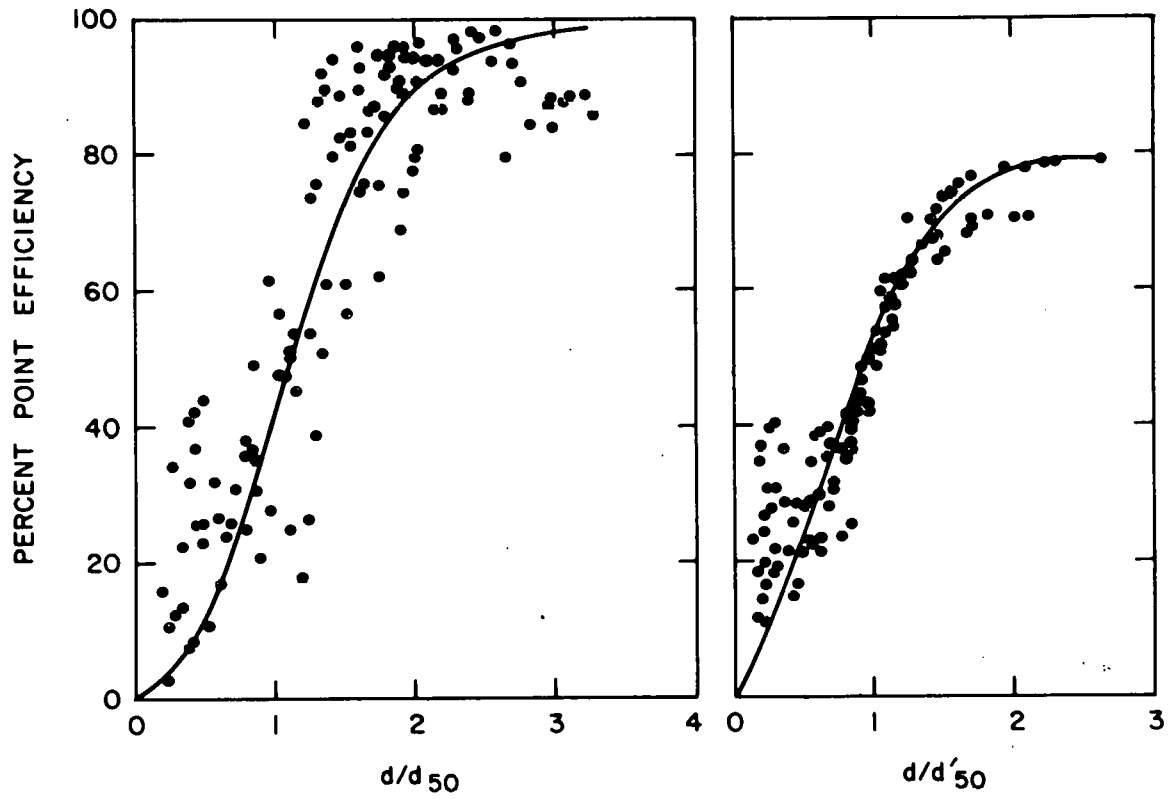


Fig. 11. Reduced efficiency curves for differential and cumulative methods.

effect of the abrasive solid particles in the slurry feed. The original and final dimensions of the cyclone, overflow, and underflow diameters are given in Table 10.

Table 10. Hydroclone dimensions

	Initial	Final	% change
Cyclone diameter, cm	1.006	1.024	1.8
Overflow diameter, cm	0.246	0.240	-2.4
Underflow diameter, cm	0.241	0.268	11.2

6. CORRELATION OF DATA AND DISCUSSION OF RESULTS

6.1 Pressure Drop as a Function of Flow Rate and Viscosity

A plot of inlet-to-overflow pressure drop, ΔP , as a function of feed flow rate, Q_f , at various viscosities is shown in Fig. 12 for fly ash. Similar plots for test dust and kaolin are shown in Figs. 13 and 14. As expected, pressure drop increases with increasing flow rate. The data for each viscosity experiment are linear on a log-log scale. The data for each viscosity with the solid particles studied were fit to an equation of the form

$$\Delta P = a Q_f^b \quad (22)$$

The regression coefficients for Eq. (22), a and b , are given in Table 11.

The experiments performed with fly ash and test dust were conducted over a wide range of viscosities. As seen from Figs. 12 and 13 and from Table 11, the viscosity of the fluid has a pronounced effect on the

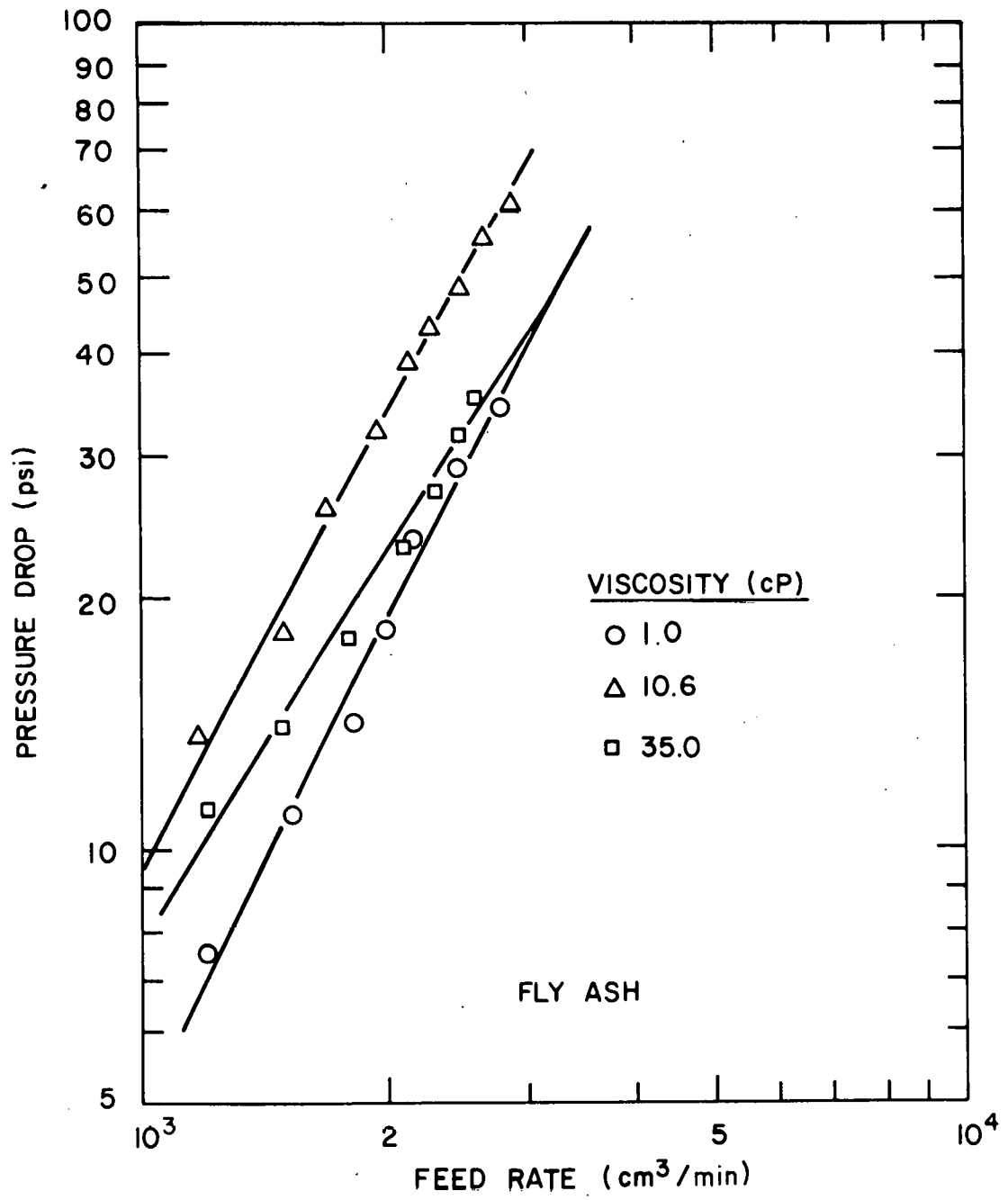


Fig. 12. Pressure drop as a function of feed rate for fly-ash slurries.

ORNL DWG 78-22240

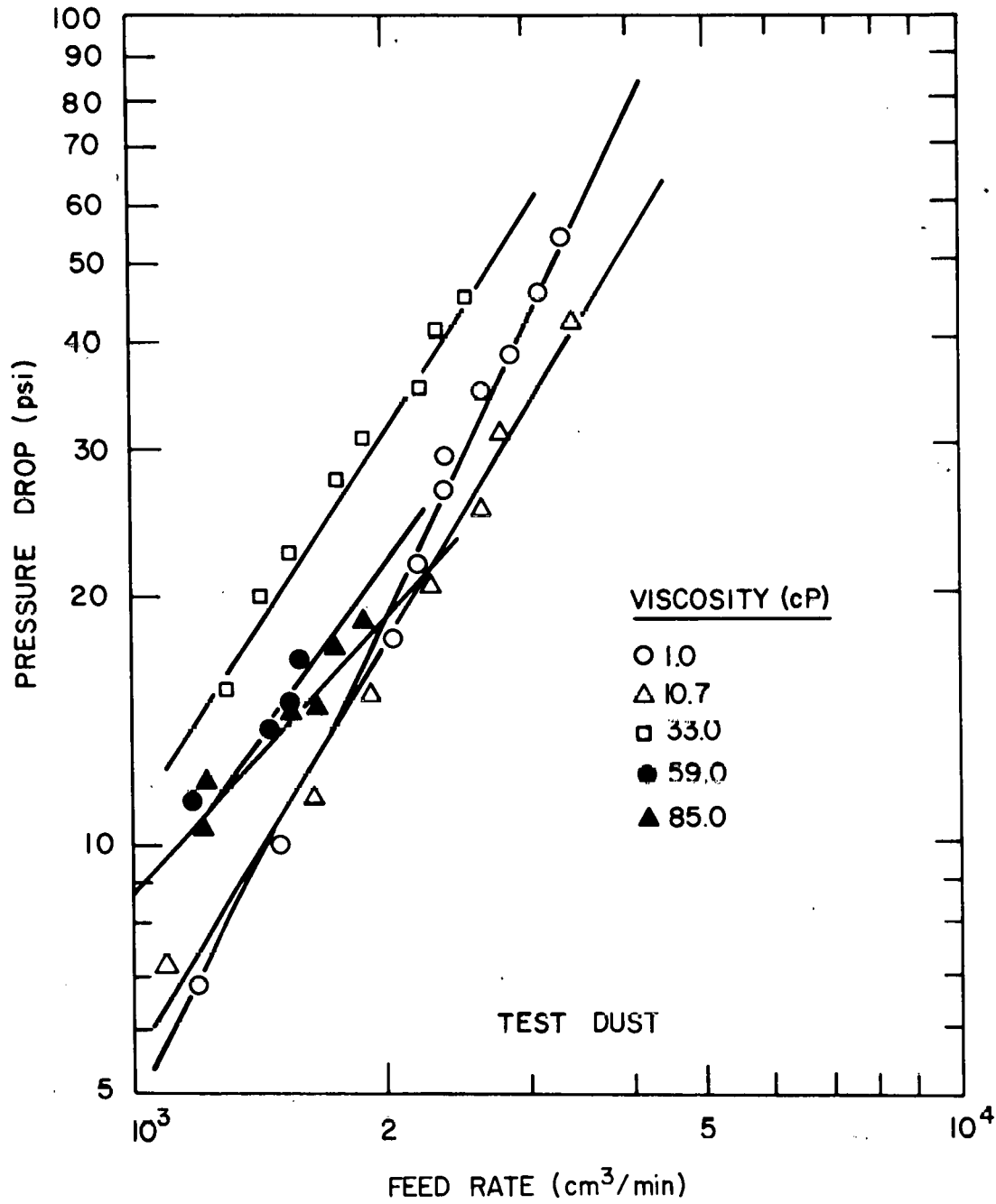


Fig. 13. Pressure drop as a function of feed rate for test-dust slurries.

ORNL-DWG 78-17914 R

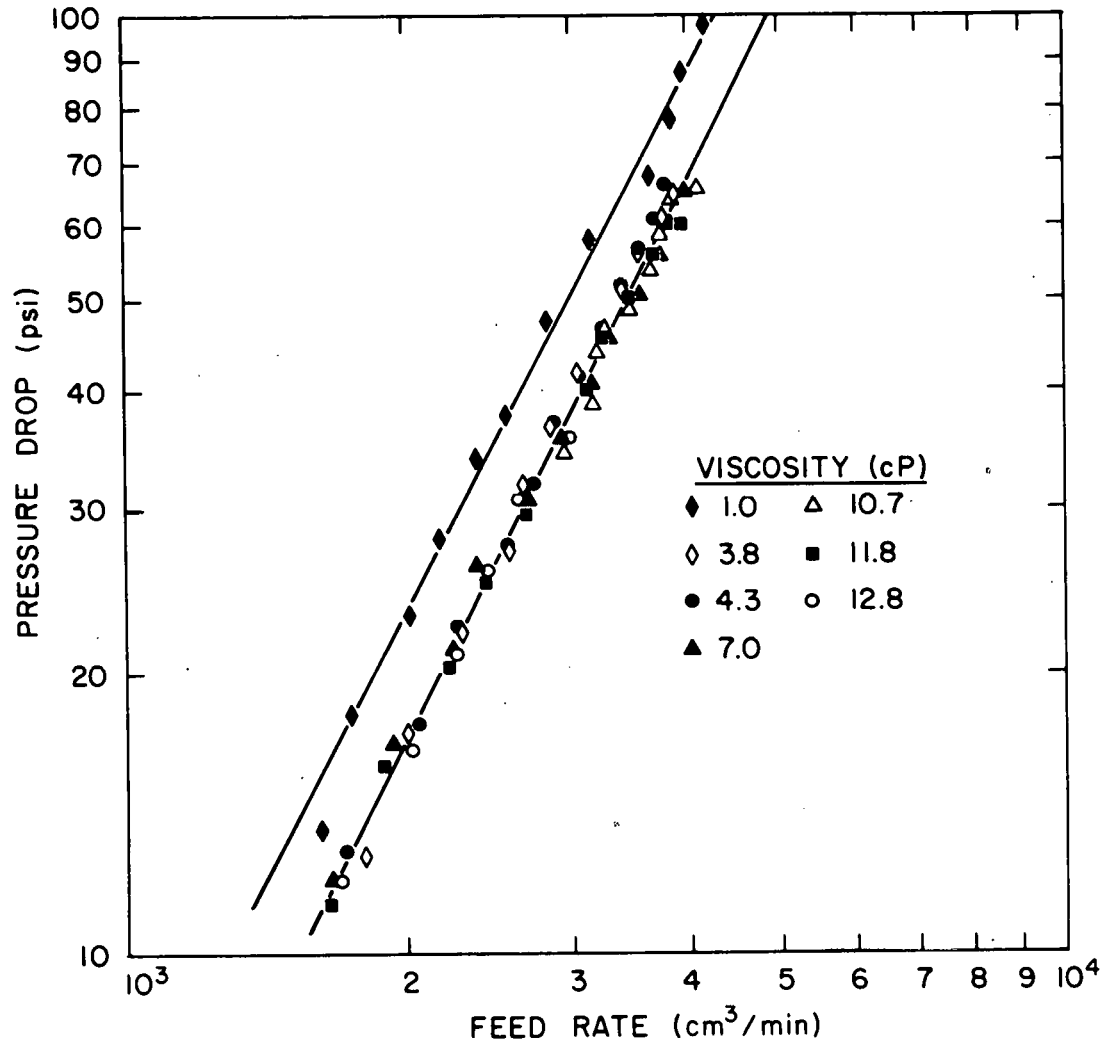


Fig. 14. Pressure drop as a function of feed rate for kaolin slurries.

Table 11. Regression coefficients for pressure-drop-feed-rate correlation, $\Delta P = a Q_f^b$

Type of solid	Viscosity (cP)	a	b	Coefficient of determination, r^2
Aluminum oxide	1.0	2.30×10^{-6}	2.09	1.00
Fly ash	1.0	6.40×10^{-6}	1.96	0.99
	10.6	3.56×10^{-5}	1.81	0.99
	35.0	1.73×10^{-4}	1.55	0.98
Test dust	1.0	2.45×10^{-6}	2.09	0.99
	10.7	7.77×10^{-5}	1.62	0.99
	33.0	2.62×10^{-4}	1.54	0.99
	59.0	7.19×10^{-4}	1.36	0.94
	85.0	3.80×10^{-3}	1.12	0.97
Kaolin	1.0	8.35×10^{-6}	1.95	0.99
	3.8	1.67×10^{-6}	2.12	1.00
	4.3	1.67×10^{-6}	2.12	1.00
	7.0	9.32×10^{-6}	1.90	1.00
	10.7	2.08×10^{-6}	2.08	0.97
	11.8	6.24×10^{-6}	1.95	1.00
	12.8	4.90×10^{-6}	1.98	0.99

pressure-drop-flow-rate correlation. Two general effects are observed as viscosity increases: the slope, b , decreases and the intercept, a , increases. The data for all viscosities using fly ash and test dust were fit to an equation of the form

$$\Delta P = a Q_f^b \mu^c . \quad (23)$$

The regression coefficients for Eq. (23) are given in Table 12. A study using a 5 wt % suspension of 2.69 sp. gr. silty clay in sucrose solutions¹⁸ dealt with the effects of liquid viscosity on the performance of miniature hydroclones. This study also showed that the slope of the individual pressure-drop-feed-rate curves decreases with increasing viscosity. They applied multiple regression analysis to their data in the turbulent regime, $N_{Re} > 20,000$, to yield the following relationship:

$$\Delta P \propto Q_f^2 \mu^{0.42} . \quad (24)$$

(The exact equation is presented in Table 1.) This equation indicates an even more pronounced effect of viscosity on the operation of the hydroclone than the regression coefficients in Table 12. From runs using fly ash and test dust slurries,²⁰ the slope of the pressure-drop-flow-rate correlation, as indicated in Eq. (22), appears to approach an asymptotic value of unity at high viscosities. At low viscosities, the centrifugal acceleration, which is proportional to the square of the velocity, is more important than viscous drag. But as viscosity increases, the viscous force becomes more important, and the pressure drop becomes proportional to the velocity. To account for the decrease

in slope with increasing viscosity, the following correlation was developed to fit the experimental data using test dust:²⁰

$$\Delta P = 2.13 \times 10^{-6} \mu^{1.52} Q_f (1 + 1.03 e^{-0.02\mu}) \quad (25)$$

Table 12. Regression coefficients for pressure drop as a function of feed rate and viscosity, $\Delta P = a Q_f^b \mu^c$

Type of solid	a	b	c	Coefficient of determination, r^2
Fly ash	1.72×10^{-5}	1.85	0.079	0.83
Test dust	7.12×10^{-5}	1.64	0.066	0.84

The data for the kaolin slurry experiments were taken with relatively low feed viscosities, <15 cP. The regression coefficients for the pressure-drop-flow-rate correlation, Eq. (22), for kaolin (see Table 11) vary only slightly with viscosities >1 cP. Figure 14 shows a least-squares fit of 60 data points for the kaolin-glycerol runs, excluding those at 1 cP, which can be described by the following equation:

$$\Delta P = 4.25 \times 10^{-6} Q_f^{2.00} \quad (26)$$

The coefficient of determination, r^2 , is 0.99. This equation and the data at 1 cP agree well with a relationship in the literature⁵ which states that the pressure drop is proportional to the square of the feed rate. Increasing viscosity did not seem to affect the slope of the pressure drop correlation with the kaolin-glycerol experiments, whereas

data from runs using fly ash and test dust indicated that the slope decreases with increasing viscosity.

The pressure-drop-feed-rate correlation for the water capacity test (i.e., the solids-free runs) is as follows:

$$\Delta P = 2.18 \times 10^{-6} Q_f^{2.15}, r^2 = 1.00 . \quad (27)$$

Figure 15 compares pressure-drop data for solids-free runs with the 1 cP viscosity runs for all of the solids studied. The correlation for the 1 cP viscosity runs containing different solids shown in Fig. 15 is as follows:

$$\Delta P = 3.05 \times 10^{-6} Q_f^{2.07}, r^2 = 0.98 . \quad (28)$$

As shown in Fig. 15, the pressure drop is higher for the solids-free data than with solids at the same feed rate. Chaplin⁹ studied the effects of solids concentration on the general pressure-drop-flow-rate relationship, $\Delta P = aQ_f^b$, and found for $\Delta P > 7$ psi, the value of b decreased from 1.84 without solids to 1.11 with 62% solids content in the feed solution. The higher solids content increases the apparent feed slurry viscosity, as demonstrated by the data in Table 6, therefore having the same effect as increasing liquid viscosity. The effect of particle density at a viscosity of 1 cP is negligible, as seen from the data in Fig. 15. However, at a higher viscosity of ~ 10.7 cP, the effect of particle density can be observed. Figure 16 compared the pressure-drop-flow-rate data for three types of solids. Since the solids concentration is small (~ 5 wt %) in this study, no correlation between pressure-drop data and solids concentration and density was attempted.

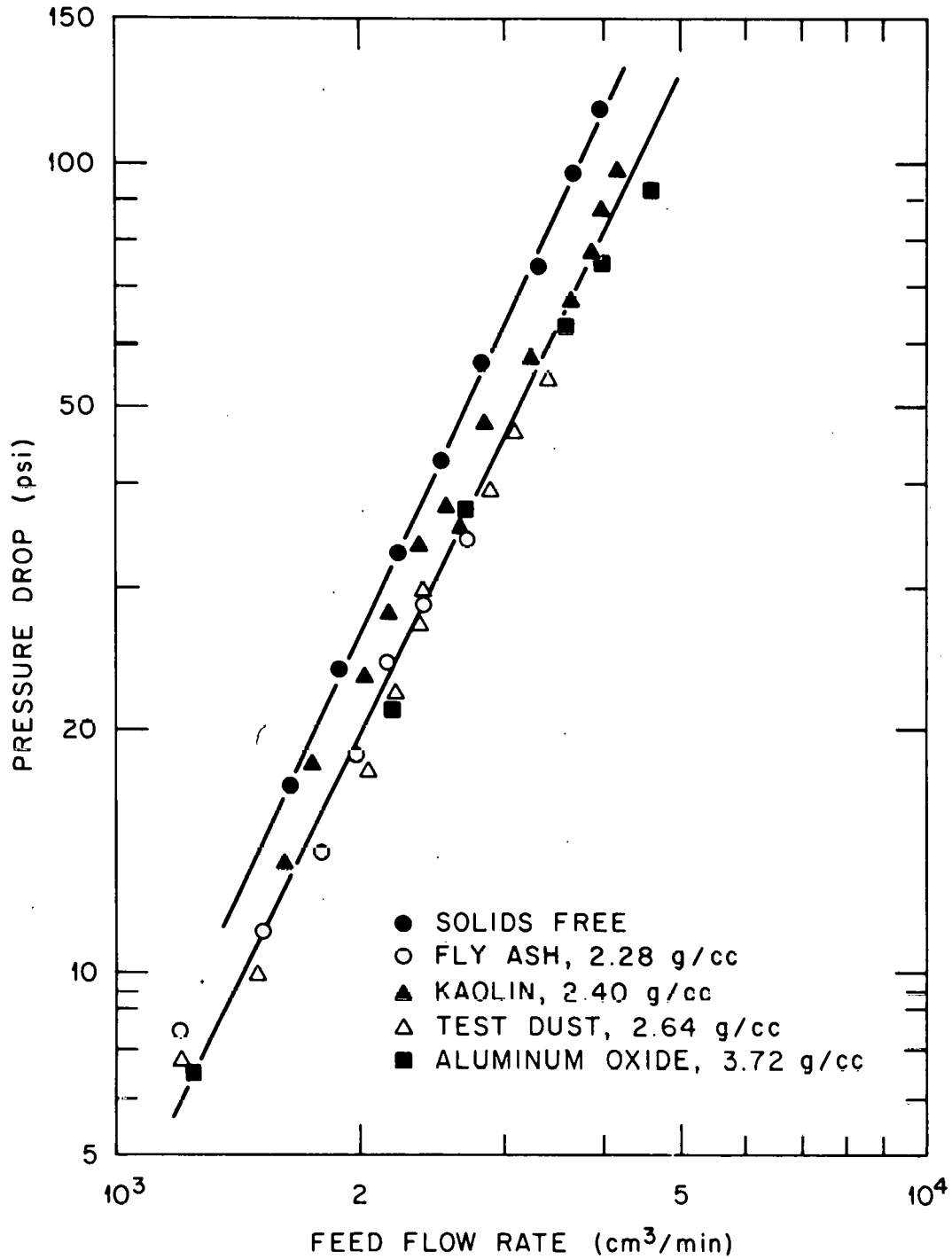


Fig. 15. The effect of feed rate on pressure drop for solids-free and 1-cP-viscosity runs.

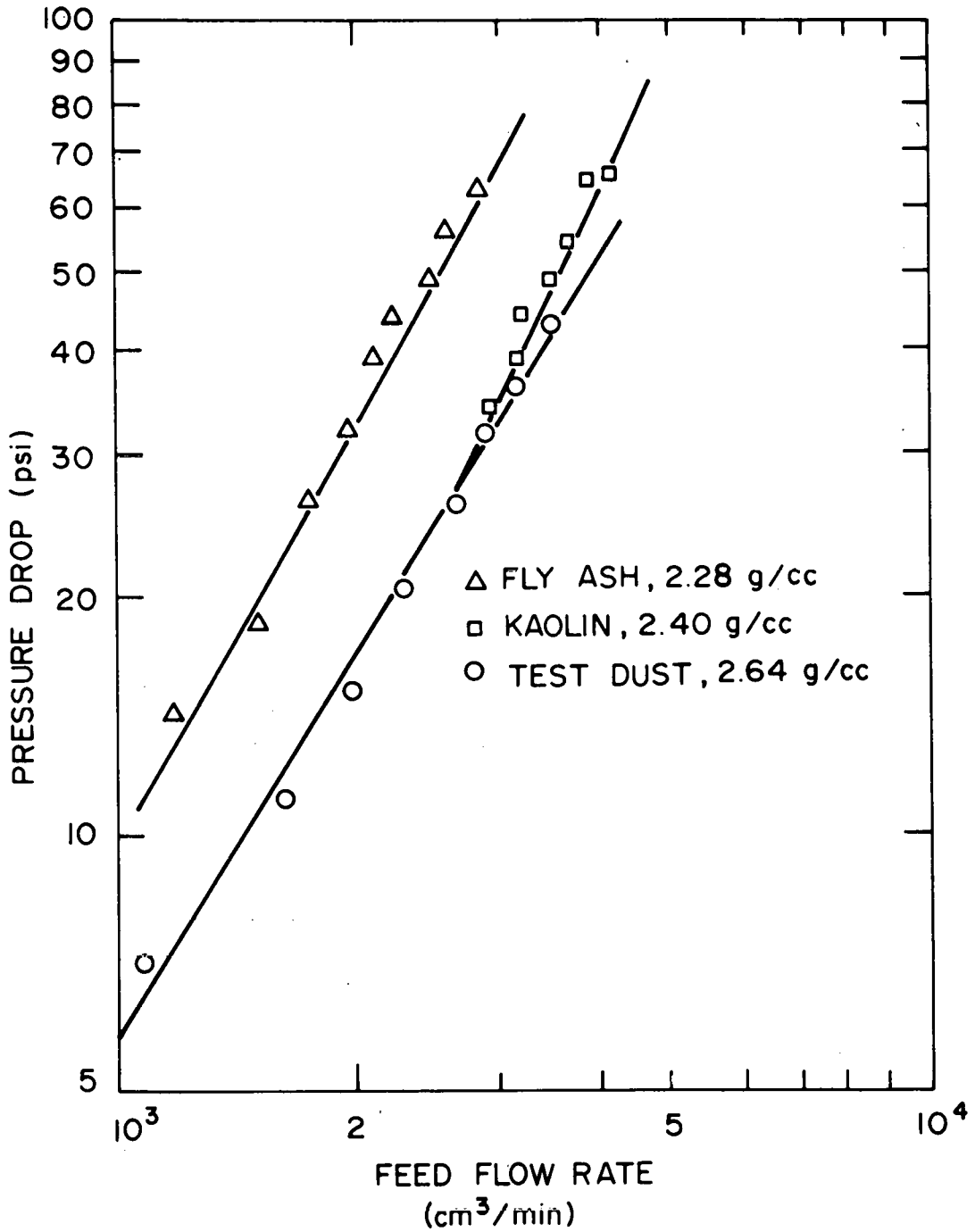


Fig. 16. The effect of feed rate on pressure drop for ~ 10.7 -cP-viscosity runs.

The empirical correlation for pressure drop as a function of feed rate for the 1 cP slurry runs [Eq. (28)] is compared in Fig. 17 with the theoretical correlation developed by Bradley [Eq. (5)] and the empirical correlation given by the hydroclone manufacturer, Dorr-Oliver.²² The curve representing the Bradley model was obtained using the dimensions of the hydroclone and values of $\alpha = 1.195$ and $n = 0.8$ in Eq. (5). The Dorr-Oliver data were based on separations using a 2.7 sp. gr. solid [a quartz-and-sand mixture of a known particle-size distribution²³] at a feed concentration below 25 wt % in water. Table 13 compares the correlations for each curve presented in Fig. 17 along with the empirical correlations given in Table 1 using the characteristic hydroclone dimensions in this study.

Table 13. Comparison of experimental and theoretical pressure-drop=flow-rate correlations

Experimental least-squares fit of 1 cP data	$\Delta P = 3.05 \times 10^{-6} Q_f^{2.07}$
Dorr-Oliver correlation	$\Delta P = 6.97 \times 10^{-6} Q_f^{1.91}$
Bradley model	$\Delta P = 4.31 \times 10^{-6} Q_f^2$
Haas correlation	$\Delta P = 3.94 \times 10^{-6} Q_f^{2.27}$
Matschke and Dahlstrom correlation	$\Delta P = 0.73 \times 10^{-6} Q_f^2$
Wagner and Murphy correlation	$\Delta P = 0.91 \times 10^{-6} Q_f^2$

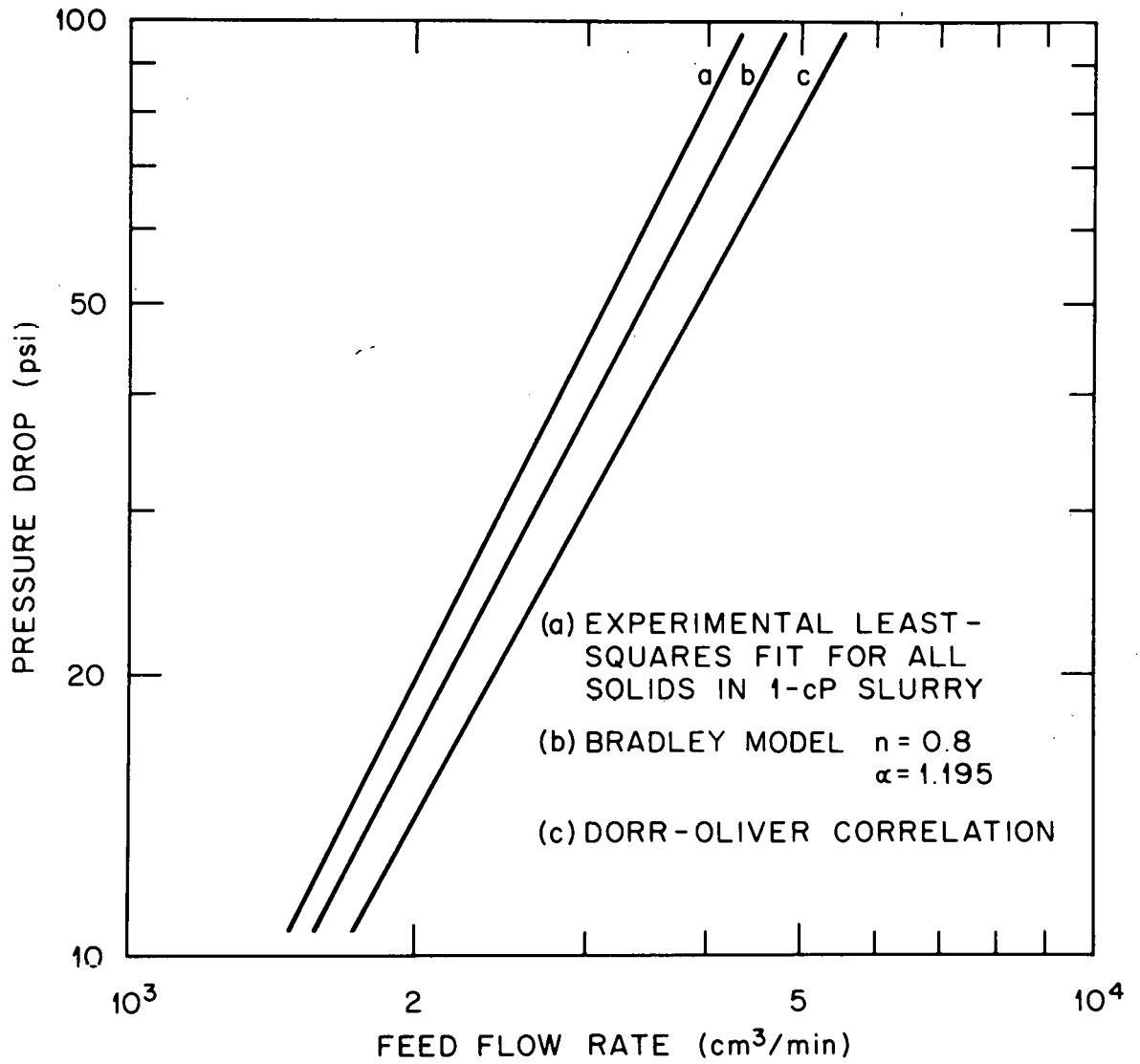


Fig. 17. Comparison of pressure-drop-flow-rate correlations.

6.2 Hydroclone Performance Parameters

An important parameter that describes hydroclone performance is volume split, S , which is defined as the ratio of the underflow to overflow rate. For the 1-cm Dorr-Oliver hydroclone used in this study, the natural feed split (free discharge conditions, i.e., no back pressure on the exiting streams) is 60% to the overflow and 40% to the underflow;²² $S = 0.67$. The normal operating condition for a hydroclone would be for $S < 1$, or the overflow rate to be greater than the underflow rate. Feed rate affects the split, but in a complex manner which Bradley⁵ explains as follows:

"At low flow rates to a particular cyclone, the air core is not well developed, and increase in flow rate causes an increase in underflow rate as the exit energy increases. As the air core develops, there comes a stage, however, where it obscures exit area and further increase in flow rate decreases the underflow rate."

The work done with small-diameter hydroclones⁵ has shown conditions where the volume split has increased, remained constant, or decreased with an increase in flow rate. Generally, with small-diameter hydroclones, when $S > 0.5$, the split was independent of feed rate, and when $S < 0.5$, the split decreased with an increase in feed rate.

Values for volume split, S , are presented in Table 7 for the solids-free runs and Table 8 for the slurry tests. The results show that all the values of S are >0.5 and most of the values are >1.0 . The values of S for the water capacity test (Table 7) are less than unity, which is the normal operation condition for a hydroclone; however, all of the values are greater than the split given by the vendor, $S = 0.67$.

For the majority of test runs, the volume split increased with an increase in feed rate. Figure 18 shows split as a function of feed rate for test dust slurries at viscosities of 1.0, 10.7, 33.0, and 59.0 cP. The slope of the least-squares fit increases with increasing viscosity with the exception of the 59.0 cP data. An increase in viscosity should result in sluggish rotational flow and also lower centrifugal forces. The air core would then become smaller, and the output to the underflow stream would increase. Therefore, S should increase with an increase in viscosity. Figure 19 also shows split vs feed rate for kaolin slurries with viscosity >7.0 cP. The range of S values is much smaller than the data shown in Fig. 18 for test dust. Table 14 lists the correlation coefficients for the following relationship between split and feed rate:

$$S = a Q_f^b \quad (29)$$

The average values and standard deviations for the test runs in which it appeared that volume split was independent of feed rate are also listed in Table 14.

The flow ratio, Rf (ratio of underflow rate to feed rate) also increased with increasing feed rate for the test runs where S increased with increasing feed rate. Since Rf is related to volume split by the following:

$$Rf = \frac{S}{1 + S} \quad (30)$$

the correlation coefficients are not calculated for Rf as a power function of Q_f .

ORNL DWG 78-22239

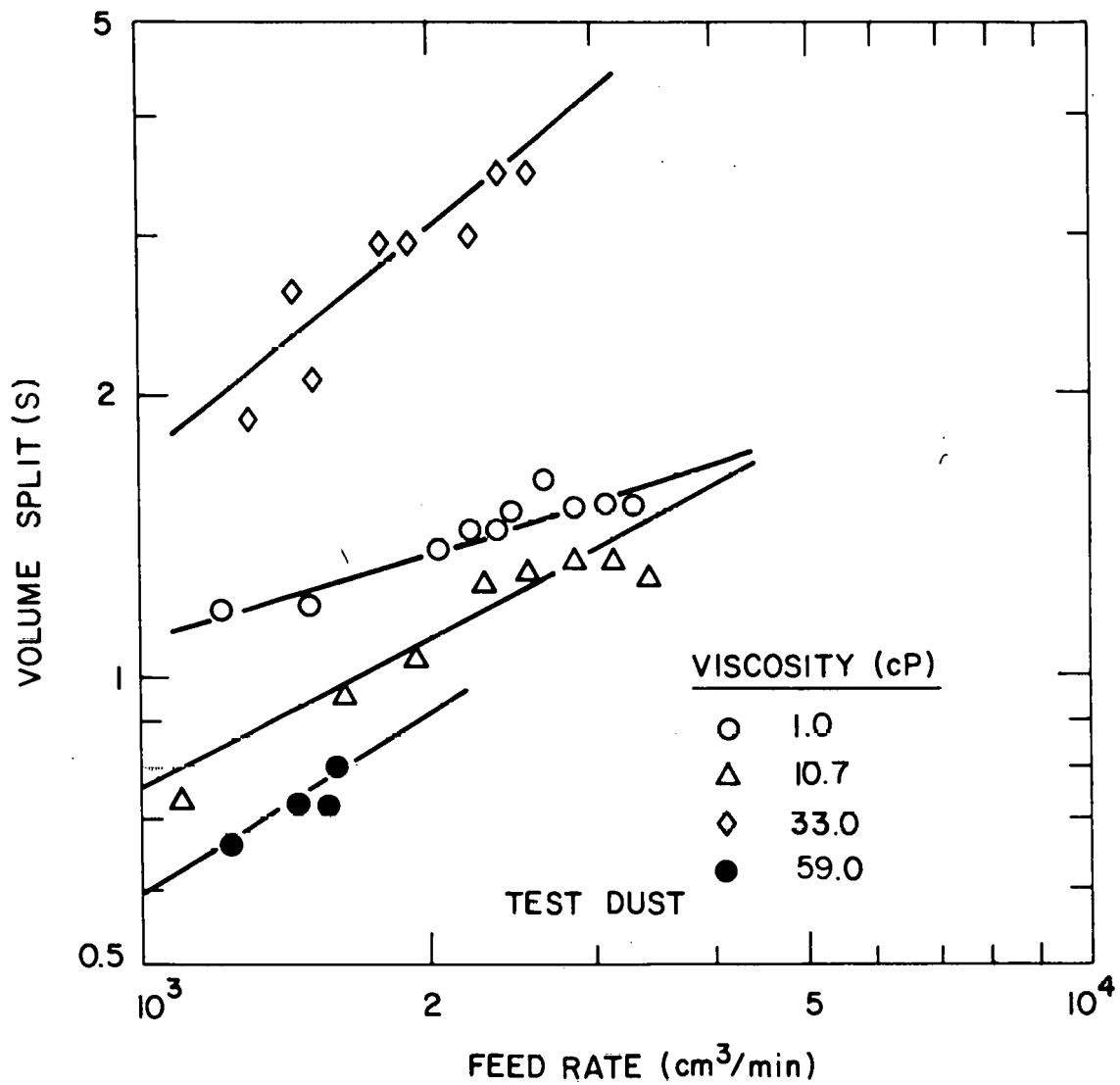


Fig. 18. Volume split as a function of feed rate for test-dust slurries.

ORNL DWG 78-22245

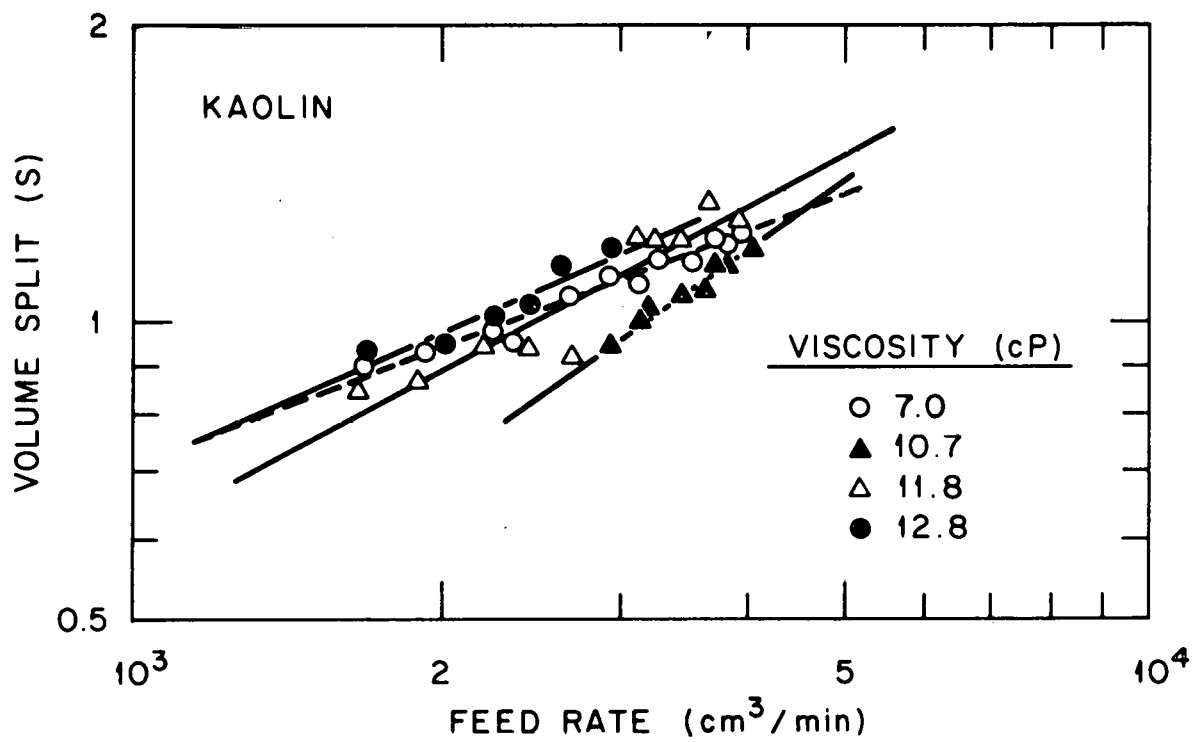


Fig. 19. Volume split as a function of feed rate for kaolin slurries with viscosities >7.0 cP.

Table 14. Correlation coefficients for volume split as a function of feed rate, $S = a Q_f^b$, or average values of volume split, \bar{S}

Type of solid	Viscosity (cP)	a	b	r^2	\bar{S}	s^a
Solids free	1.0				0.844	0.061
Aluminum oxide	1.0	0.0236	0.49	0.97		
Test dust	1.0	0.1227	0.32	0.86		
	10.7	0.0184	0.54	0.93		
	33.0	0.0056	0.83	0.83		
	59.0	0.0077	0.63	0.82		
	85.0				0.766	0.098
Fly ash	1.0				1.380	0.173
	10.6	0.0351	0.46	0.85		
	35.0	0.0471	0.38	0.81		
Kaolin	1.0				1.148	0.047
	3.8				1.185	0.033
	4.3				1.254	0.017
	7.0	0.0519	0.38	0.96		
	10.7	0.0027	0.73	0.95		
	11.8	0.0138	0.55	0.87		
	12.8	0.0294	0.46	0.91		

^a_s = standard deviation of \bar{S} .

Since a large number of variables are involved in the operation of a hydroclone, the experimental results of some investigations have been expressed in terms of dimensionless groups, in particular, Reynolds number and Euler number. The Reynolds number can be thought of as the ratio of inertial to viscous forces, and the Euler number as the ratio of pressure to inertial forces. Therefore, the dimensionless numbers can be expressed as follows:

$$N_{Re} = \frac{DV\rho}{\mu}, \quad (31)$$

and

$$N_{Eu} = \frac{\Delta P g_c}{\rho V^2}. \quad (32)$$

However, definitions of both dimensionless groups vary throughout the literature because of the different characteristic hydroclone diameters (i.e., main, inlet, overflow, and underflow). The Reynolds numbers and Euler numbers in Tables 7 and 8 were calculated using the mean velocity in the inlet feed, V_i , and the feed port, D_f . Therefore, the dimensionless groups (Tables 7 and 8) are defined by the following equations:

$$N_{Re \text{ inlet}} = \frac{D_f V_i \rho}{\mu} = \frac{4Q_f \rho}{\pi D_f \mu}, \quad (33)$$

and

$$N_{Eu} = \frac{\Delta P g_c}{\rho V_i^2} = \frac{\Delta P g_c \pi^2 D_f^4}{16 \rho Q_f^2}. \quad (34)$$

A Reynolds number can also be defined using the main diameter of the hydroclone, D_c ($N_{Re} = \frac{D_c V_i \rho}{\mu}$).⁷ For a given hydroclone design,

$$N_{Re} = \frac{D_c N_{Re \text{ inlet}}}{D_f} \quad (35)$$

For the Dorr-Oliver hydroclone used in this study,

$$N_{Re} = \left(\frac{1.00 \text{ cm}}{0.325 \text{ cm}} \right) N_{Re \text{ inlet}} = 3.08 N_{Re \text{ inlet}} \quad (36)$$

Rearrangement of Eq. (5), the correlation for pressure drop developed by Bradley, in dimensionless form gives:

$$\frac{2\Delta P g_c}{\rho V_i^2} = \frac{\alpha^2}{n} \left[\left(\frac{D_c}{D_f} \right)^{2n} - 1 \right] \quad (37)$$

The dimensionless group on the left-hand side of the equation is referred to as the loss coefficient.⁵ The loss coefficient is twice the magnitude of the Euler number.

In this study (see Tables 7 and 8), Reynolds numbers ranged from 73.7 to 2.9×10^4 , and Euler numbers varied from 6.4 to 16.3. The effect of inlet Reynolds number on the pressure loss coefficient is shown in Fig. 20. Other studies⁵ have found the pressure loss coefficient or the Euler number to decrease as N_{Re} increased until it reached a minimum level. This minimum corresponds to conditions where inertial forces predominate at the hydroclone wall. As N_{Re} is increased further, the Euler number increases, becoming solely dependent on changes in centrifugal head. The normal operating condition⁵ for a 1-cm-diam hydroclone using water should correspond to an inlet N_{Re} in the range of $\sim 10^4$ to 5×10^4 . The Reynolds numbers for the 1-cP runs are within this range. The loss coefficients (see Fig. 20) do not vary significantly in this

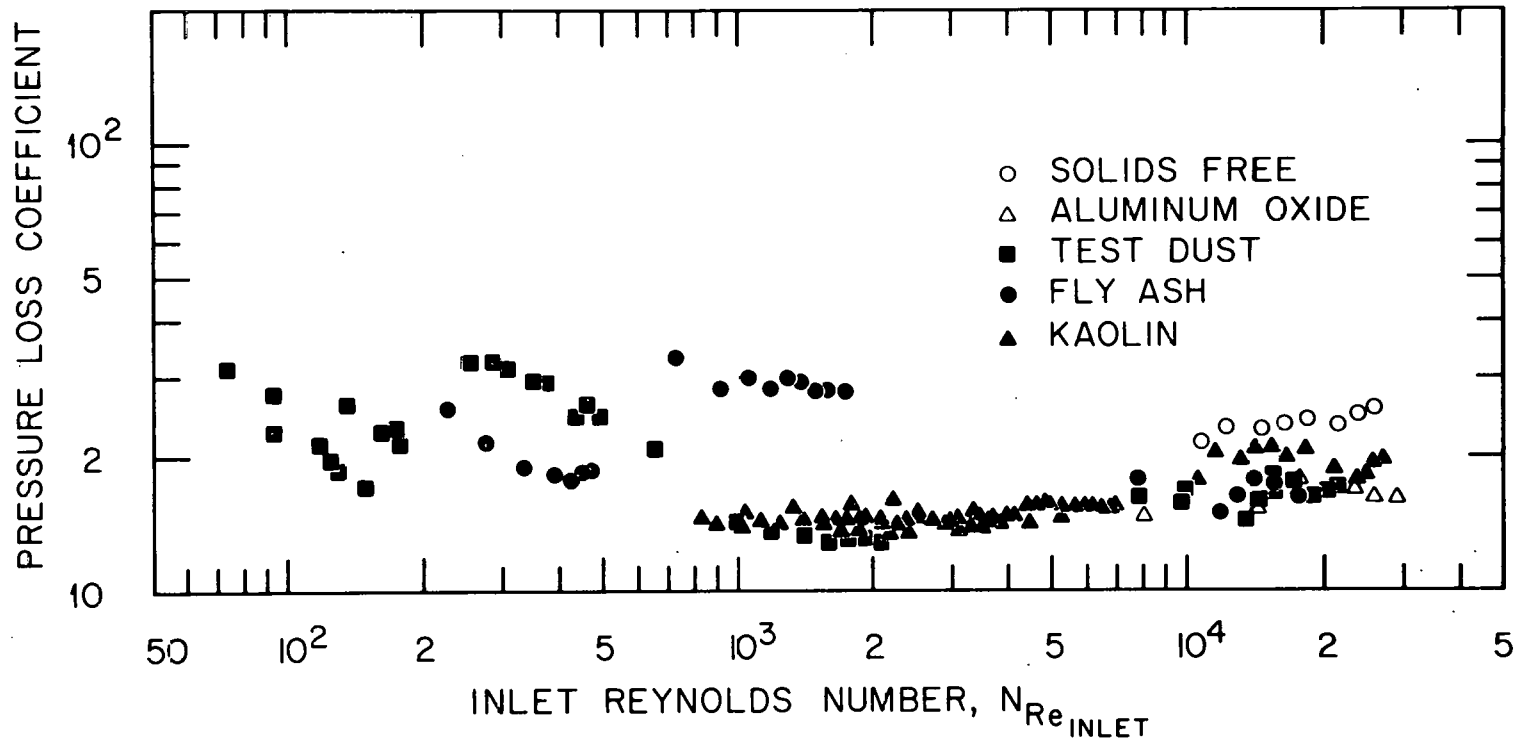


Fig. 20. Effect of inlet Reynolds number on the pressure loss coefficient.

study; however, there is a slight decrease with the inlet Reynolds numbers between 10^2 and 10^3 , a flattening off in the range of 10^3 to 10^4 , and a slight increase with the Reynolds numbers $>10^4$. Gerrard and Liddle²⁴ fitted the following function to data in the literature and found:

$$N_{Eu} = 0.186 N_{Re \text{ inlet}}^{0.3748}, \text{ for } N_{Re \text{ inlet}} > 5000. \quad (38)$$

Since most of the data in this study were for $N_{Re \text{ inlet}} < 5000$, no correlation such as this was attempted.

The effect of the Reynolds number on hydroclone efficiency has also been examined to some extent in the literature.⁷ This will be included in the next section with the discussion of the hydroclone efficiency results.

6.3 Hydroclone Efficiency

Hydroclone efficiencies (gross, centrifugal, and point efficiency) are calculated as described in Sects. 5.2 and 5.3. Gross efficiency (G), the ratio of solids underflow rate and solids feed rate, and centrifugal efficiency (E), as defined by Eq. (7), are calculated from the flow rates and solids concentrations of the overflow and underflow streams. Therefore, G and E are not referenced to a particle size distribution but describe the bulk stream separation.

The effect of feed rate on gross efficiency for test-dust, fly-ash, and kaolin particles is shown in Figs. 21, 22, and 23 respectively. Gross efficiency increases with increasing feed rate; however, viscosity has a pronounced effect on the magnitude of gross efficiency. Table 15

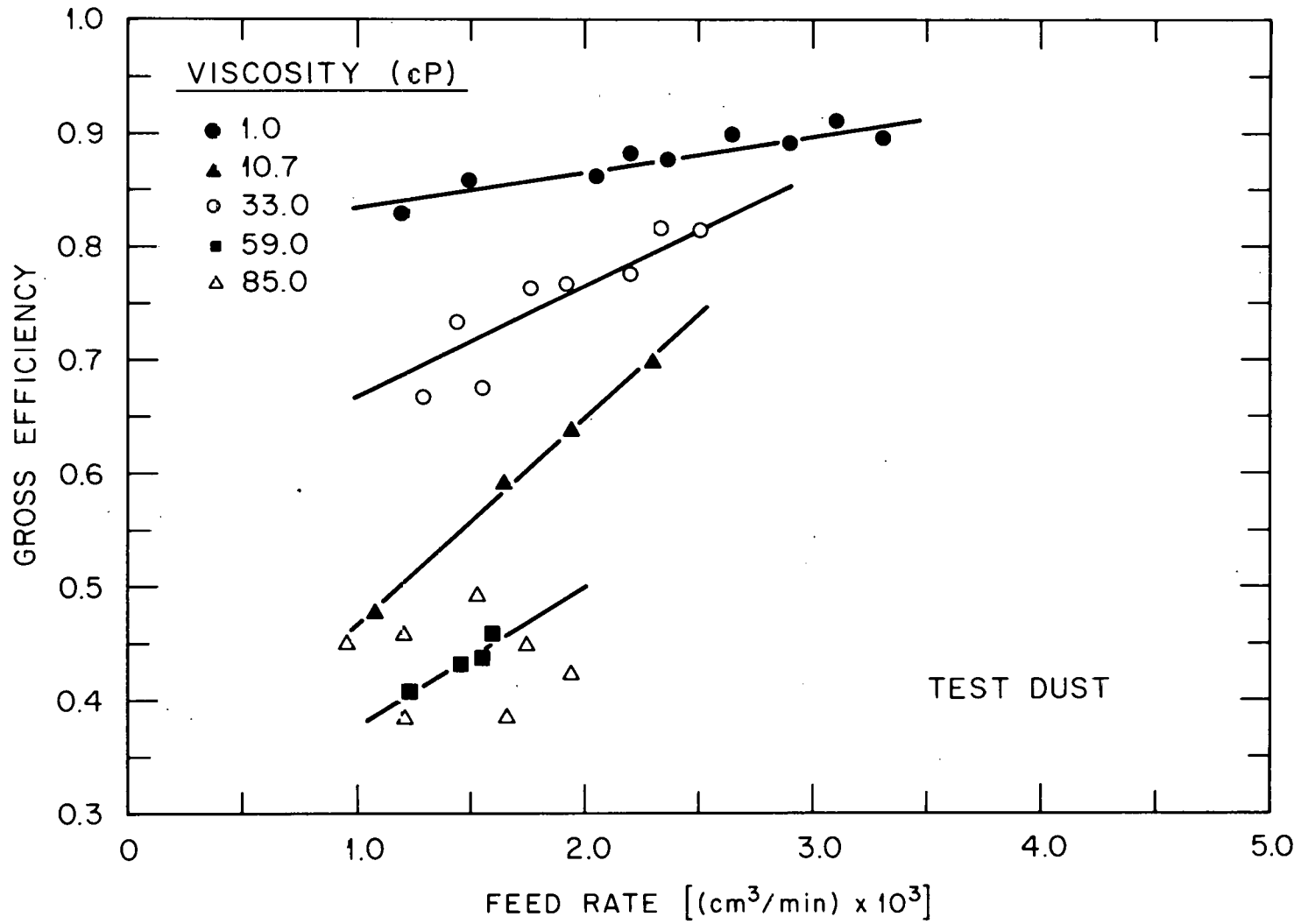


Fig. 21. Gross efficiency as a function of feed rate for test-dust slurries.

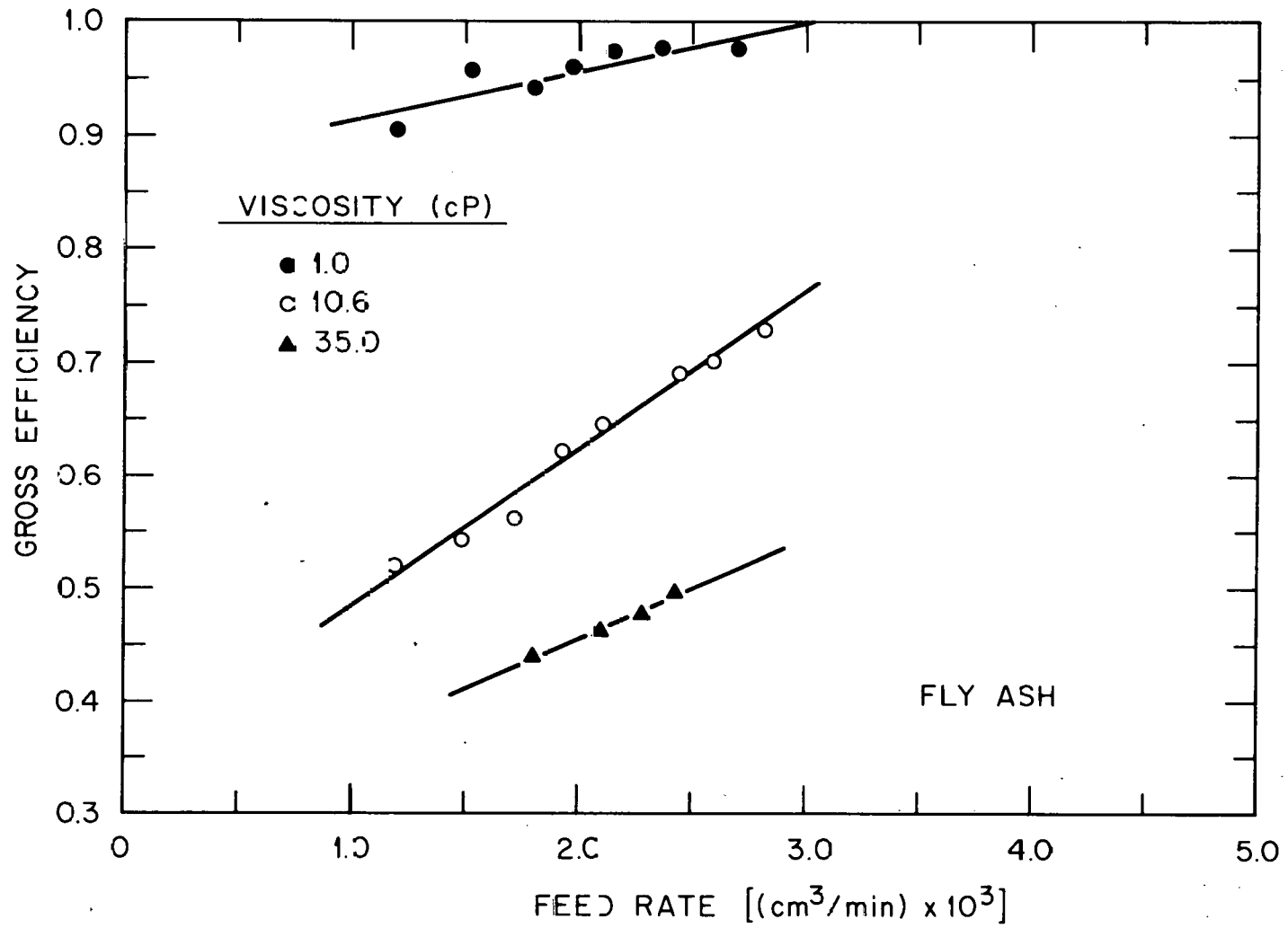


Fig. 22. Gross efficiency as a function of feed rate for fly-ash slurries.

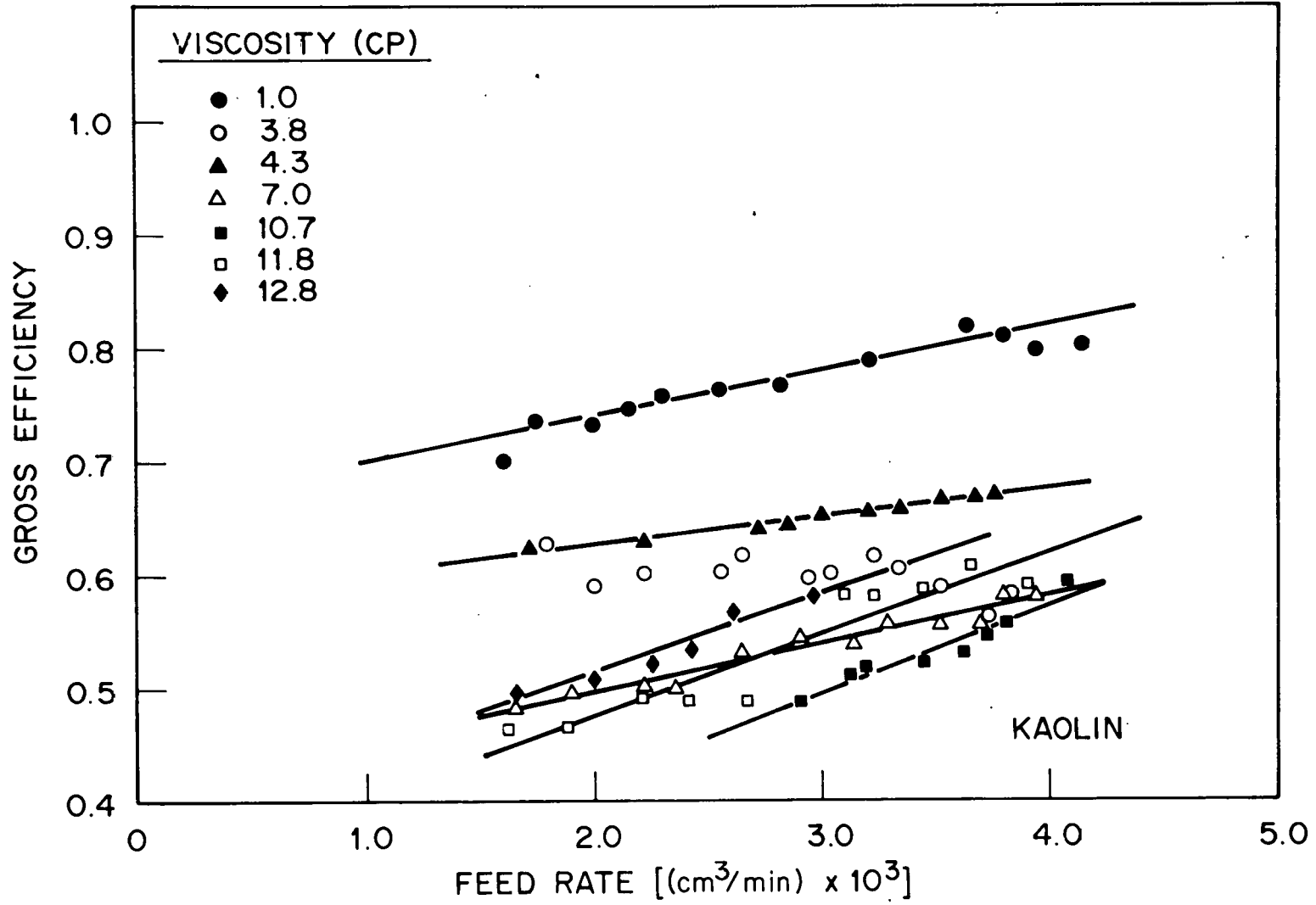


Fig. 23. Gross efficiency as a function of feed rate for kaolin slurries.

Table 15. Correlation coefficients for a linear least-squares fit of gross efficiency as a function of feed rate, $G = a + bQ_f$

Type of solid	Viscosity (cP)	a	b	r^2
Test dust	1.0	0.802	3.23×10^{-5}	0.85
	10.7	0.288	1.82×10^{-4}	1.00
	33.0	0.539	1.13×10^{-4}	0.82
	59.0	0.255	1.22×10^{-4}	0.90
Fly ash	1.0	0.870	4.35×10^{-5}	0.73
	10.6	0.346	1.39×10^{-4}	0.97
	35.0	0.276	8.96×10^{-5}	0.98
Kaolin	1.0	0.660	3.82×10^{-5}	0.90
	4.3	0.576	2.44×10^{-5}	0.96
	7.0	0.409	4.31×10^{-5}	0.94
	10.7	0.255	7.95×10^{-5}	0.92
	11.8	0.334	7.12×10^{-5}	0.89
	12.8	0.371	7.08×10^{-5}	0.95

lists the correlations coefficients of the linear least-squares fit of the curves in Figs. 21-23. As viscosity increases, both the slope and intercept of these curves decrease. The data for the test dust at 85.0 cP (Fig. 21) and kaolin at 3.8 cP (Fig. 23) are shown, but due to scatter, no correlations were made for those particular data. The maximum values of G occurred at 1 cP at the highest feed rate.

A similar effect of feed rate on centrifuged efficiency can be observed in Figs. 24, 25, and 26. Centrifugal efficiency increased with increasing feed rate. Table 16 lists the correlation coefficients of the linear least-squares fit of E as a function of feed rate. As with gross efficiency, an increase in viscosity causes a decrease in the slope and intercept of the centrifugal efficiency curves.

To show the effect of viscosity on efficiency, Figs. 27 and 28 show gross and centrifugal efficiency, respectively, as a function of viscosity at a feed rate of 2500 cm³/min. The values of efficiency in Figs. 27 and 28 are interpolated from Figs. 21-26. A least-squares fit of all the data and the kaolin runs only are also shown in these figures. Both gross and centrifugal efficiencies decrease with increasing viscosity. The equations for the curves shown in Figs. 27 and 28 are as follows:

$$\text{Overall: } G = 0.804 - 0.075 \ln \mu, r^2 = 0.42 ; \quad (39)$$

$$E = 0.572 - 0.164 \ln \mu, r^2 = 0.62 . \quad (40)$$

$$\text{Kaolin: } G = 0.751 - 0.102 \ln \mu, r^2 = 0.85 ; \quad (41)$$

$$E = 0.427 - 0.175 \ln \mu, r^2 = 0.88 . \quad (42)$$

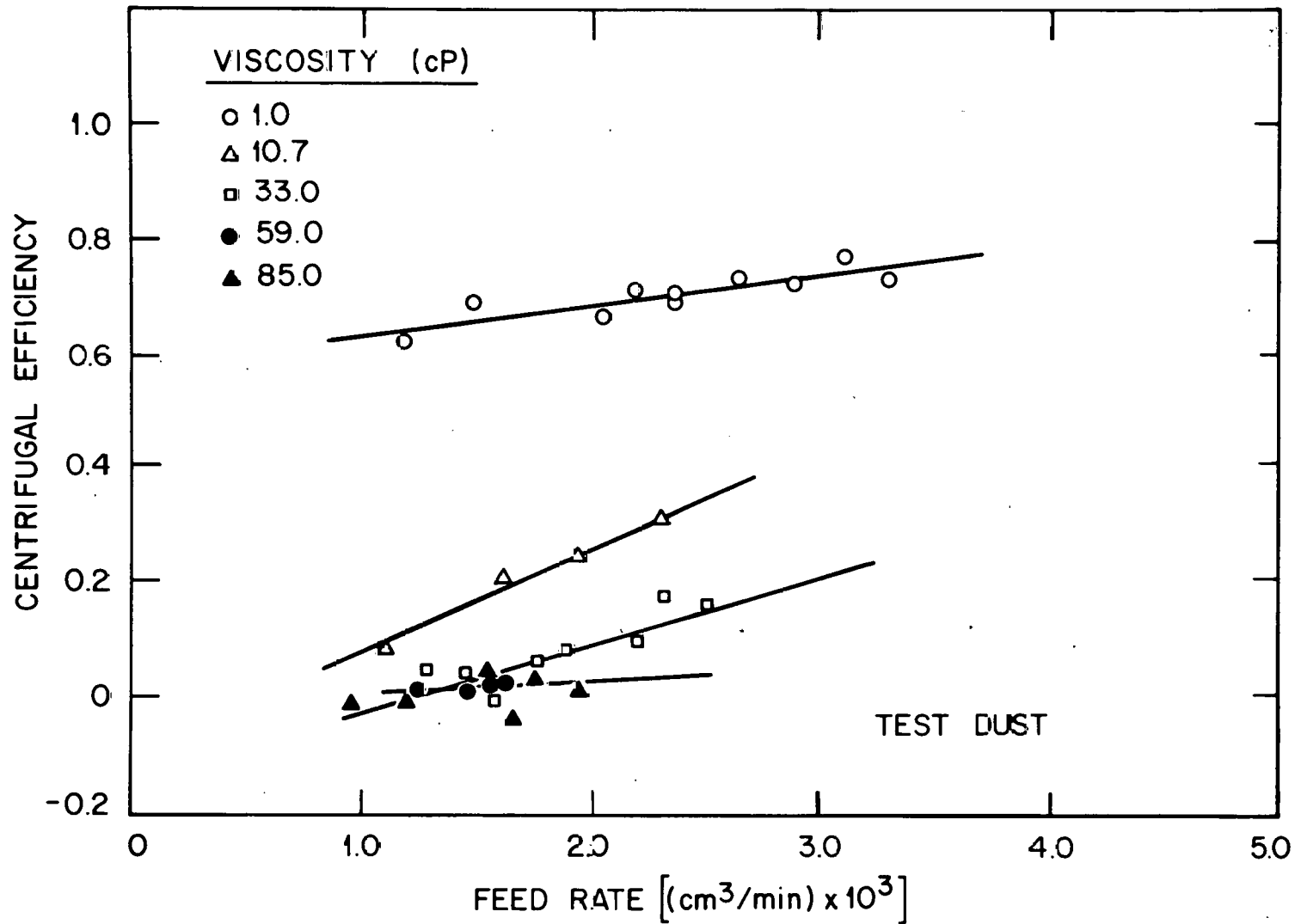


Fig. 24. Centrifugal efficiency as a function of feed rate for test-dust slurries.

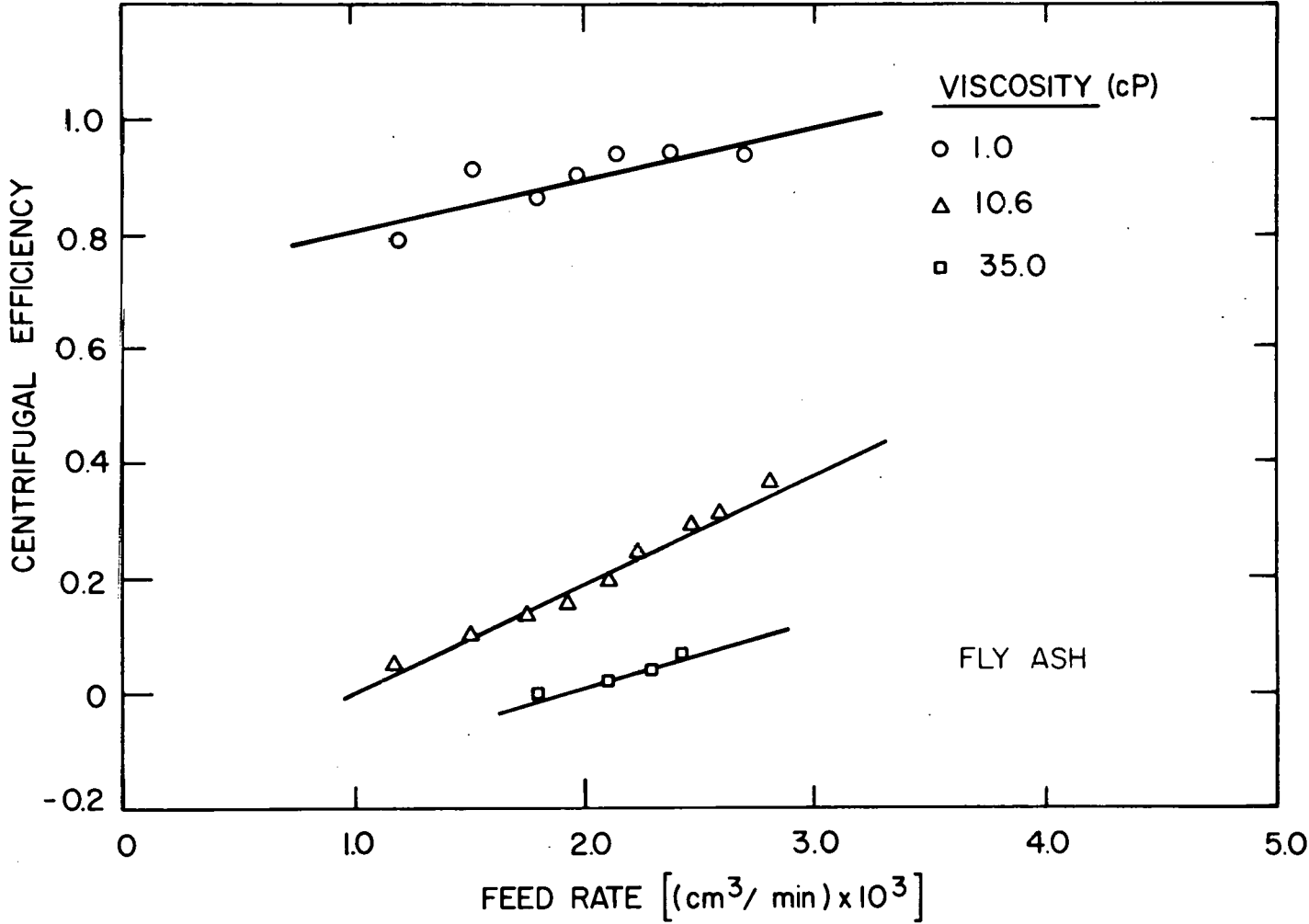


Fig. 25. Centrifugal efficiency as a function of feed rate for fly-ash slurries.

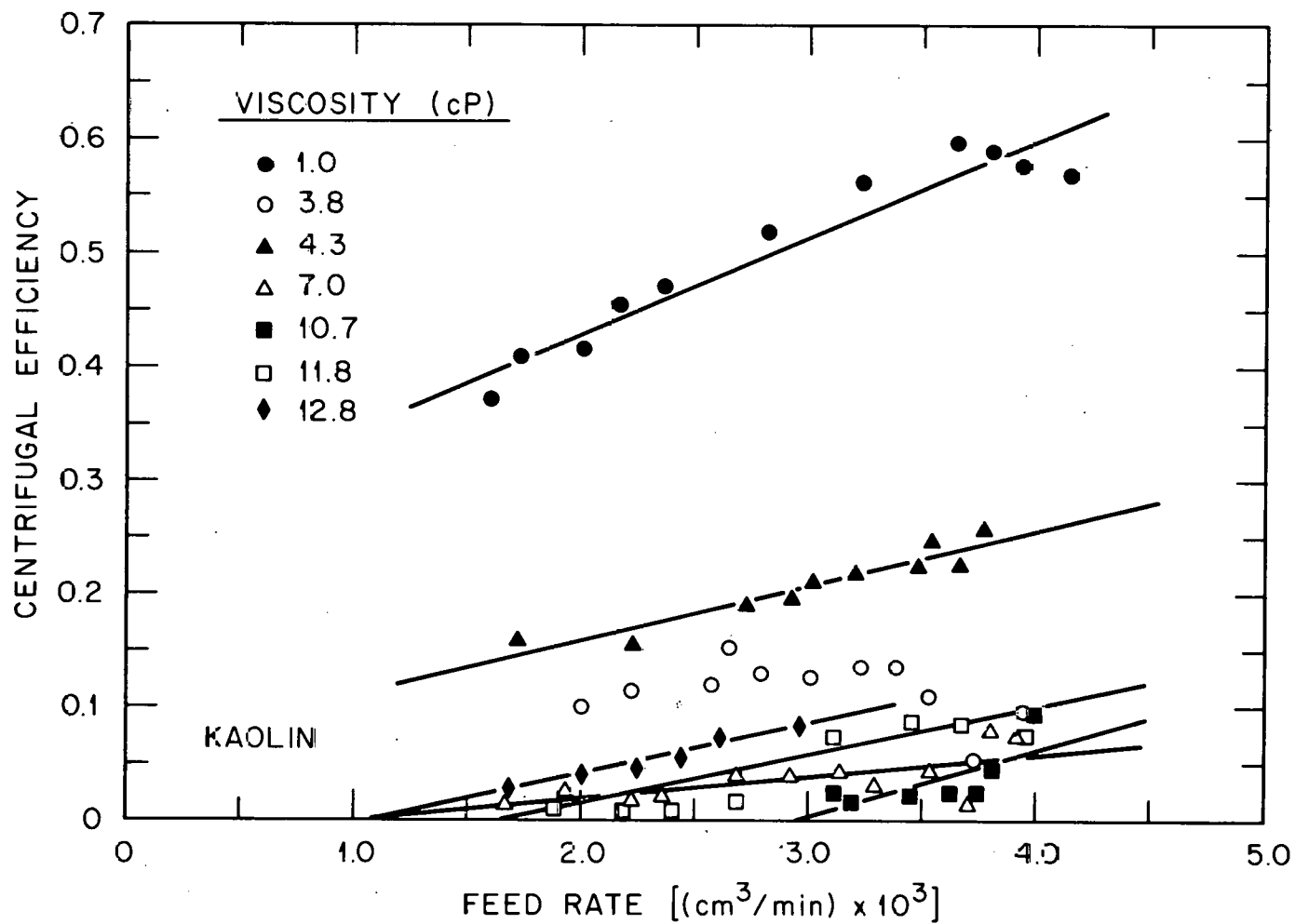


Fig. 26. Centrifugal efficiency as a function of feed rate for kaolin slurries.

Table 16. Correlation coefficients for a linear least-squares fit of centrifugal efficiency as a function of feed rate, $E = a + bQ_f$

Type of solid	Viscosity (cP)	a	b	r^2
Test dust	1.0	0.585	5.12×10^{-5}	0.75
	10.7	-0.112	1.85×10^{-4}	1.00
	33.0	-0.152	1.24×10^{-4}	0.77
	59.0	-0.020	2.56×10^{-5}	0.62
Fly ash	1.0	0.716	9.13×10^{-5}	0.68
	10.6	-0.198	1.95×10^{-4}	0.99
	35.0	-0.230	1.19×10^{-4}	0.93
Kaolin	1.0	0.259	8.57×10^{-5}	0.90
	4.3	0.059	4.99×10^{-5}	0.90
	7.0	-0.018	1.9×10^{-5}	0.46
	10.7	-0.177	5.98×10^{-5}	0.69
	11.8	-0.077	4.38×10^{-5}	0.82
	12.8	-0.050	4.52×10^{-5}	0.95

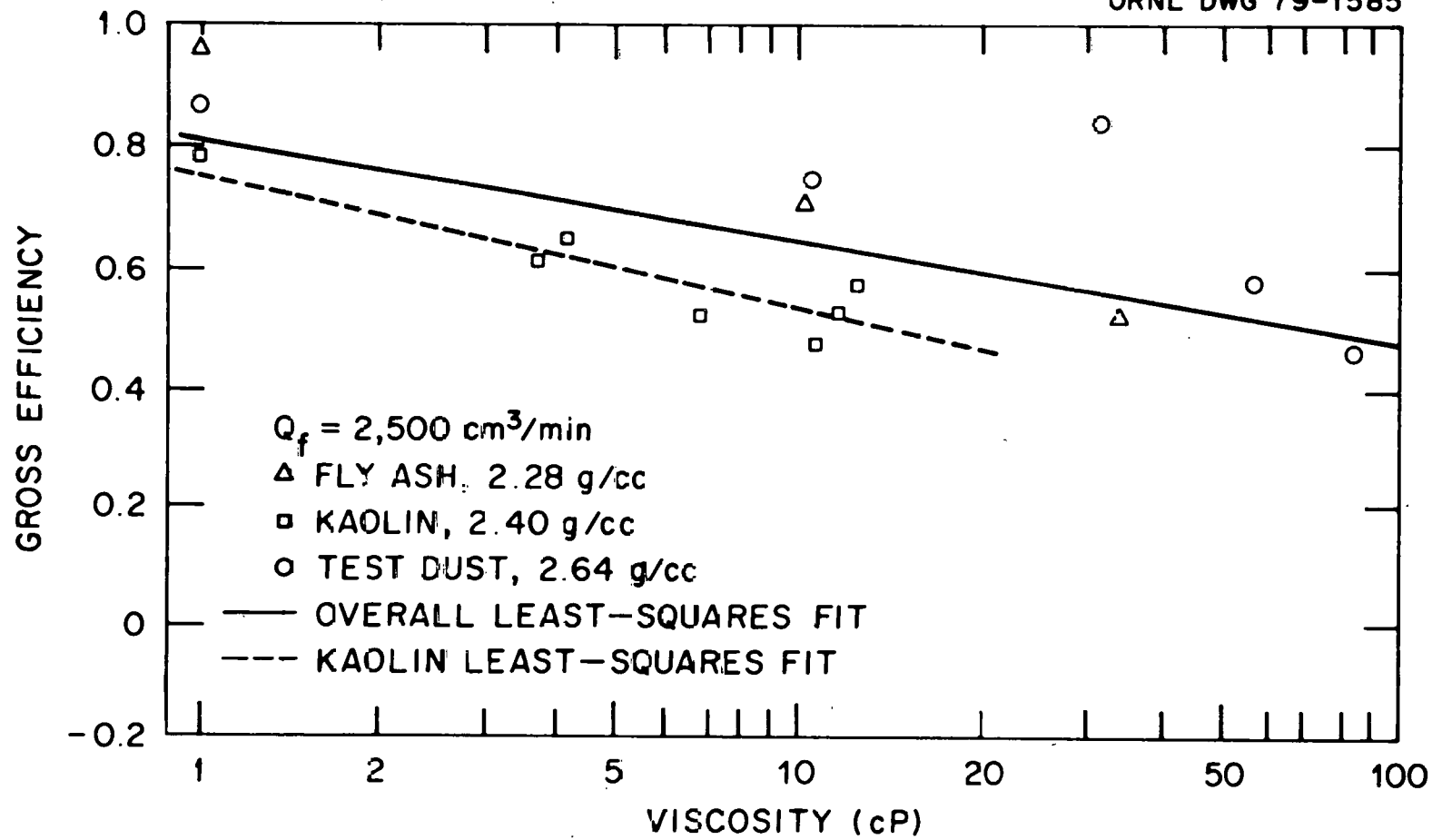


Fig. 27. Effect of viscosity on gross efficiency at a feed rate of 2500 cm³/min.

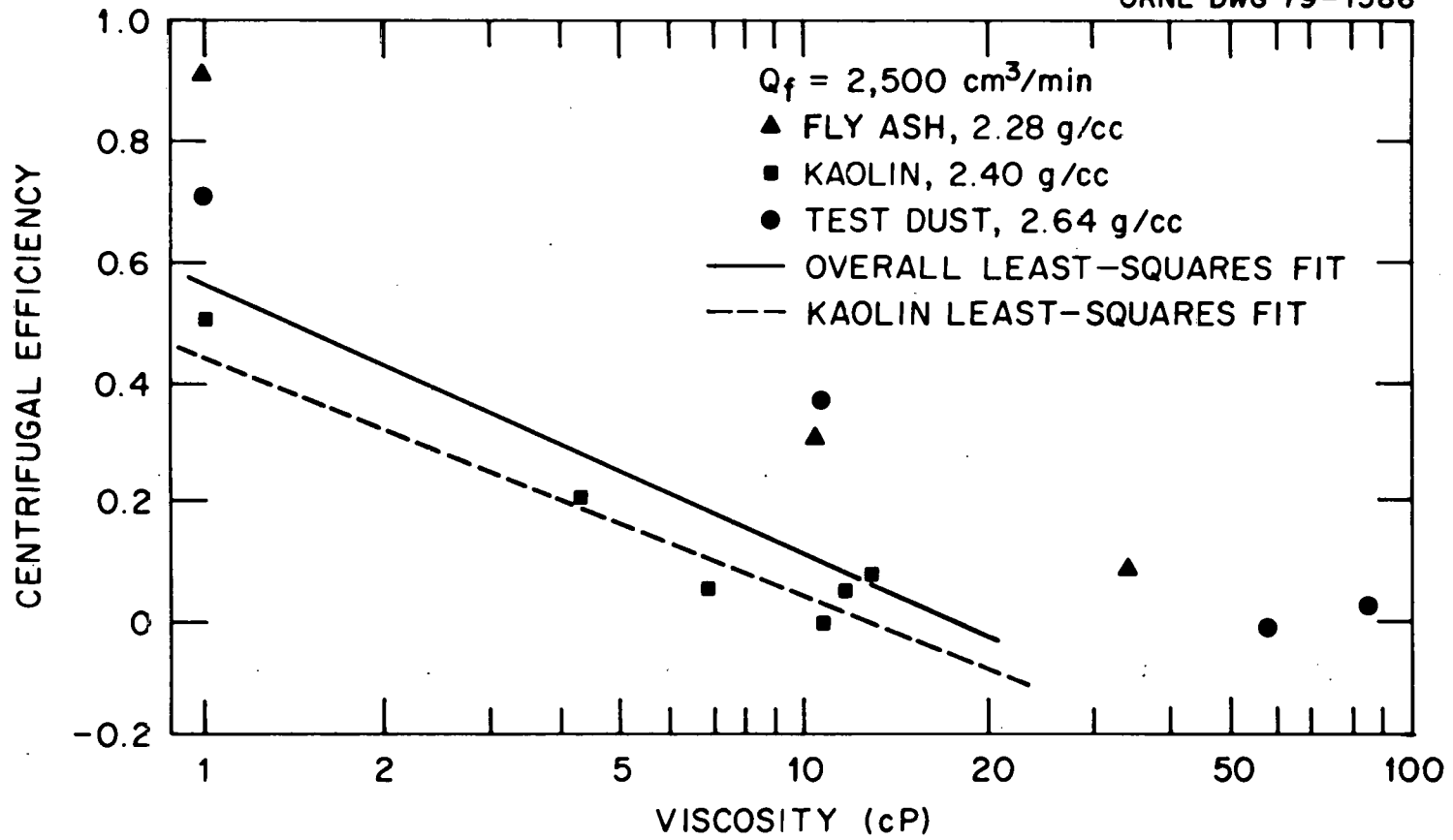


Fig. 28. Effect of viscosity on centrifugal efficiency at a feed rate of $2500 \text{ cm}^3/\text{min}$.

The least-squares fit of all the data in Fig. 27 indicates that the fraction of solids and the fraction of liquid that go to the underflow are essentially equal (gross efficiency = 0.5) at a viscosity of 55 cP. With kaolin particles at the same feed rate, a gross efficiency of 0.5 occurs at an even lower viscosity of ~ 11 cP.

The centrifugal efficiencies shown in Fig. 28 are also significantly influenced by viscosity. The least-squares fit of all the centrifugal efficiency data at a feed rate of $2500 \text{ cm}^3/\text{min}$ shows $E = 0$ at viscosity of ~ 16 cP. The kaolin data show $E = 0$ at a viscosity of 11 cP. Negative centrifugal efficiencies are shown in Table 8 and in Fig. 28. Efficiencies usually are chosen to range from 0 to 1 by definition; however, a negative centrifugal efficiency does occur if R_f is greater than G because more liquid than solid material is discharging to the underflow port of the hydroclone. At higher viscosities the rotational flow is sluggish, resulting in lower centrifugal forces and an increased underflow rate as discussed previously in Sect. 6.2. This, however, is an improper region for hydroclone operation.

The effect of the Reynolds number on both gross and centrifugal efficiency was determined. Figure 29 shows gross efficiency for test dust, fly ash, and kaolin as a function of N_{Re} . The least-squares equations for the data in Fig. 29 are the following:

$$\text{Test dust: } G = 0.233 N_{Re}^{0.126}, r^2 = 0.68 . \quad (43)$$

$$\text{Fly ash: } G = 0.116 N_{Re}^{0.202}, r^2 = 0.96 . \quad (44)$$

$$\text{Kaolin: } G = 0.143 N_{Re}^{0.153}, r^2 = 0.81 . \quad (45)$$

ORNL DWG 78-22228

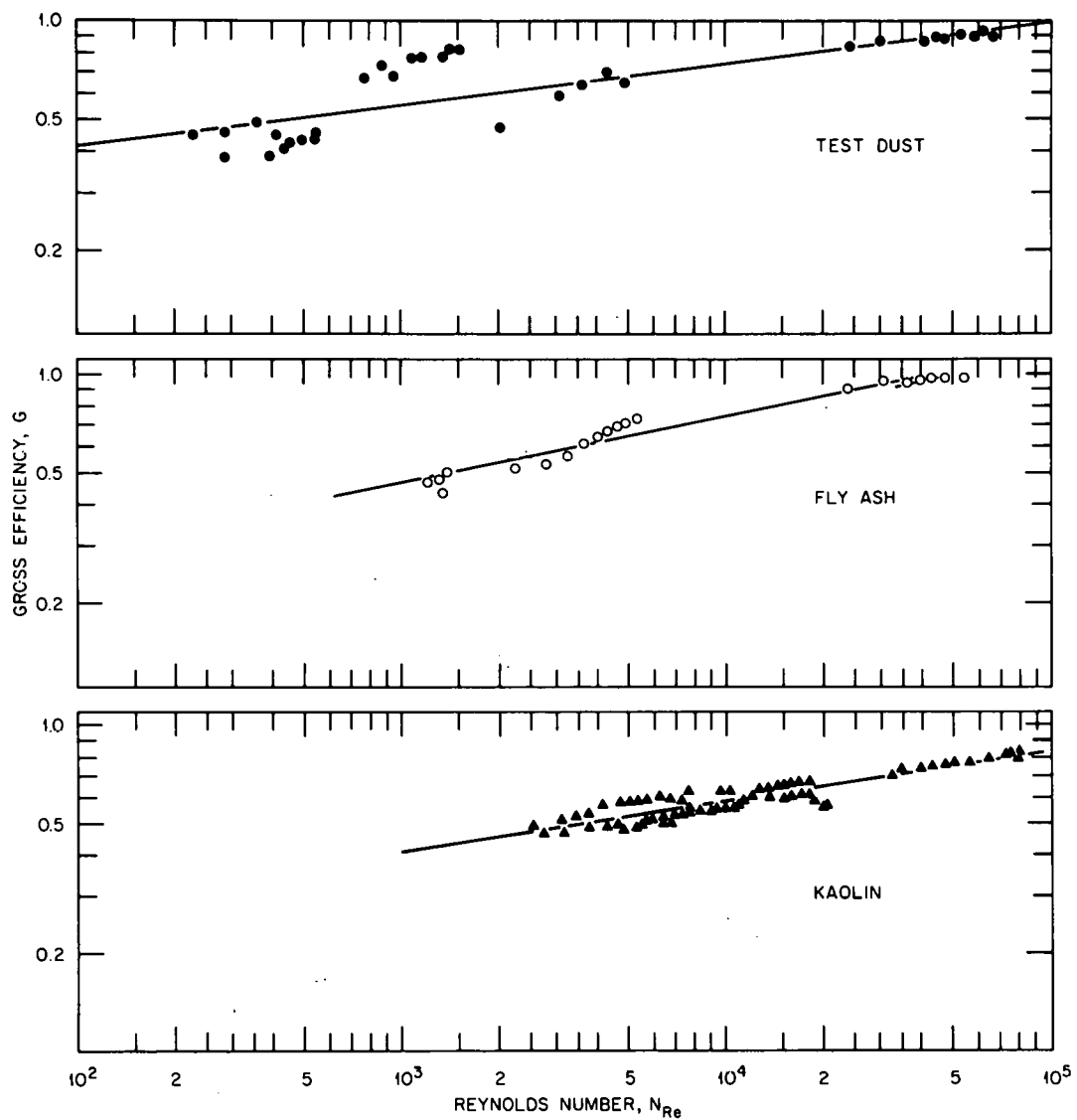


Fig. 29. Gross efficiency as a function of Reynolds number.

Gross efficiency increases with an increasing Reynolds number. The Reynolds numbers that correspond to a maximum gross efficiency ($G = 1$) for test dust, fly ash, and kaolin are about 1.0×10^5 , 4.3×10^4 , and 3.3×10^5 respectively.

Centrifugal efficiency also increases with increasing Reynolds number, as shown in Fig. 30. The least-squares equations for the data in Fig. 29 are the following:

$$\text{Test dust: } E = 1.74 \times 10^{-4} N_{\text{Re}}^{0.795}, r^2 = 0.86 . \quad (46)$$

$$\text{Fly ash: } E = 7.43 \times 10^{-5} N_{\text{Re}}^{0.905}, r^2 = 0.84 . \quad (47)$$

$$\text{Kaolin: } E = 1.38 \times 10^{-6} N_{\text{Re}}^{1.179}, r^2 = 0.64 . \quad (48)$$

The Reynolds numbers which correspond to a maximum centrifugal efficiency ($E = 1$) for test dust, fly ash, and kaolin are about 5.4×10^4 , 3.6×10^4 , and 9.3×10^4 respectively.

Figure 31 shows centrifugal efficiency as a function of Reynolds number for kaolin-glycerol slurries. Centrifugal efficiency increases with increasing Reynolds number, as shown previously, and with decreasing viscosity (see Fig. 31). Therefore, the runs at 1 cP have the highest Reynolds numbers and centrifugal efficiencies.

For a complete description of the efficiency of a hydroclone, efficiency must be related to a particle size distribution. Therefore, point efficiencies from the size-distribution curves, using both a differential and cumulative technique, were calculated. Figure 10 shows point efficiency curves for the two methods for a kaolin-aqueous solution (1 cP) at a $\Delta P = 18.0$ psi. It was not expected that the two

ORNL DWG 78-22237

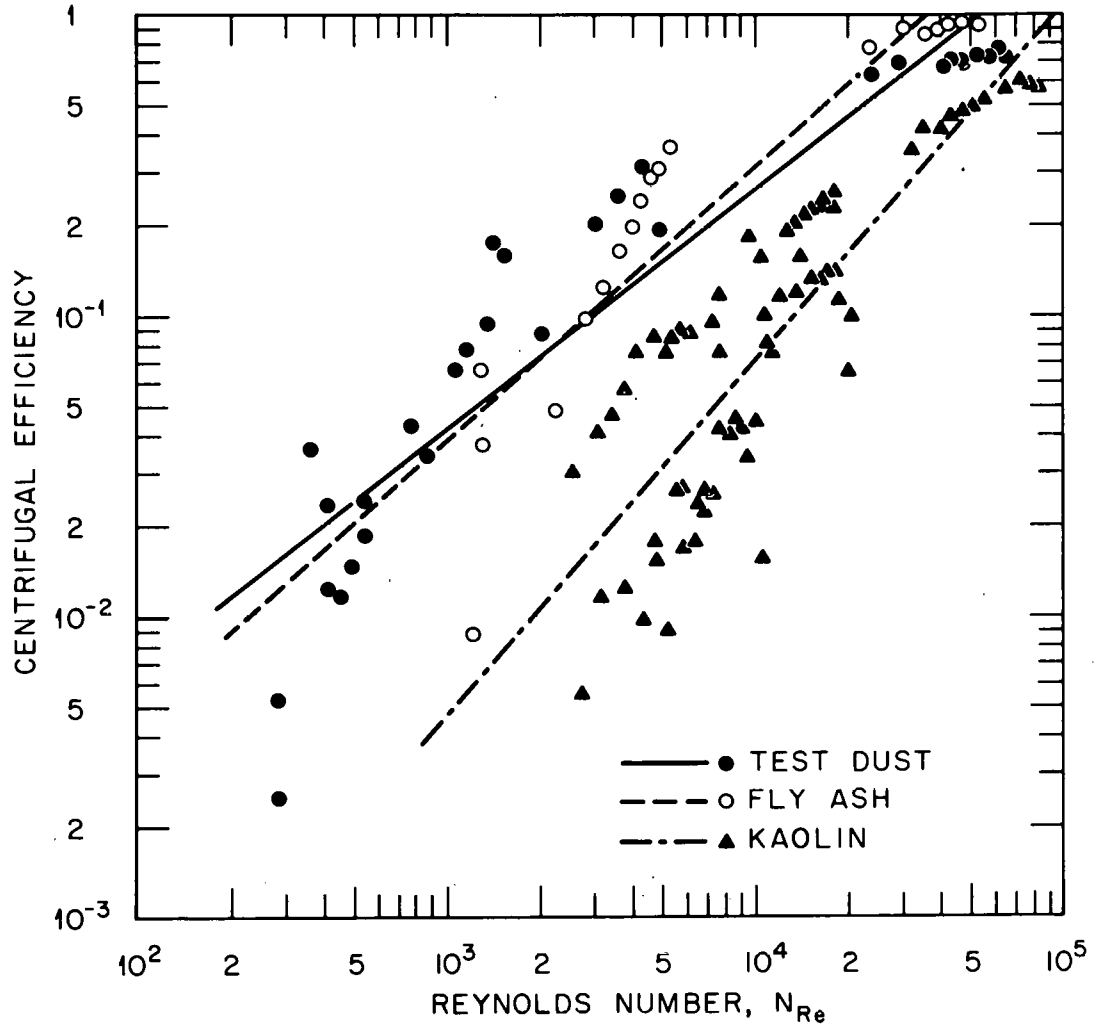


Fig. 30. Centrifugal efficiency as a function of Reynolds number.

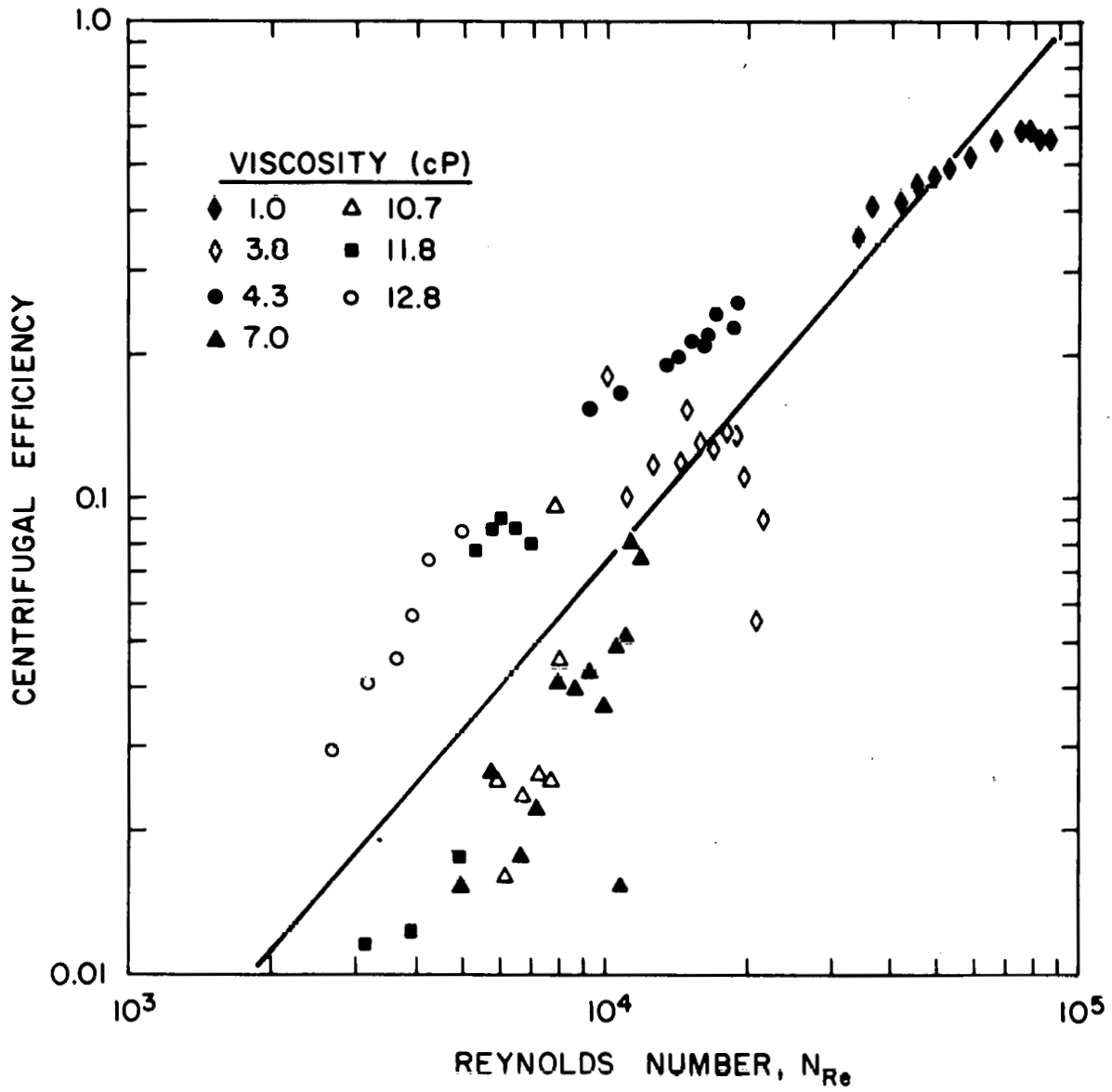


Fig. 31. Centrifugal efficiency as a function of Reynolds number for kaolin slurries.

methods of determining point efficiencies would differ. As displayed in Fig. 10, the differential method gives higher values of point efficiency than the cumulative method. However, values from the differential method are more scattered than efficiencies calculated by the cumulative method. The differential method seems more accurate since the percent point efficiencies range from 0 to 100%, whereas the cumulative method gives a maximum percent point efficiency of only 80%. Since the two techniques were not analyzed to determine a reason for the differences, the results of each method are shown in Sect. 5.3 and will be discussed in this section.

From point efficiency curves, similar to Fig. 10, d_{50} values could be interpolated, as presented in Table 9. Although particle size distributions and subsequent point efficiency curves were determined for the kaolin slurries with average viscosities of 1.0, 4.3, 10.7, 11.8, and 12.8 cP, only a few d_{50} values could be interpolated. The particle size analyses for the overflow and underflow streams were nearly identical for runs not listed in Table 9. Therefore, the point efficiency data were too scattered to be useful. There are two possible explanations for the similarity of the overflow and underflow size distribution curves. First, if the size distributions are accurate, essentially no separation occurred according to specific particle size ranges. The gross efficiency calculations indicated that G approached 0.5 as viscosity increased. Therefore, the bulk solids are splitting nearly evenly between the overflow and underflow streams. The second possibility is that the particle size distributions are not accurate and,

therefore, do not show the actual separation by particle size when used to determine point efficiencies.

The d_{50} values in Table 9 range from 1.3 to 3.8 μm . The literature²⁵ states that a plot of d_{50} vs $(\text{Re inlet})(\sigma-\rho)/\rho$ should give a straight line. Also, by rearrangement of the d_{50} correlations in Table 1, d_{50} is proportional to the product of Re inlet and $(\sigma-\rho)/\rho$. The values of d_{50} in Table 9 are plotted as suggested²⁵ in Fig. 32. The number of d_{50} values are small, and there is much scatter; however, a least-squares linear line is drawn through all the d_{50} values and also two separate dashed lines are drawn for $(N_{\text{Re inlet}})(\sigma-\rho)/\rho$ values less than and greater than 10^4 . The efficiency correlations in Table 1 are rearranged and the hydroclone dimensions substituted to obtain similar correlations that relate d_{50} to $(N_{\text{Re inlet}})(\sigma-\rho)/\rho$. These correlations and the relationships from Fig. 32 are presented in Table 17. The values predicted by the Bradley model are consistently lower than the experimental values of d_{50} . The three empirical correlations (see Table 17) give d_{50} values much higher than the experimental d_{50} values in Table 9. The least-squares fit of all the experimental d_{50} values in Fig. 32 does not indicate a negative slope of one-half. By separating the d_{50} values in Fig. 32 into two regimes, the experimental relationship is closer to those found in the literature. There is not enough d_{50} data to give an acceptable correlation.

Reduced efficiency curves (using both differential and cumulative methods) for the kaolin-aqueous slurries (1 cP) are shown in Fig. 11. A reduced efficiency curve is a complete description of the hydroclone efficiency. Several empirical relationships for reduced efficiency

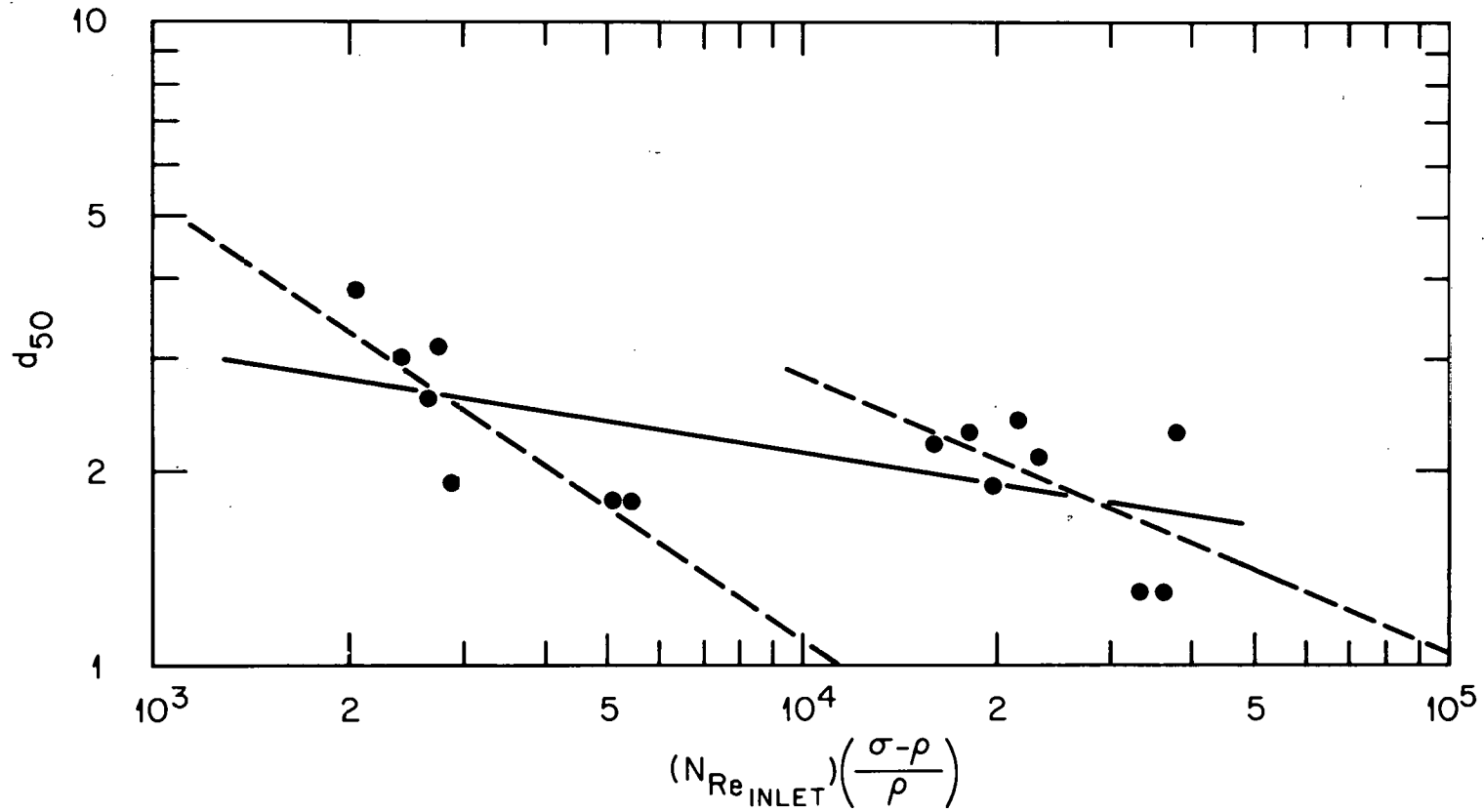


Fig. 32. Effect of $(N_{Re\ inlet}) \frac{(\sigma - \rho)}{\rho}$ on d_{50} values.

Table 17. Comparison of experimental and theoretical d_{50} efficiency correlations, $\gamma = (N_{Re \text{ inlet}})(\sigma - \rho)/\rho$

Correlations	
	<u>Experimental Least-Squares Fit^a</u>
Overall	$d_{50} = 9.5 \gamma^{-0.16}$, $r^2 = 0.38$;
$\gamma < 10^4$	$d_{50} = 585 \gamma^{-0.68}$, $r^2 = 0.73$;
$\gamma > 10^4$	$d_{50} = 154 \gamma^{-0.43}$, $r^2 = 0.32$;
	<u>Theoretical</u>
Bradley model	$d_{50} = 182 (1 - Rf)^{0.5} \gamma^{-0.5}$
Ilaas model	$d_{50} \approx 1957 \gamma^{-0.5}$
Matschke and Dahlstrom correlation (for $\mu = 1 \text{ cP}$)	$d_{50} \approx 1802 \gamma^{-0.5}$
Wagner and Murphy correlation	$d_{50} \approx 1014 \gamma^{-0.5}$

^aLeast-squares fit from data in Fig. 32.

curves have been deduced. Yoshioka and Hoffa¹² obtained a curve to which Bradley⁵ fitted the following analytical function:

$$E' = 1 - \exp \left[- \left(\frac{d}{d_{50}} - 0.115 \right)^3 \right]. \quad (49)$$

Another equation deduced²⁵ from similar observations is

$$E' = \frac{\exp (\beta d/d_{50}) - 1}{\exp (\beta d/d_{50}) + \exp \beta - 2}. \quad (50)$$

The constant β was found to depend on the slurry feed; previous work indicated $\beta = 2.5$ for silica ore and 2.0 for copper ore. Equation (49) and Eq. (50) for $\beta = 2.0$ and $\beta = 3.0$ are shown in Fig. 33, with the reduced efficiency from the experimental data determined from the differential technique. The data follow the S-shaped curves; however, Eq. (51), using $\beta = 3.0$, seems to fit the best.

Particle removal data obtained from Dorr-Oliver for the hydroclone used in this study are given in Fig. 34 as a function of feed rate and pressure drop. The Dorr-Oliver d_{95} values indicate the particle diameters in microns at which 95% of the solids were discharged to the underflow stream. As seen in Fig. 33, $d_{95}/d_{50} \cong 2$, where $\beta = 3.0$. By comparing the experimental values with the Dorr-Oliver correlation at the same pressure drop (see Fig. 34), the particle removal efficiencies observed in experiments with 1 cP slurries appear comparable to the manufacturers specifications.

ORNL DWG 78-22238

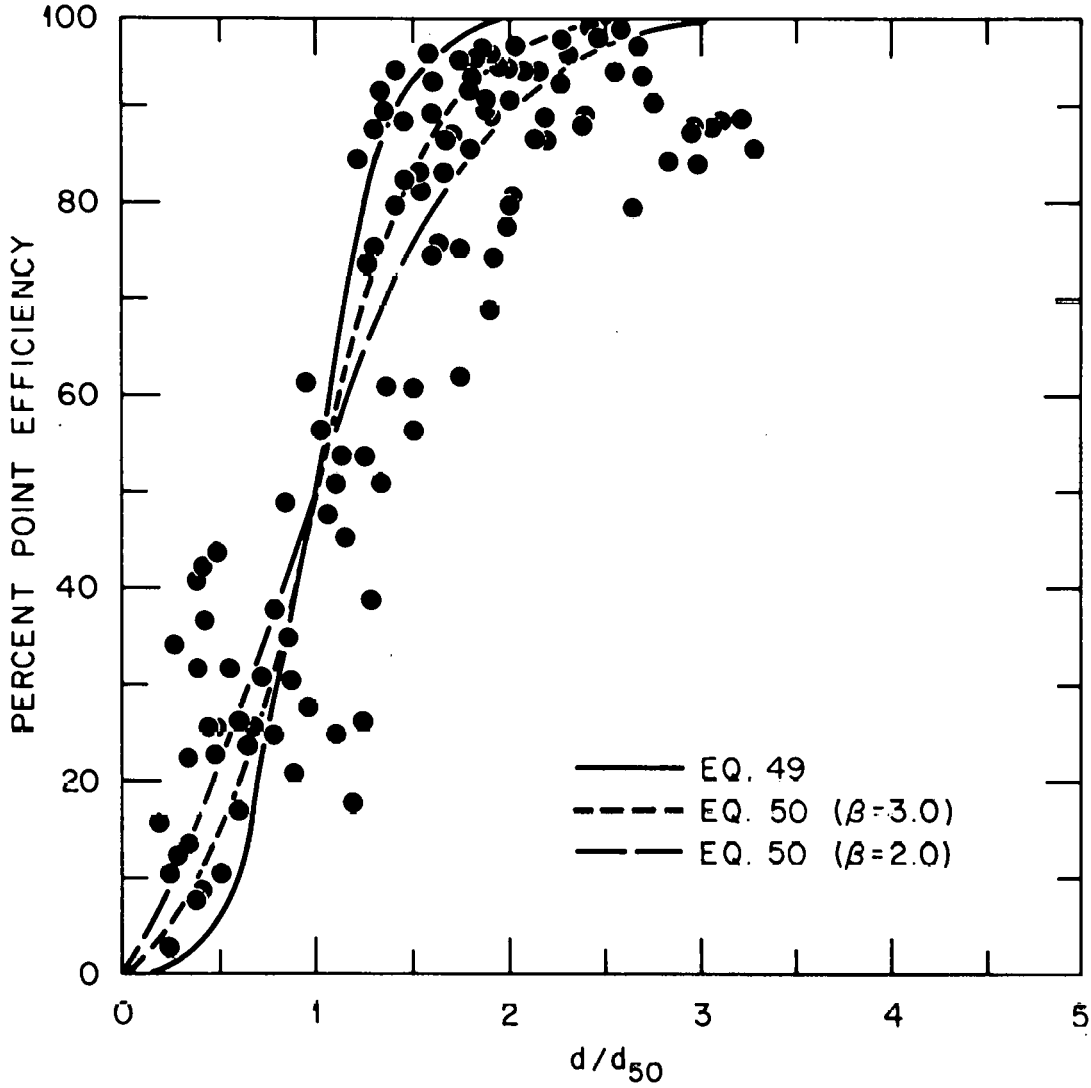


Fig. 33. Reduced efficiency data (differential method) showing literature correlations.

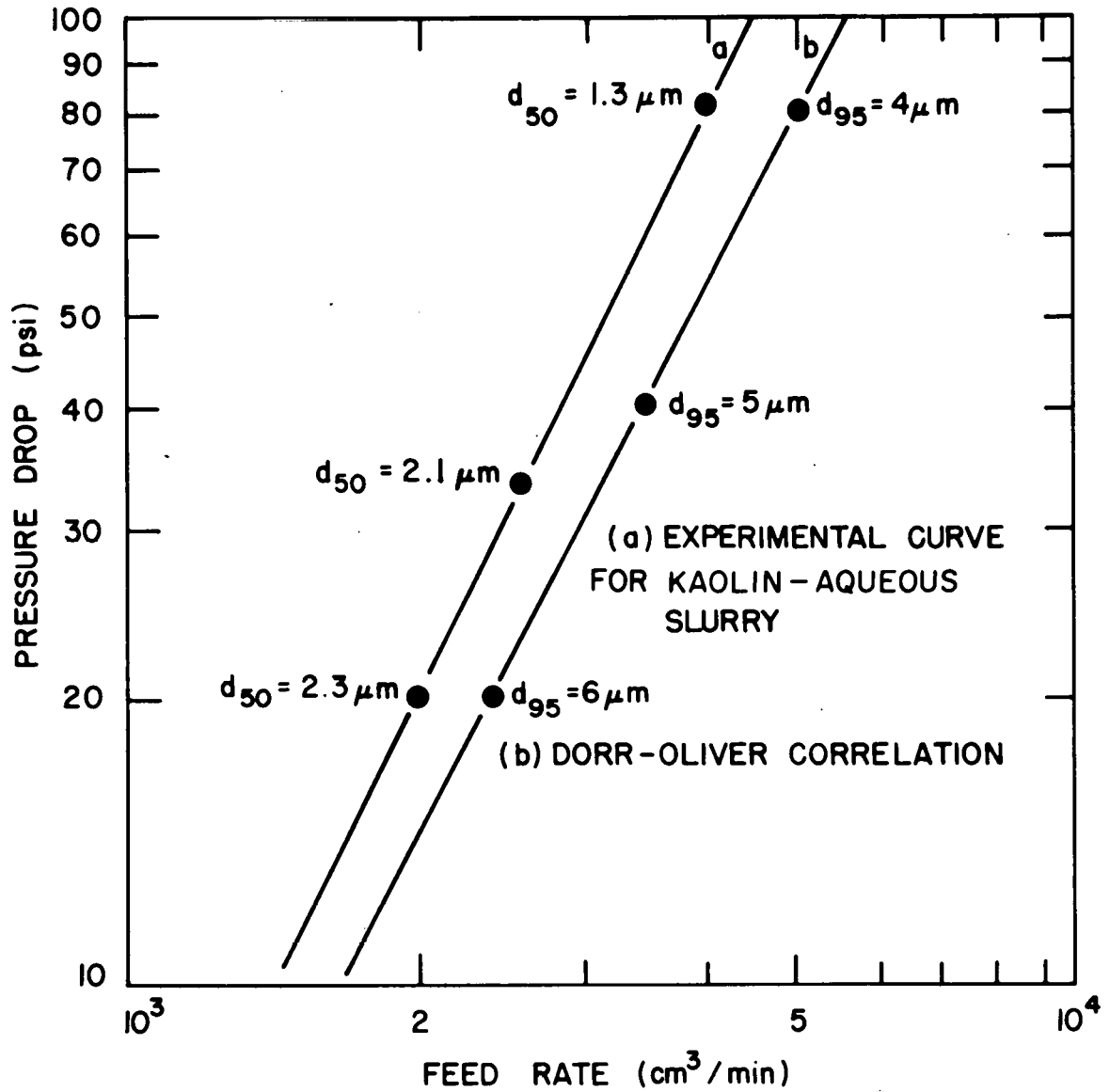


Fig. 34. Comparison of experimental and manufacturer particle removal data.

7. CONCLUSIONS

For the experimental results and data analysis of the performance of the 1-cm-diam hydroclone studied, several conclusions can be reached:

1. Pressure drop increases with increasing feed rate and increasing viscosity. The following correlations show this result for the fly-ash and test-dust slurries tested (viscosities 1-35 cP for fly ash and 1-85 cP for test dust):

$$\text{Fly ash: } \Delta P = 1.72 \times 10^{-5} Q_f^{1.85} \mu^{0.079} . \quad (51)$$

$$\text{Test dust: } \Delta P = 7.12 \times 10^{-5} Q_f^{1.64} \mu^{0.066} . \quad (52)$$

2. For the kaolin-glycerol mixtures (viscosities <13 cP), the pressure-drop-flow-rate correlation was not affected by viscosity. For viscosities other than 1 cP, the correlation is

$$\Delta P = 4.25 \times 10^{-6} Q_f^{2.00} . \quad (53)$$

3. For all slurries with a liquid viscosity of 1 cP, the following relationship between pressure drop and feed rate agrees well with theoretical and other empirical correlations given in the literature:

$$\Delta P = 3.05 \times 10^{-6} Q_f^{2.07} . \quad (54)$$

4. For most of the experimental runs, volume split and flow ratio increased with an increase in feed rate and viscosity. All values of volume split are >0.5 , and most are greater than unity.
5. Euler numbers do not vary significantly for this study (range from 6.4-16.3). However, Euler numbers decreased slightly with increasing inlet Reynolds number, reaching a minimum at a $N_{Re \text{ inlet}}$ range of 10^3 to 10^4 , and then increasing slightly for $N_{Re \text{ inlet}} > 10^4$. This trend had been observed previously in the literature.
6. Gross and centrifugal efficiency increased with increasing feed rate and decreasing viscosity. Therefore, gross and centrifugal efficiency increased with increasing Reynolds number as follows:

$$\text{Test dust: } G = 0.233 N_{Re}^{0.126} ; \quad (43)$$

$$E = 1.74 \times 10^{-4} N_{Re}^{0.795} . \quad (46)$$

$$\text{Fly ash: } G = 0.116 N_{Re}^{0.202} ; \quad (44)$$

$$E = 7.43 \times 10^{-5} N_{Re}^{0.905} . \quad (47)$$

$$\text{Kaolin: } G = 0.143 N_{Re}^{0.153} ; \quad (45)$$

$$E = 1.38 \times 10^{-6} N_{Re}^{1.179} . \quad (48)$$

7. When point efficiency is plotted against particle diameter, the data follow the expected S-shaped curve. The interpolated d_{50} values, the particle diameter corresponding

to a point efficiency of 50%, decreased as the product $(N_{Re \text{ inlet}})(\sigma-\rho)/\rho$ increased.

8. Reduced efficiencies for the kaolin-aqueous slurry were calculated to characterize the hydroclone operation. The following relationship for reduced efficiency was determined using the differential method:

$$E^i = \frac{\exp(3.0 d/d_{50}) - 1}{\exp(3.0 d/d_{50}) - \exp 3.0 - 2} \quad (53)$$

This evaluation of a 1-cm-diam hydroclone studied its performance at the limits of operation by combining the parameters of high liquid viscosity, micron-sized particles, and small solid-liquid density difference (which simulated the properties of coal-derived liquids). As mentioned in the literature and concluded in this study, the performance criteria of pressure drop and hydroclone efficiency are greatly influenced by the parameters of interest. The results of experiments with test-dust and fly-ash particles illustrate the effects of high liquid viscosity. Pressure drop increased with increasing viscosity and feed rate; however, the maximum ΔP which could be attained decreased with increasing viscosity. Table 18 compares pressure drop [from Eqs. (26), (51), and (52)], Reynolds number, gross efficiency [from Eqs. (43)-(45)], and centrifugal efficiency [from Eqs. (46)-(48)] for test dust, fly ash, and kaolin solutions at the same feed rate and the maximum liquid viscosity studied for each slurry. The feed rate of 2500 cm³/min is a maximum capacity at viscosities >30 cP. These results in Table 18 show that the gross and centrifugal efficiencies are prohibitively low.

Therefore, liquid viscosities greater than ~ 10 cP are not recommended due to the deleterious effects on the pressure drop (flow rate) and efficiency.

Table 18. Comparison of calculated results at a feed rate of $2500 \text{ cm}^3/\text{min}$

Solids	Maximum liquid viscosity (cP)	Pressure drop (psi)	N_{Re}	G	E
Test dust	85.0	35.7	591	0.521	0.028
Fly ash	33.0	44.0	1520	0.510	0.056
Kaolin	12.8	26.6	3930	0.507	0.024

Thus the results of the kaolin studies, where the liquid viscosity was < 13 cP and the particle diameters were $< 10 \mu\text{m}$, are particularly interesting. The maximum feed rates for liquid viscosities of 1 cP and 12.8 cP are ~ 4000 and $3000 \text{ cm}^3/\text{min}$ respectively. Table 19 compares pressure drop [Eq. (26)], Reynolds number, and efficiencies [Eqs. (45) and (48)] for kaolin at the above conditions. This comparison shows the pronounced effect of viscosity on efficiency. Notice, however, that the maximum feed rate and lowest viscosity for a kaolin slurry resulted in a maximum gross efficiency of 80.5% and centrifugal efficiency of 83.8%.

Viscosity has a noticeable effect on the particle-size-distribution curves, as shown in Figs. 6 and 7. As viscosity increases, the smaller sized particles are not separated from the bulk fluid to the underflow stream. At the most favorable conditions of high feed rate and with a

liquid viscosity of 1 cP, a d_{50} value of 1.3 μm is determined from Fig. 34; this corresponds to a d_{95} value of $\sim 3 \mu\text{m}$. Therefore, at higher viscosities it can be assumed that this d_{50} value (and d_{95}) would only increase. Therefore, with the most favorable operating conditions using kaolin slurries ($\sigma = 2.64 \text{ g/cm}^3$) at a feed capacity of 4000 cm^3/min and liquid viscosity of 1 cP, 95% of the particles $>3 \mu\text{m}$ in diameter can be separated to the underflow stream.

Table 19. Comparison of calculated results for kaolin particles

Maximum feed rate (cm^3/min)	Liquid viscosity (cP)	Pressure drop (psi)	N_{Re}	G	E
4000	1	68.0	80,400	0.805	0.838
3000	12.8	38.3	4,710	0.522	0.030

8. ACKNOWLEDGMENTS

The author wishes to acknowledge T. Trinh, J. J. Monge, and W. A. Chrusciel of the MIT School of Chemical Engineering Practice who collected the experimental data for the aluminum-oxide, fly-ash, and test-dust slurries. Special thanks are due R. O. Payne who conducted the kaolin slurry experiments and compiled much of the experimental data for analysis. Particle size analyses were performed by the Analytical Chemistry Division by L. D. Jones under the supervision of W. R. Laing.

9. APPENDIX

THIS PAGE
WAS INTENTIONALLY
LEFT BLANK

Table A-1. Test data for aluminum oxide, test dust, and fly-ash particles^a

Run number	Viscosity (cP)	Pressure drop (psi)	Solids concentration		Overflow rate (cm ³ /min)	Underflow rate (cm ³ /min)
			Overflow (g/cm ³)	Underflow (g/cm ³)		
<u>Aluminum Oxide Particles</u>						
(Solids density = 3.72 g/cm ³)						
1	1.0	6.6			700	540
2		21.2			1090	1095
3		37.0			1235	1450
4		62.7			1610	1960
5		74.8			1700	2267
6		92.8			1770	2667
<u>Test Dust Particles</u>						
(Solids density = 2.64 g/cm ³)						
18	1.0	6.8	0.0166	0.0688	550	650
19		10.0	0.0144	0.0734	680	810
20		17.7	0.0151	0.0667	860	1190
21		22.0	0.0132	0.0678	900	1300
22		27.0	0.0128	0.0651	980	1380
23		39.7	0.0116	0.0618	1140	1750
24		46.5	0.0110	0.0726	1220	1880
25		54.2	0.0108	0.0600	1300	2000
26		29.7	0.0129	0.0612	950	1420
27		35.5	0.0123	0.0667	1000	1640
35	10.7	7.1	0.0533	0.0651	620	460
36		11.2	0.0490	0.0740	840	800
37		15.0	0.0451	0.0743	940	1000
38		20.4	0.0424	0.0770	1010	1280

Table A-1 (continued)

Run number	Viscosity (cP)	Pressure drop (psi)	Solids concentration		Overflow rate (cm ³ /min)	Underflow rate (cm ³ /min)
			Overflow (g/cm ³)	Underflow (g/cm ³)		
<u>Test Dust Particles</u>						
(Solids density = 2.64 g/cm ³)						
39		25.5	0.0394	0.0560	1140	1460
40		31.2			1220	1640
41		36.8			1340	1780
42		43.0			1480	1920
45	33.0	22.2	0.0607	0.0598	500	1050
46		15.5	0.0737	0.0574	440	840
47		19.8	0.0551	0.0578	400	1040
48		27.0	0.0539	0.0591	450	1320
49		30.5	0.0535	0.0596	480	1410
50		35.5	0.0535	0.0609	550	1660
51		41.5	0.0500	0.0636	520	1810
52		45.5	0.0506	0.0630	560	1950
60	59.0	11.5	0.0607	0.0626	740	490
61		15.1	0.0613	0.0649	900	660
62		17.0	0.0609	0.0635	830	710
63		14.0	0.0600	0.0621	840	620
11	85.0	11.8	0.0464	0.0467	750	460
12		14.9	0.0470	0.0426	980	680
13		18.8	0.0445	0.0458	1150	810
14		17.5	0.0515	0.0543	990	760
15		8.5	0.0564	0.0546	520	440
16		10.5	0.0527	0.0533	660	550
17		14.5	0.0512	0.0553	810	720

Table A-1 (continued)

Run number	Viscosity (cP)	Pressure drop (psi)	Solids concentration		Overflow rate (cm ³ /min)	Underflow rate (cm ³ /min)
			Overflow (g/cm ³)	Underflow (g/cm ³)		
<u>Fly-Ash Particles</u>						
(Solids density = 2.28 g/cm ³)						
28	1.0	7.4	0.0057	0.0435	530	660
29		11.2	0.0042	0.0793	700	820
30		14.1	0.0066	0.0797	780	1010
31		18.6	0.0050	0.0767	770	1200
32		24.1	0.0029	0.0730	860	1290
33		28.5	0.0023	0.0718	1040	1330
34		34.5	0.0031	0.0719	1030	1660
64		10.6	13.8	0.0546	0.0603	600
65	18.5		0.0524	0.0640	760	730
66	26.0		0.0504	0.0647	860	860
67	32.0		0.0479	0.0652	870	1060
68	39.0		0.0459	0.0663	930	1180
69	43.7		0.0433	0.0676	990	1270
70	48.3		0.0399	0.0689	1060	1380
71	55.2		0.0384	0.0683	1120	1480
72	62.0		0.0360	0.0715	1200	1620
53	35.0		11.2			720
54		14.0			840	640
55		18.0	0.0602	0.0589	1000	800
56		23.5	0.0605	0.0617	1140	960
57		27.0	0.0576	0.0626	1240	1040
58		31.8	0.0526	0.0607	1310	1120
59		35.0			1260	1270

^aData obtained from ref. 18.

Table A-2. Test data for kaolin particles^a

Run number	Viscosity (cP)	Pressure drop (psi)	Solids concentration		Overflow rate (cm ³ /min)	Underflow rate (cm ³ /min)
			Overflow (g/cm ³)	Underflow (g/cm ³)		
1	1.0	13.6	0.0272	0.0555	750	867
2	1.0	18.0	0.0243	0.0553	785	957
3	1.0	23.0	0.0243	0.0565	918	1084
4	1.0	27.8	0.0223	0.0574	1008	1152
5	1.0	33.8	0.0223	0.0596	1097	1260
6	1.0	37.5	0.0213	0.0596	1179	1364
7	1.0	47.5	0.0203	0.0628	1360	1463
8	1.0	57.8	0.0182	0.0639	1570	1667
9	1.0	67.5	0.0179	0.0670	1648	1985
10	1.0	77.5	0.0182	0.0670	1765	2045
11	1.0	87.3	0.0183	0.0660	1875	2069
12	1.0	97.7	0.0179	0.0620	1915	2234
13	3.8	12.7	0.0263	0.0370	820	980
14	3.8	17.3	0.0332	0.0400	915	1091
15	3.8	22.1	0.0361	0.0447	1022	1256
16	3.8	27.0	0.0381	0.0476	1162	1400
17	3.8	31.7	0.0391	0.0521	1205	1449
18	3.8	36.4	0.0436	0.0560	1325	1517
19	3.8	41.6	0.0444	0.0566	1387	1646
20	3.8	46.4	0.0455	0.0588	1443	1792
21	3.8	51.2	0.0461	0.0598	1562	1830
22	3.8	56.2	0.0449	0.0555	1635	1891
23	3.8	61.0	0.0422	0.0468	1732	2007
24	3.8	64.7	0.0432	0.0522	1805	2042
37	4.5	12.8	0.0142	0.0191	775	950
38	4.5	17.6	0.0155	0.0131	910	1150
39	4.4	22.3	0.0160	0.0213	1001	1269
40	4.4	27.0	0.0100	0.0244	1137	1428
41	4.3	31.8	0.0165	0.0235	1219	1515
42	4.2	36.6	0.0175	0.0254	1274	1576

Table A-2 (continued)

Run number	Viscosity (cP)	Pressure drop (psi)	Solids concentration		Overflow rate (cm ³ /min)	Underflow rate (cm ³ /min)
			Overflow (g/cm ³)	Underflow (g/cm ³)		
43	4.2	41.2	0.0186	0.0277	1352	1691
44	4.2	46.5	0.0182	0.0273	1425	1786
45	4.3	51.5	0.0183	0.0278	1500	1893
46	4.2	56.7	0.0183	0.0291	1571	1965
47	4.1	61.0	0.0192	0.0293	1605	2078
48	4.2	66.6	0.0185	0.0302	1673	2088
25	7.0	12.0	0.0430	0.0444	882	792
26	7.0	16.7	0.0420	0.0444	1000	930
27	7.0	21.3	0.0465	0.0482	1136	1105
28	7.0	26.0	0.0472	0.0494	1212	1156
29	7.0	30.7	0.0474	0.0514	1296	1385
30	7.0	35.4	0.0494	0.0533	1386	1535
31	7.0	40.6	0.0529	0.0573	1509	1634
32	7.0	45.5	0.0525	0.0559	1526	1768
33	7.0	50.3	0.0512	0.0557	1648	1891
34	7.0	55.7	0.0531	0.0546	1679	2038
35	7.0	60.2	0.0518	0.0602	1738	2080
36	7.0	65.0	0.0504	0.0578	1771	2171
54	11.3	34.0	0.0555	0.0556	1509	1421
55	11.1	38.7	0.0547	0.0577	1573	1566
56	10.9	43.7	0.0564	0.0583	1575	1622
57	10.8	48.7	0.0571	0.0598	1680	1773
58	10.5	53.8	0.0581	0.0611	1758	1878
59	10.2	58.4	0.0570	0.0598	1735	1987
60	10.1	64.0	0.0578	0.0629	1781	2039
72	11.1	65.3	0.0419	0.0499	1839	2244
49	12.0	11.2	0.0419	0.0424	893	759
50	12.0	15.8	0.0434	0.0445	1014	879
51	11.8	20.1	0.0468	0.0480	1137	1073
52	11.4	24.9	0.0487	0.0497	1251	1175

Table A-2 (continued)

Run number	Viscosity (cP)	Pressure drop (psi)	Solids concentration		Overflow rate (cm ³ /min)	Underflow rate (cm ³ /min)
			Overflow (g/cm ³)	Underflow (g/cm ³)		
53	11.4	29.4	0.0513	0.0532	1403	1285
67	12.3	40.0	0.0375	0.0430	1409	1703
68	12.0	44.3	0.0383	0.0447	1478	1764
69	12.0	50.4	0.0390	0.0460	1565	1888
70	11.9	55.4	0.0409	0.0477	1585	2095
71	11.7	59.7	0.0419	0.0480	1738	2189
61	13.3	12.0	0.0251	0.0267	870	810
62	13.0	16.5	0.0277	0.0301	1038	980
63	13.0	21.0	0.0301	0.0330	1123	1128
64	13.0	25.7	0.0324	0.0362	1194	1246
65	12.8	30.5	0.0342	0.0394	1229	1394
66	12.5	35.2	0.0362	0.0424	1361	1613

^aSolids density = 2.40 g/cm³.

10. REFERENCES

1. E. Bretney, U.S. Pat. No. 453, 105 (May 26, 1891).
2. M. G. Driessen, Journ. Inst. Fuel 67, 327 (1939).
3. M. S. Edwards, B. R. Rodgers, and R. Salmon, Coal Technology Program, Supporting Research and Development on Separations Technology, Phase I Report, ORNL/TM-4801 (March 1975).
4. Hydrocarbon Research, Inc., H-Coal Integrated Pilot Plant, Phase I - Final Report, Dec. 1973-June 1976, HCP/T-1544/1 (Vol. II), Hydrocarbon Research, Inc., Lawrenceville, New Jersey (November 1977), pp. 306-19.
5. D. Bradley, The Hydroclone, Pergamon Press, N.Y., 1965.
6. D. Bradley, Ind. Chem. 34, 473 (September 1958).
7. J. G. van Kooy, "The Influence of the Reynolds' Number on the Operation of a Hydroclone," p. 70 in Cyclones in Industry, Elsevier, Amsterdam, The Netherlands, 1961.
8. D. Bradley, A Contribution to the Theory of the Hydraulic Cyclone, and Data on the Performance of Small Diameter Cyclones - Part 3, AERE-R3146 (1959).
9. G. M. Chaplin, A Mathematical Description of Hydroclone Dynamics, Thesis, University of Arizona, 1972, p. 14.
10. D. Bradley and D. J. Pulling, Trans. Inst. Chem. Eng. 37, 34 (1959).
11. K. Rietema, "The Mechanism of the Separation of Finely Dispersed Solids in Cyclones," Cyclones in Industry, Elsevier, Amsterdam, 1961.
12. H. Yoshioka and Y. Hotta, Chem. Eng. (Japan) 19, 632 (1955).
13. A. N. Zhevnovaty, Int. Chem. Eng. 2(4), 580-84 (October 1962).
14. F. J. Fontein, J. G. van Kooy, and H. A. Leniger, Br. Chem. Eng. 7(6), 410-21 (June 1962).
15. P. A. Haas, E. O. Nurmi, M. E. Whatley, and J. R. Engel, Chem. Eng. Prog. 53(4), 203-207 (April 1957).
16. W. L. Oliver III, Chem. Eng. Prog. 59(4), 87-90 (April 1963).
17. D. E. Matschke and D. A. Dahlstrom, Chem. Eng. Prog. 54(12) (December 1958); 55(1) (January 1959).

18. J. Wagner and R. S. Murphy, *Ind. Eng. Chem. Process Des. Dev.* 10(3), 346-52 (1971).
19. 1974 SAE Handbook, Part 2, p. 908, Society of Automotive Engineers, New York, 1974.
20. T. Trinh, J. J. Monge, and W. A. Chrusciel, Efficiency of Particle Removal from Viscous Liquids with a Hydroclone, ORNL/MIT-237 (October 1976).
21. C. S. Miner and N. N. Dalton, pp. 278-81 in Glycerol, Reinhold Publishing Co., New York, 1953.
22. The Dorrclone (brochure), Dorr-Oliver Inc., Stamford, Conn., 1976.
23. M. Leonard, Dorr-Oliver Inc., Stamford, Conn., personal communication, August 17, 1976.
24. A. M. Gerrard and C. J. Liddle, *Chem. Eng.*, 298 (1975).
25. L. Svaravsky, ed., p. 109 in Solid-Liquid Separation, Butterworths, Boston, 1978.

INTERNAL DISTRIBUTION

- | | |
|---------------------|---------------------------------|
| 1. R. E. Barker | 15. C. H. Shappert |
| 2. J. M. Begovich | 16-20. J. B. Talbot |
| 3. R. M. Canon | 21. D. B. Trauger |
| 4. S. D. Clinton | 22. J. S. Watson |
| 5. H. D. Cochran | 23. A. Zucker |
| 6. P. W. Fisher | 24-25. Central Research Library |
| 7. D. E. Ferguson | 26. Document Reference Section |
| 8. T. M. Gilliam | 27-28. Laboratory Records |
| 9. R. W. Glass | 29. Laboratory Records - RC |
| 10. P. A. Haas | 30. ORNL Patent Office |
| 11. J. R. Hightower | 31. L. Burris, Jr. (consultant) |
| 12. L. E. McNeese | 32. G. R. Choppin (consultant) |
| 13. B. R. Rodgers | 33. W. H. Corcoran (consultant) |
| 14. C. D. Scott | |

EXTERNAL DISTRIBUTION

- 34. R. P. Epple, Office of Basic Energy Sciences, DOE, Mail Station J-309, GTN, Washington, DC 20545
- 35. W. J. Haubach, Office of Basic Energy Sciences, DOE, Mail Station J-309, GTN, Washington, DC 20545
- 36. H. T. Jones, Office of Fossil Energy, DOE, Mail Station E-333, GTN, Washington, DC 20545
- 37. E. S. Pierce, Office of Basic Energy Sciences, DOE, Mail Station J-309, GTN, Washington, DC 20545
- 38. D. K. Stevens, Office of Basic Energy Sciences, DOE, Mail Station J-309, GTN, Washington, DC 20545
- 39. F. Dee Stevenson, Office of Basic Energy Sciences, DOE, Mail Station J-309, GTN, Washington, DC 20545
- 40. Office of Assistant Manager for Energy Research and Development, DOE-ORO, Oak Ridge, TN 37830
- 41-67. Technical Information Center, Oak Ridge, TN 37830